VIRTUAL METHODOLOGY FOR ACTIVE FORCE CANCELLATION IN AUTOMOTIVE APPLICATION USING MASS IMBALANCE AND CENTRIFUGAL FORCE GENERATION (CFG) PRINCIPLE

by

ABHISHEK PAUL

A dissertation submitted in partial fulfillment of the
requirements for the degree of Degree of

DOCTOR OF PHILOSOPHY IN MECHANICAL ENGINEERING

2024

Oakland University
Rochester, Michigan

Doctoral Advisory Committee:

Michael A. Latcha, Ph.D., Chair
Zissimos P. Mourelatos, Ph.D.
Christopher Cooley, Ph.D.
Syed Haider, Ph.D.
Darrell Schmidt, PhD.

To my family, friends, mentors, and Max

ACKNOWLEDGMENTS

I would like to acknowledge sincere gratitude towards my advisor, Professor Michael A. Latcha for his continuous guidance and support during this research. He has been a constant source of expertise and inspiration to complete this dissertation.

I also wish to express my appreciation to the members of my advisory committee, Professors Zissimos P. Mourelatos, Professor Christopher Cooley, Professor Darrell Schmidt of Oakland University, and Dr. Syed Haider of Stellantis for their comments and suggestions throughout this journey.

Special thanks are due to Dr. Francisco Sturla and Kevin Thomson from Stellantis for providing valuable advice and support in my research.

Abhishek Paul

ABSTRACT

VIRTUAL METHODOLOGY FOR ACTIVE FORCE CANCELLATION IN AUTOMOTIVE APPLICATION USING MASS IMBALANCE AND CENTRIFUGAL FORCE GENERATION (CFG) PRINCIPLE

by

ABHISHEK PAUL

Advisor: Michael A. Latcha, PhD.

Structures under the influence of an external force are excited to resonance when the frequency of the external force and the natural frequency of the structure align with each other. Resonance leads to large deformation, which may cause damage to the integrity of the structure. There have been numerous applications of external devices that dampen the effects of excitation to the structure, such as tuned mass dampers, semi-active and active dampers, which have been implemented in buildings, bridges, and other large structures. One of the methods used for active cancellation uses the principle of centrifugal forces generated by the rotation of an imbalanced mass. These forces help counter the external excitation force applied to the structure. This research focuses on the working principle of active force cancellation using centrifugal forces due to mass imbalance and provides a virtual solution to simulate and predict the forces required to cancel the external excitation to an automotive structural system. This research addresses the challenges to miniaturize the CFG used for a Body on Frame truck and effectively reduce the amplitudes of the response due to a forcing function. The virtual tool presented in this thesis will help predict the maximum amplitude cancellation at resonance for given imbalance mass and frequency of forced excitation.

TABLE OF CONTENTS

LIST OF FIGURES

LIST OF ABBREVIATIONS

TMD	Tuned Mass Damper
SDOF	Single Degree of Freedom
MDOF	Multiple Degree of Freedom
CFG	Centrifugal Force Generator
AC	Alternating Current
PID	Proportional Integral Derivative
LQR	Linear Quadratic Regulator
DC	Direct Current
ATMD	Active Tuned Mass Damper
EMF	Electro Magnetic Force
RHS	Right Hand Side
LHS	Left Hand Side
BIBO	Bounded Input Bounded Output
MIMO	Multi Input Multi Output
LTI	Linear Time Invariant
Hz	Hertz
KN	Kilo Newton
N	Newton
RPM	Rotations per minute
MM	Millimètre
KG	Kilogram

LIST OF ABBREVIATIONS – Continued

DMAP	Direct Matrix Abstraction Program
ADAS	Advanced Driver Assistance Systems

CHAPTER ONE

INTRODUCTION

1.1 LITERATURE REVIEW

In the past there have many techniques that have been used to reduce vibrations or to dissipate energy in a system to improve comfort, design, durability, and product life. These techniques have been utilized and implemented in many fields, such as civil, aerospace, marine and vehicle engineering. Most of these techniques comprise of mass damping or force cancellation. With advent of new technologies and automations, active control has become very popular in various industries. Active control attempts to change state variables using components such as mass dampers or force cancelling actuators during the operation cycle of the structure. For example, when an engine is operating, the acoustic vibrations coming from the engine can be reduced by generating forces with equal amplitude and opposite phase which cancel out the noise. This can be done by building a closed loop controller which can modify the feedback based on the input of the system within milliseconds. Some of these techniques will be elaborated in this dissertation.

1.1.1 MASS DAMPERS

Mass dampers essentially work on the principle that an added mass, spring and damper system will help reduce the amplitudes of resonance of the exciting force and natural mode of a system or move the natural modes of a system away from the exciting frequency, since natural modes are functions of mass and stiffness. A tuned mass damper (TMD) is tuned to a particular frequency such that, when a particular frequency is excited by the exciting force, the tuned mass resonates out of phase with the structural motion hence dissipating the energy [1]. Tuned mass dampers have been used in many applications such as crankshaft torsional dampers, steering wheel torsional dampers etc. Smith [2] has presented a simulation model of a centrifugal pendulum absorber which has been analyzed to reduce vibrations within the drivetrain. Smith [2] also provides a list of limitations to the simulation model analyzed, such as the Coriolis forces are neglected, only torsional vibrations have been considered, one vehicle configuration with single gear and six cylinders have been used for simulation etc. In the above-mentioned study, the author placed masses on rollers on either side of a flywheel at and offset from the carrier. The carriers have large cutout paths for the rollers to roll and move the masses to act as a pendulum. Since the flywheel is connected to the gearbox and engine, the centrifugal forces generated due the rotation of these pendulum masses at different velocities are used to regulate unwanted torsional vibrations coming from the engine due to the firing pulses [2]. Alsuwaiyan and Shaw [3] considered the epicyloidal paths of the rollers to have tautochronus motion (the same oscillatory frequency through the range of amplitudes) for a system dominated by centrifugal forces, as in the case of a flywheel system. Alsuwaiyan and Shaw [3] also illustrated an ADAMS model for the flywheel subsystem and used MATLAB to define the epicycloidal curved path which the pendulum masses follow during the drivetrain simulation. The centrifugal forces produced with these masses are directed towards the center of flywheel, which helps counter the incoming torsional vibrations. The authors also conclude the study by listing out limitations for the presented simulation model and scope of improvement. Future work recommended includes improvement in the centrifugal pendulum absorber geometry with inclusion of cutouts, end-stops, rollers, mirrored masses etc.

1.1.2 ACTIVE/SEMI-ACTIVE MASS DAMPERS

The application and development of semi-active dampers have been presented by Ferreira, et al. [4]. A numerical method to define semi active dampers to control the appropriate tuning of tuned mass dampers has been discussed. This model has been developed to control and/or dampen the lateral vibrations of long suspension bridges. The initial numerical model is built using a simple 2-degree of freedom system, one degree of freedom representing the structure and the other degree of freedom representing the tuned mass damper (TMD). An additional damper is placed in the system between the structure and TMD, which has a control switch. When the velocity of the TMD and the displacement of the structure are in opposite phase then the control of the semi-active damper remains off and when they are not in opposite phase then the control is switched on, allowing the semi-active damper to either create impulses causing a phase lead or locking the mass of the TMD causing a phase lag [4]. Ferreira et al. [4], also presented numerical modelling of semi-active dampers for multi degree of freedom (MDOF) structures. This principle has been used to model the MDOF system for this thesis as a starting point.

Active mass dampers have also been developed for slender structures, high rises, bridges, automotive vehicles etc. These basically work by moving masses and incorporate a control loop to regulate this movement. As masses are accelerated, they generate forces which can be utilized to counter or dampen input vibrations. One such application has been presented by Scheller and Starossek, [5]. In this paper, Scheller and Starossek presented a working principle and development of an active mass damper for bridges. The focus of the paper is on lateral vibration reduction of bridges due to pedestrian forces and flutter control of a bridge deck section. The authors also present a test setup to validate the functioning of the developed active mass damper system. The rotating mass unbalances creating centrifugal forces have been presented in the above paper, which is the main principle used for developing the virtual force cancellation technique presented in this thesis. As stated above, the basic principle of CFGs are that the rotating masses produce forces tangential to the axis of rotation, termed centrifugal forces. These forces can be controlled by number of unbalanced rotating masses, as presented by by Scheller and Startossek. The system relies on the fact that there are two actuators on the sides of the device with masses attached to a rod which rotate with the same angular frequency but in the opposite direction. The centrifugal force generated, therefore, is the sum of two vertical forces as the horizontal components cancel out each other. An assumption here is that the rod connecting the mass to the actuator is massless. Scheller and Starossek [5] also illustrate that the direction of the generated centrifugal force can be manipulated by changing the relative position between the left and right rotors. The paper also mentions the additional moments created in the model and how they can be eliminated to generate pure horizontal control forces. Scheller and Starossek [5] describe combinations of damper units for various applications.

Yang et al. [6] theoretically modeled an active mass damper with negative acceleration feedback control of single degree of freedom structure and showed theoretically and experimentally the application of the Negative Acceleration Feedback

(NAF) control algorithm to reduce vibrations in multi-degree of freedom structures. The authors have used AC servo motors controlled by PID controller to control the movement of the active masses. A multi-input and multi-output feedback control for vibration suppression in buildings has also been proposed by Talib, Shin and Kwak [7]. They modeled a negative acceleration feedback control to support multiple accelerometers and multiple active mass dampers. This has also been validated theoretically and experimentally using a two-story building-like structure. Chang and Yang [8] also presented a closed loop control system to control vibrations in building structures modeled as a SDOF system. An active tuned mass damper system with velocity feedback and complete feedback has been presented in the paper.

Samali and Al-Dawod [9] presented a five-story benchmark model with an active tuned mass damper with fuzzy control. The advantages of the fuzzy controller are its ability to handle nonlinear behavior and robustness. Samali and Al-Dawod have also compared active control between a fuzzy controller and a LQR controller. The benchmark model has been analyzed under earthquake excitations. In the conclusions from this research study, it was found that response reduction using fuzzy controllers is comparable to, and in some cases, better than, the LQR controller, although one needs to have a good knowledge base and an expert understanding of fuzzy logic to build the control system [9].

Active control of coupled structures has been demonstrated by Christenson et al. [10]. Acceleration feedback control and DC servo motor have been used to design and validate the control system developed. An H2/LQG approach has been implemented to design the control strategy and minimize accelerations in building structures under seismic excitations. In another paper [11], Zhang, Li, Cheng, and Zhang modeled active mass dampers using rotating actuators. A mathematical model has been derived to suppress vibrations in SDOF system due to external excitations. In this paper [11], Lagrange equations were used to derive the system of equations and hierarchical sliding mode controller has been presented to control the state variables. Numerical and experimental analysis has been performed to validate the model and reduce vibrations in the system due to external excitations. Vertical vibrations in the system are neglected as they are deemed to be negligible in comparison with the horizontal vibrations in the system considered [11]. The forces generated by an actuator in an ATMD, controlled by linear quadratic Gaussian controller, has been presented by Kim et al. [12]. They have presented a composite tuned mass damper, controlled using a LQG controller, to minimize vibrations due to wind responses in tall buildings. A composite tuned mass damper consists of both passive and active tuned mass dampers, which are used to suppress the vibrations in a structure.

In control theory, optimal control is deduced when all states of the system and output are a combination of all the states [12]. Due to the random nature of the wind-induced vibrations, the input and output are a function of random vibrations with a constant power spectral density of Gaussian white noise and an observer modeled to estimate all the state variables of the system. An LQG controller is used to define the system of equations and state variables in which the linear dynamic system is a function of Gaussian white noise with constant power spectral density. An active hybrid control, which is a combination of an active tuned mass damper and base isolation, has been presented by Djedoui, Ounis and Abdeddaim [13]. A proportional integral derivative (PID) controller with negative feedback closed-loop error has been used to control the system under earthquake excitations. The required control forces are computed using feedback error which is calculated as the difference between desired response and actual output [13]. A SIMULINK model has also been presented in the paper. Ge, et al. [14] highlight the use of active disturbance rejection control to mitigate vibrations in electric drive systems of electric vehicles. Ge, et al. [14] focus on vibrations due to impact such as potholes and bumps and reducing them with use of active disturbance rejection and electric current compensation. The electric current compensation helps in managing the sudden changes in the motor current during impact. A set of data on electric drive system response with and without the active vibration control has been presented. Stabilization of the current variation using current compensation technique has also been demonstrated.

The design and construction of the car's body and the perception of vehicle dynamics felt by the occupant has been presented by Roessler and Baier [15]. Experimental studies conducted on the vehicle structure and drivers' response to various road surfaces have been presented. The authors observed that certain frequencies and amplitudes of vibrations were more strongly associated with specific driving characteristics, such as acceleration, braking, and cornering. The study concluded that low frequency vibrations from 4-8 Hz were influential in determining the driver's perception of the driving dynamics. The paper suggests that by reducing or modifying specific vibrations, manufacturers may be able to create a more desirable driving sensation that aligns with the intended performance characteristics of the vehicle. Overall, the article highlights the role of feelable structure vibrations in shaping the perceived driving dynamics and emphasizes the potential for car manufacturers to leverage these insights to improve the overall driving experience for their customers.

Derrix and Prokop [16] investigated the impact of body stiffness on the drivability and dynamic behavior of a vehicle through on-road experiments. The authors observed that higher body stiffness was associated with improved steering response, increased stability, and reduced body roll during cornering. On the other hand, lower body stiffness resulted in a more comfortable ride but potentially compromised the vehicle's handling and responsiveness. The paper concluded with highlighting the importance of finding an optimal balance between comfort and performance when it comes to adjusting body stiffness. Wang et al. [17] have shown use of PID controller to control electric drives and power converters using MATLAB/Simulink. They have shown the importance of electric drives in energy conversion and the automatic control of electrical drives and grid connected three phase power converters, and to recent developments in design and implementation. PID control system implementation with anti-windup mechanisms and tuning of PID control systems have also been presented. A deep understanding of PID controller has been provided by Astrom and Hagglund [18]. Many implementation details, such as limitation of derivative gain, anti-windup, improvement of set point response, etc. have also been discussed.

1.2 RESEARCH OUTLINE

Even though physical prototypes have been built in large-scale, the development of small-scale units for implementation in cars is new and limited. The control system designed for these systems are proprietary to the corporations developing these products, limiting the application of the products to physical prototypes. Also as mentioned above, the majority of the research has been done in civil structures with rectilinear actuators. Different control algorithms have also been studied in the past to control the systems and state variables, each having their advantages and disadvantages. Having a control system design integrated with finite element modelling will help build a virtual tool which can be used as a directional/predictive tool to aid in vehicle product development and suppress vibrations in automotive structures. The purpose of this research is to firstly understand the downscaling of a CFG cancelation device to effectively use it for automotive application, and secondly to understand the efficiency of this tool to cancel a specific frequency of excitation for a given mass. The proposed research also dives deeply into the working principles and characteristics of the DC motors used in this system to drive the actuators used to generate the cancelation forces.

CHAPTER TWO

DC MOTORS EQUATION DERIVATION AND EFFICIENCIES

The primary function of a DC motor is to convert electrical energy into mechanical energy. In general, motors depend on magnetic fields to generate forces. To understand the working principle of a DC motor, the equations governing the calculation of the angular speed ω and the electrical current i with respect to time will be derived. A model for a simple, frictionless DC motor is developed, and then a more realistic DC motor with friction is derived to fundamentally understand the governing equations. Following this, a Simulink model is built to represent the final DC motor equations which will help simulate generation of ω for a given voltage and load and help determine the active cancelation force from the actuator.

2.1 EQUATIONS OF DC MOTOR

Figure 1 shows a circuit containing current, resistance, inductance, source voltage and back electro-magnetic force (EMF) voltage.

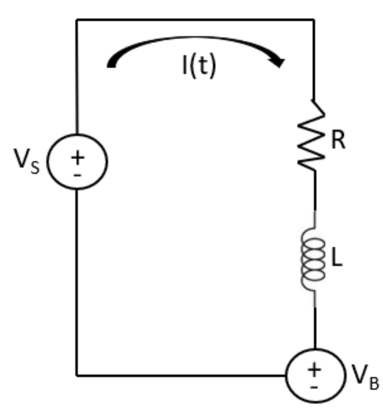

FIGURE 1 – Electrical Circuit

$$V_s = R * i(t) + L * \frac{d(i(t))}{dt} + V_B \tag{1}$$

V_s is source voltage, R is armature resistance, $i(t)$ is current at given time, L is armature inductance and V_B is the back EMF given by,

$$V_B = \omega * K_B \tag{2}$$

ω is rotation velocity of the shaft and K_B is back EMF constant.

$$T = J * \dot{\omega} \tag{3}$$

T is motor torque, J is moment of inertia and $\dot{\omega}$ is rotational acceleration

$$T = K_T * i(t) \tag{4}$$

K_T is motor torque constant

From Equations (3) and (4),

$$K_T * i(t) = J * \dot{\omega}(t) \tag{5}$$

From Equations (1) and (2),

$$V_s = R * i(t) + L * \frac{d(i(t))}{dt} + (K_B * \ \omega(t)) \tag{6}$$

From Equation (5),

$$\dot{\omega}(t) = \frac{K_T * i(t)}{J} \tag{7}$$

From Equation (6),

$$\frac{d(i(t))}{dx} = \frac{V_s - R * i(t) - (K_B * \omega(t))}{L} \tag{8}$$

Integrating Equations (7) and (8) with initial condition = 0 over time period,

$$\omega(t) = \omega(0) + \frac{K_T}{J} * \int\big(i(t)\big)\,dt$$

(9)

And

$$i(t) = i(0) + \frac{1}{L} * \int\{V_s - R * i(t) - (K_B * \ \omega(t))\}$$

(10)

$\omega(0) = 0$ and $i(0) = 0$

From Equation (10), ω varying with time has been calculated for a given current varying with time, source voltage, resistance, inductance and constant K_B.

However, the above set of equations represent a theoretical DC motor rather than a practical DC motor since it assumed to be frictionless. Next, the equations for a more realistic DC motor including friction are derived.

$$T - (B_f * \omega) = J * \dot{\omega}$$

(11)

where B_f is the rotational friction damping coefficient.

From Equations (4) and (11),

$$K_T * i(t) - (B_f * \omega) = J * \dot{\omega}(t)$$

(12)

Assuming for now $K_T = K_B = K$

Therefore Equations (6) and (12) can be written as

$$V_s = R * i(t) + L * \frac{d(i(t)}{dt} + (K * \ \omega(t))$$

(13)

$$K * i(t) - (B_f * \omega(t)) = J * \dot{\omega}(t)$$

(14)

Taking Laplace transform of Equations (13) and (14)

$$V_s - R * I(s) - L * s * I(s) - \big(K * \ s * \theta(s)\big) = 0$$

(15)

$$K * I(s) - \left(B_f * s * \theta(s)\right) = J * s^2 * \theta(s)$$

(16)

I(s) and $s * \theta(s)$ are Laplace transform of $i(t)\ and\ \omega(t)$ respectively and the initial conditions are considered to be zero.

From Equation (16),

$$I(s) = \frac{(s*\theta(s))*(J*s+B_f)}{K}$$

(17)

Substituting Equation (17) in Equation (15) and since $s * \theta(s) = \dot{\theta}(s)$,

$$V_s = \left\{\frac{(L*s+R)*\left(J*s+B_f\right)}{K} + K\right\} * \dot{\theta}(s)$$

(18)

which gives,

$$\frac{Vs}{\dot{\theta}(s)} = \left\{\frac{(L*s+R)*\left(J*s+B_f\right)}{K} + K\right\}$$

(19)

This can be rewritten as,

$$\frac{\dot{\theta}(s)}{V_s} = \left\{\frac{K}{(L*s+R)*\left(J*s+B_f\right)+K^2}\right\}$$

(20)

Assuming i and ω as state variables,

$$\dot{\theta} = K / J * i - {}^{B_f}\!/_{J} * \omega = \frac{d\omega}{dt}$$

(21)

And,

$$\frac{di}{dt} = {}^{V_s}\!/_{L} - {}^{R}\!/_{L} * i - {}^{K}\!/_{L} * \ \omega$$

(22)

This can be written in state space form as,

$$\frac{d}{dt}\begin{bmatrix}\omega \\ i\end{bmatrix} = \begin{bmatrix}-B_f/J & K/J \\ -K/L & -R/L\end{bmatrix} * \begin{Bmatrix}\omega \\ i\end{Bmatrix} + \begin{bmatrix}0 \\ 1/L\end{bmatrix} * V_s$$

(23)

This can now be represented in the Simulink model as shown in Figure 2.

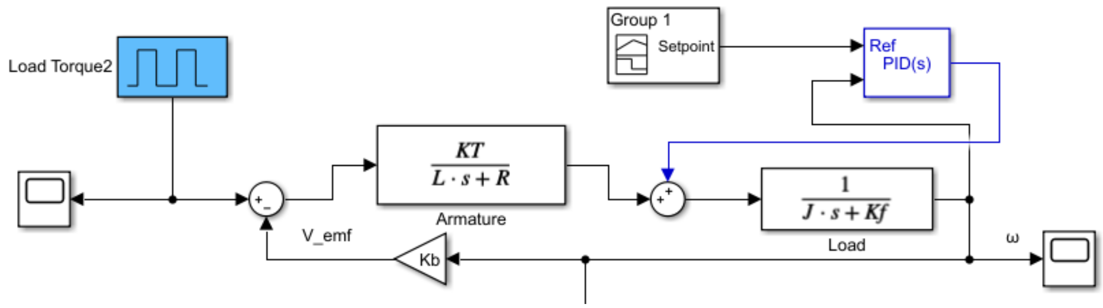

FIGURE 2 Simulink representation of the DC motor.

Here Kf represents the friction coefficient shown as "B_f" in above derived equations and K_b and KT denote the back EMF coefficient and motor torque coefficient respectively.

2.2 EFFICIENCIES AND TYPES OF DC MOTORS

The ratio of motor energy output to input defines the efficiency of a motor. There are several factors which can lead to losses of energy in the motor, hence reducing the overall efficiency of the motor [19]. Therefore, for a given current supplied with respect to time, the angular velocity varying with respect to time may not be achieved as shown by the equations above. There primarily two types of losses in a DC motor, electrical and mechanical. Therefore, the electrical and mechanical efficiencies can be computed using the equations below.

$$\eta_e = \frac{(converted\ power\ in\ armature)}{(input\ electrical\ power)} = \frac{TT*\omega}{V_s*I}$$

(24)

where η_e is defined as electrical efficiency. TT is total torque, ω is angular velocity, V_s is source voltage and I is armature current.

Similarly,

$$\eta_m = \frac{(converted\ power\ in\ armature)}{(output\ mechanical\ power)} = \frac{TT*\omega}{T*\omega} \tag{25}$$

where η_m is defined as the mechanical efficiency. TT is total torque, ω is angular velocity, and T is motor torque.

The overall efficiency of the motor can then be written as

$$\eta = \frac{(output\ mechanical\ power)}{(input\ electrical\ power)} = \frac{(input\ power - total\ losses)}{(input\ electrical\ power)} = \frac{P_i - (P_a + P_f + P_k)}{P_i} = \frac{V_s * I - (I - I_{sh})^2 * R_a - P_k}{V_s * I} \tag{26}$$

where $P_i, P_a, P_f\ and\ P_k$ are defined as the input power, the armature copper loss power, the field copper loss power and the core and mechanical loss power, respectively. I_{sh} is the shunt current and R_a is the armature resistance. FIGURE 3 below shows a schematic diagram of losses that occur in a DC motor.

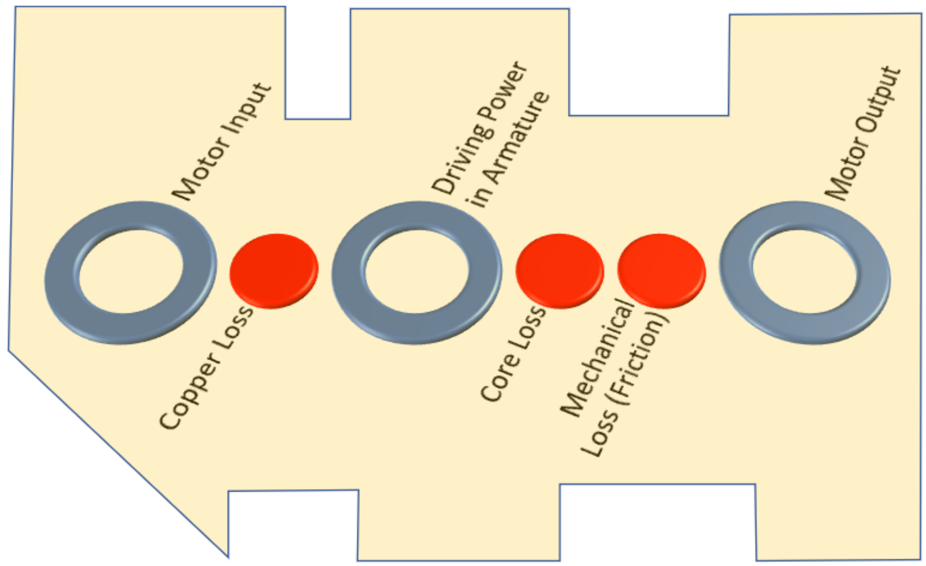

FIGURE 3 with loss stages in a DC motor.

In this research the efficiency of a DC motor has not been included in the final Simulink tool but can be explored in the future to further improve on the accuracy of the tool's prediction of cancelation forces for a given system.

There are primarily three types of DC motors, brushed DC motor, brushless DC motor and coreless or ironless DC motor.

2.2.1 BRUSHED DC MOTOR

These motors primarily consist of brushes with a DC source, commutators, windings, and armature. Figure 4 below shows a diagram of a brushed DC motor. The commutators are used to connect a stationary circuit with a rotating circuit. The rotor windings are energized using the conductive brushes [20,23]. These can be categorized into three variants, 1) separately excited DC motors, 2) self-excited DC motors and 3) permanent magnet DC motors. As the name suggests, separately excited DC motors have different power supplies for the field windings and the armature windings and hence are energized separately. In a self-excited DC motor, the field windings are electrically connected with the armature windings and are energized by a single power supply. They can be connected in one of the following three ways: 1) series connection which has the armature windings and field windings connected in series therefore having same current flow through both, 2) shunt connection which have the armature windings and the field windings connected in parallel with each other, resulting in full source voltage across the field windings and the current is divided into a field current and an armature current, and 3) compound connection which uses features of both series and shunt wound DC motors. Compound connections can be divided into two groups, 1) cumulative compound, in which the series and shunt fields generate flux in same direction, the shunt field's flux helps increase the series field's flux and the total flux is always greater than the original flux, and 2) differentially compound, in which the series and shunt fields generate flux in opposite directions and the total flux is always less than the original flux. In certain types of differential compound DC motors, if the field windings are in parallel to the armature windings and in series to the field winding then it is called a short shunt DC motor and if it is in parallel to both then it is called a long shunt DC motor. Finally, the permanent magnet DC motor does not have a stator (field windings) and the magnetic field is generated using a permanent magnet [23]. The armature windings are placed inside the permanent magnet which generates a rotating force in the armature. Since no additional power supply is needed for field flux generation, these motors are compact and cheap to manufacture and can be used for low power generation.

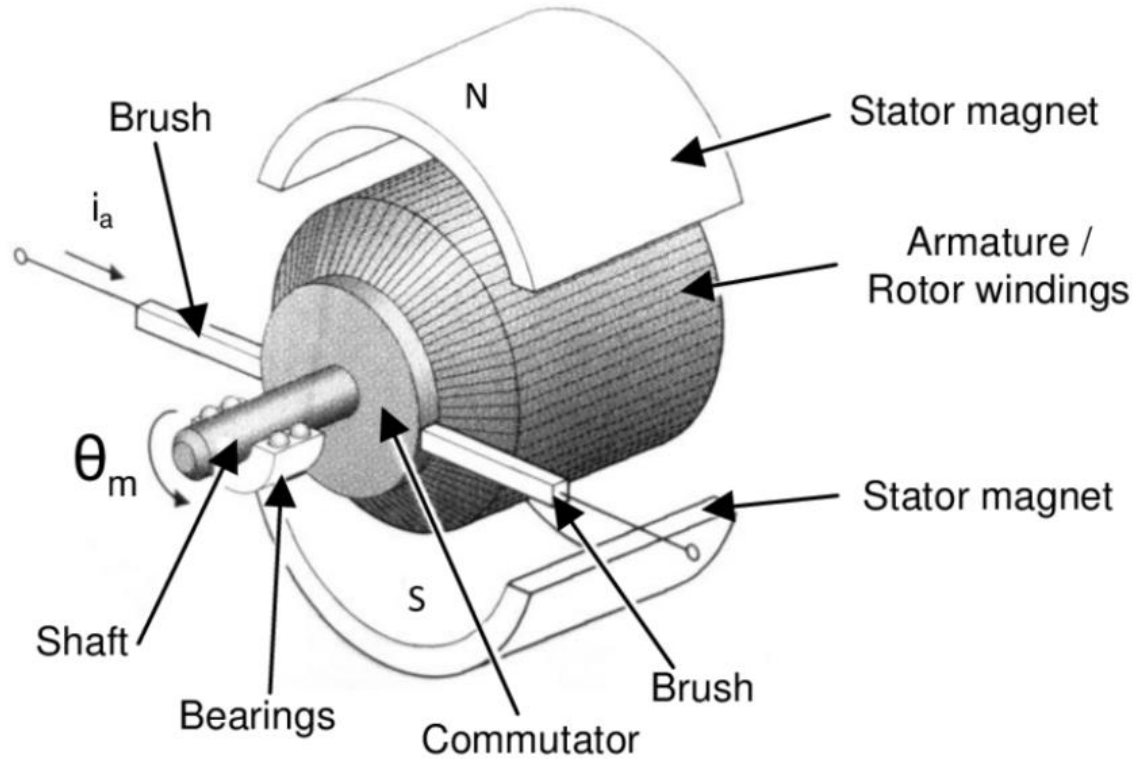

FIGURE 4 – Brushed DC Motor [21]

2.2.2 BRUSHLESS DC MOTOR

Figure 5 below shows a diagram of a brushless DC motor, which does not contain any brushes or commutators. The stator, made up of multiple windings, is supplied with power and the rotor is a permanent magnet [20,21,22]. The stator windings are situated at different angles which produce flux in different directions. The input is switched between the stator windings which generate a magnetic field that in turn influences the rotor magnetic field. Switching devices such as thyristors are used for electronic commutation. These types of motors are highly efficient and have a longer life span than brushed DC motors.

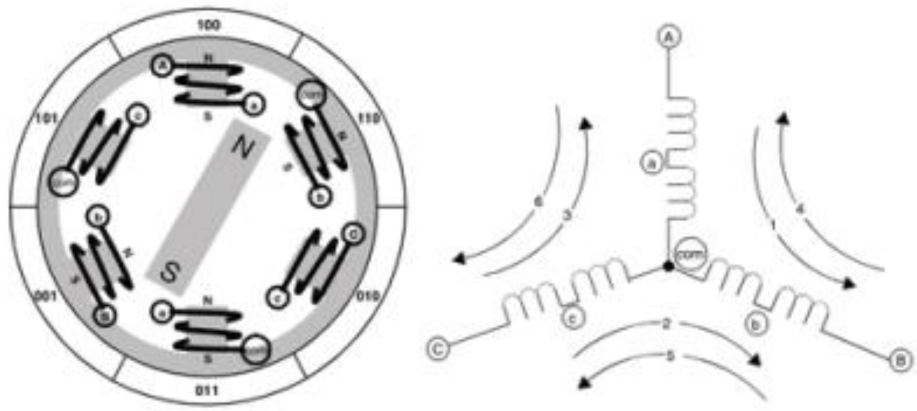

FIGURE 5 – Brushless DC Motor [19]

2.2.3 CORELESS OR IRONLESS DC MOTOR

These types of DC motors do not have a laminated iron core. The windings are skewed to form hollow cages in which the rotor, made of a permanent magnet, sits [21]. This eliminates many issues concerning traditional motors due to the absence of iron core, such as minimizing hysteresis losses, and increases the efficiency of the motor. The absence of an iron core also helps reduce the mass inertia of the motor which thereby increases the acceleration and deceleration rate of the motor.

There are also several types of AC motors in existence. This research does not consider AC motors and for the research a self-excited DC motor has been used. Other DC motors can be explored to improve efficiency and minimize losses in the future.

CHAPTER THREE

CONTROL SYSTEM, STABILITY AND CFG WORKING PRINCIPLE

The heart of this research lies in using the mass imbalance principle to generate centrifugal forces used for generating the cancellation forces. The challenge is to understand and calculate the magnitude and phase of the force being generated to accurately reduce the excitation forces coming into the system. One of the key factors is also to determine and minimize the time taken to control the angular velocity of the DC motor output shaft to generate the cancellation force. To understand this, a review of control theory is required.

3.1 SYSTEM STABILITY

There are few ways of measuring the stability of a system. For a homogenous linear system with constant coefficients, a phase portrait [25] approach can be used to determine the critical points of the system and understand its stability. To create a phase portrait, the trajectories of a system are plotted on a phase plane, demonstrated below using an example of a homogenous system [25].

Assuming a homogenous system given by

$$y' = Ay = \begin{bmatrix} -3 & 1 \\ 1 & -3 \end{bmatrix} * y, = \begin{matrix} y_1' = -3y_1 + y_2 \\ y_2' = y_1 - 3y_2 \end{matrix} \tag{27}$$

The characteristic equation can be defined as

$$\det(A - \lambda I) = \begin{vmatrix} -3 - \lambda & 1 \\ 1 & -3 - \lambda \end{vmatrix} = \lambda^2 + 6\lambda + 8 = 0 \tag{28}$$

From Equation (28)

$\lambda_1 = -2 \; and \; \lambda_2 = -4$ which are the eigenvalues of the system. Eigen vectors are obtained from $(-3-\lambda)x_1 + x_2 = 0$.

For $\lambda_1 = -2$ this is $-x_1 + x_2 = 0$ which gives $x^{(1)} = [1 \quad 1]^T$. For $\lambda_2 = -4$ this is $x_1 + x_2 = 0$, and the eigenvector is $x^{(2)} = [1 \quad -1]^T$. The general solution can be then written as

$$y = \begin{bmatrix} y_1 \\ y^2 \end{bmatrix} = c_1 y^{(1)} + c_2 y^{(2)} = c_1 \begin{bmatrix} 1 \\ 1 \end{bmatrix} e^{-2t} + c_2 \begin{bmatrix} 1 \\ -1 \end{bmatrix} e^{-4t} \tag{29}$$

Prior to understanding the stability of the system, critical points need to be defined. To define this, a generalized system with constant coefficients consisting of 2 ODEs must be observed.

$$y' = Ay = \begin{matrix} y_1' = a_{11}y_1 + a_{12}y_2 \\ y_2' = a_{21}y_1 + a_{22}y_2 \end{matrix} \tag{30}$$

Which gives,

$$\frac{dy_2}{dy_1} = \frac{y_2' dt}{y_1' dt} = \frac{y_2'}{y_1'} = \frac{a_{21}y_1 + a_{22}y_2}{a_{11}y_1 + a_{12}y_2} \tag{31}$$

For this, there is a unique tangent direction $\frac{dy_2}{dy_1}$ of trajectory passing through P for every point P:(y_1, y_2) except at P:(0,0) for which the RHS for Equation (31) becomes 0/0 which is undetermined. Such points are called critical points. There are 5 types of critical points, improper nodes, proper nodes, saddle points, spirals and centers. Figures 6A-6E shows all the types of critical points.

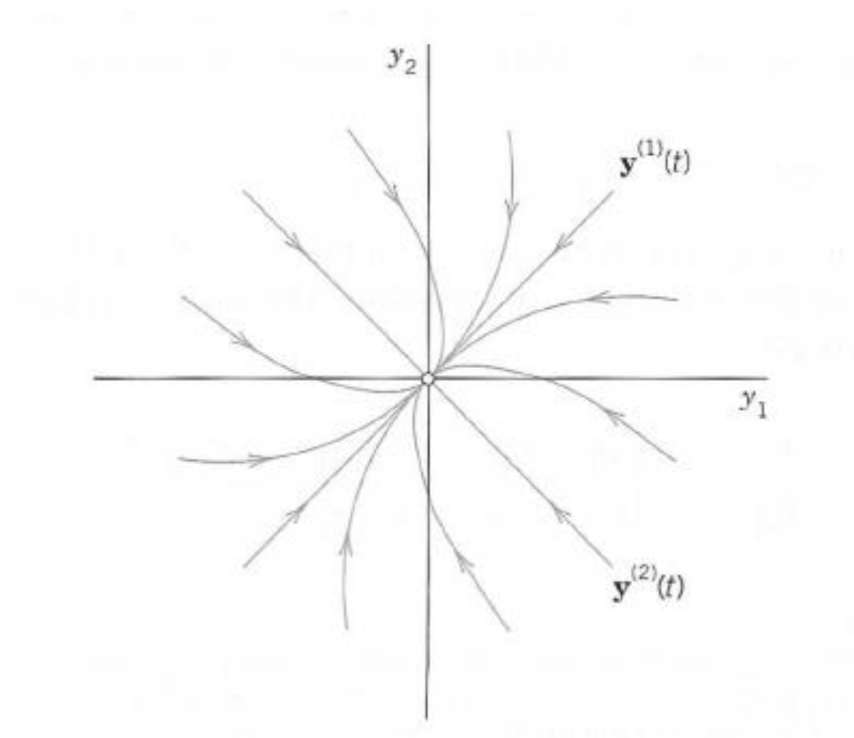

FIGURE 6A – Improper Node [25]

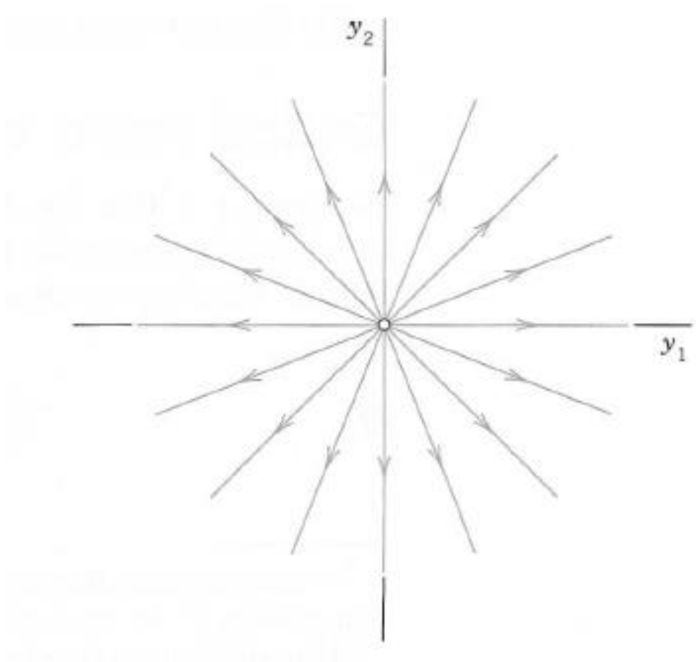

FIGURE 6B – Proper Node [25]

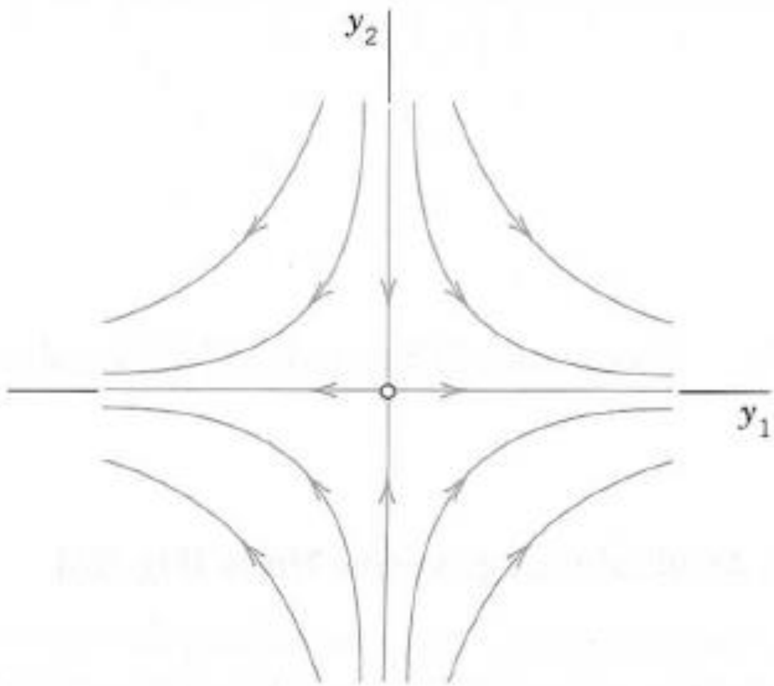

FIGURE 6C – Saddle Point [25]

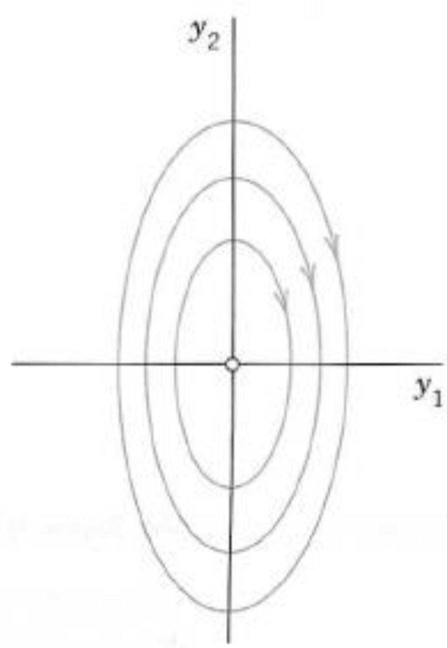

FIGURE 6D – Center [25]

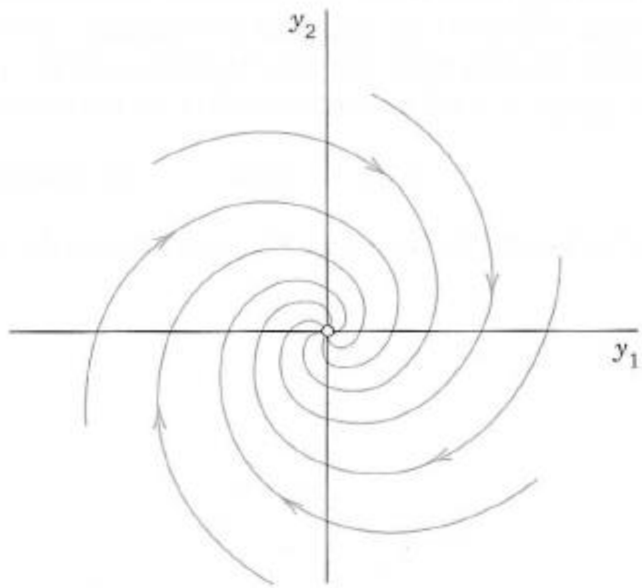

FIGURE 6E – Spiral [25]

For Equation (30), a generalized quadratic equation can be determined to calculate eigenvalue criteria given by,

$$\lambda^2 + p\lambda + q = 0 \text{ with coefficients p, q and discriminant } \Delta \tag{32}$$

Where

$$p = a_{11} + a_{22}, q = \det A = a_{11}a_{22} - a_{12}a_{21} \; and \; \Delta = p^2 - 4q \tag{33}$$

From Equation (32) and (33),

$$\lambda^2 + p\lambda + q = (\lambda - \lambda_1)(\lambda - \lambda_2) = \lambda^2 - (\lambda_1 + \lambda_2)\lambda + \lambda_1\lambda_2 \tag{34}$$

Which gives,

$$p = \lambda_1 + \lambda_2; q = \lambda_1\lambda_2 \; and \; \Delta = (\lambda_1 - \lambda_2)^2 \tag{35}$$

Figure 7 can be used to determine the stability of the system based on where the critical points lie in this phase plane.

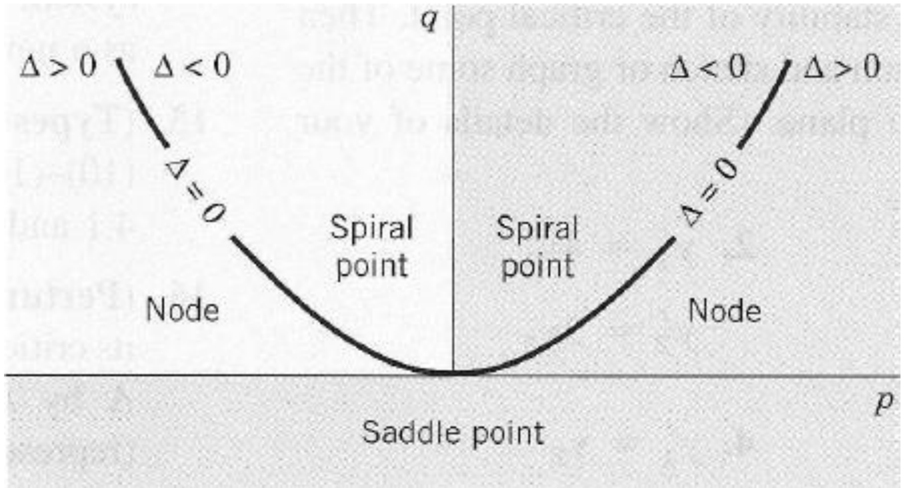

FIGURE 7 – Phase Plane [25]

Other ways to observe the stability of a system can be classified into two techniques. Firstly, Bounded Input Bounded Output (BIBO) [27,28] stability which for zero-state response and internal stability is introduced for zero-input response. A system is said to be BIBO stable (bounded-input bounded output stable) if every bounded input excites a bounded output. This stability is applicable only if the system is initially at rest. A system with a proper rational transfer matrix $\hat{G}(s) = [\hat{g}_{ij}(s)]$ is BIBO stable, if and only if every pole of every $\hat{g}_{ij}(s)$ has a negative real part where, for a given state space system,

$$\dot{x}(t) = Ax(t) + Bu(t) \; and \; y(t) = Cx(t) = Du(t) \tag{36}$$

The transfer function is defined by,

$$\hat{G}(s) = \mathrm{C}(sI - A)^{-1}B + D$$

(37)

To define the internal stability, the system is said to be stable in the sense of Lyapunov[29,30], or simply stable, if every finite initial state $x(0)$ excites a bounded response $x(t) = e^{At}x(0)$. The system is said to be asymptotically stable (in fact, exponentially stable), if in addition, $x(t) = e^{At}\, x(0) \longrightarrow 0\; as\; t \longrightarrow \infty$ $(x(t) = e^{At}\, x(0) \longrightarrow 0\; exponentially\; as\; t \longrightarrow \infty)$ which means the eigenvalues of the characteristic equation, A have zero or negative real parts and they are asymptotically stable if the eigenvalues of A have negative real parts.

3.1.1 SYSTEM CONTROLLABILITY

It is important to ensure observability and controllability of a system prior to controlling it. In this section the fundamentals behind the controllability and observability of a system are reviewed. These concepts help determine if a system defined in state space form is controllable for a given input and if the initial state can be observed from the output. Consider the continuous time multi input/multi output (MIMO) linear time invariant (LTI) system[31,32] described by

$$\dot{x}(t) = Ax(t) + Bu(t),\; x(0) = x_0 \tag{38}$$

$$y(t) = Cx + Du(t) \tag{39}$$

Which has solution,

$$x(t) = \phi_A(t, t_0)x(t_0) + \int_{t_0}^{t} \phi_A(t, \tau)Bu(\tau)d\tau = e^{(t-t_0)A}x(t_0) + \int_{t_0}^{t} e^{(t-\tau)A}Bu(\tau)d\tau \tag{40}$$

$\phi_A(t, t_0)x(t_0) + \int_{t_0}^{t} \phi_A(t, \tau)Bu(\tau)d\tau$ is called general form and $e^{(t-t_0)A}x(t_0) + \int_{t_0}^{t} e^{(t-\tau)A}Bu(\tau)d\tau$ is called LTI (Linear Time Invariant) form.

The state space Equation (38) is said to be controllable if for initial state $x(0) = x_0$ and any final state x_1, there exists an input that transfers x_0 to x_1 in a finite time. Otherwise it is uncontrollable. Controllability can also be defined if the n x n symmetric matrix given by

$$W_c(t) = \int_0^t e^{A\tau}(B)(B)^T e^{A^T\tau} d\tau = \int_0^t e^{A(t-\tau)}(B)(B)^T e^{A^T(t-\tau)} d\tau \tag{41}$$

is nonsingular(invertible) for all $t > 0$, i.e., $W_c^{-1}(t)$ exists. $W_c(t)$ is called the controllability Gramian matrix [33], which is positive definite.

For simplicity, the controllability of a system can also be determined using MATLAB. A system is controllable if and only if,

Rank $[C_{AB}] = n$,

Where,

$C_{AB} = [B\ AB\ A^2B\ ...\ A^{n-1}B]$ is the n x np constant controllability matrix associated with the pair [A,B]. C_{AB} can be computed using the MATLAB function “CTRB”.

3.1.2 SYSTEM OBSERVABILITY

Considering the continuous time multi input/multi output (MIMO) linear time invariant (LTI) system [31,32] described by Equations (38) and (39), the state space is said to be observable if for any initial state x(0), there exists finite $t_1 > 0$ such that the knowledge of the input u and output y over [0, t_1] suffices to determine uniquely the initial state x(0). Otherwise, it is said to be unobservable. Observability can be defined in terms of the Observability Gramian matrix $W_O(t)$ which is positive definite. The system is said to be observable if and only if the n x n symmetric matrix given by

$$W_O(t) = \int_0^t e^{A^T\tau} C^T C e^{A\tau} d\tau$$

(42)

is nonsingular (invertible) for all $t > 0$, i.e., $W_O^{-1}(t)$ exists.

For simplicity the observability of a system using MATLAB can also be determined. A system is observable if and only if,

Rank $[O_{AC}] = n$,

Where,

$O_{AC} = [C^T \; A^T C^T \; (A^T)^2 C^T \; \ldots \; (A^T)^{n-1} C^T]^T$ is the n x np constant controllability matrix associated with the pair [A,C]. O_{AC} can be computed using the MATLAB function "OBSV".

A system might be unstable but still controllable and observable which means that an unstable system can be controlled using suitable feedback control and the unknown initial condition x(0) can be determined from the known input u(t) and known output y(t).

3.1.3 CFG WORKING PRINCIPLE

In this section, the fundamental principle on which the proposed force cancellation is based is discussed. To begin, define the mass imbalance and dynamic behavior of a system under the influence of the mass imbalance.

In Figure 8, a single degree of freedom (SDOF) system can be seen. The system consists of a lumped mass m, spring stiffness k and damper c. Force f is applied to the right-hand side of the system, the equation of motion can be defined, and the acceleration, velocity and displacement can be computed as following,

$$m\ddot{x}(t) + c\dot{x}(t) + kx(t) = f(t)$$

(43)

Which gives,

$\ddot{x}(t) = (f(t) - c\dot{x}(t) - kx(t))/m$

(44)

Where $\ddot{x}(t)$ is the acceleration, $\dot{x}(t)$ is the velocity and $x(t)$ is the displacement of the lumped mass under forced excitation $f(t)$.

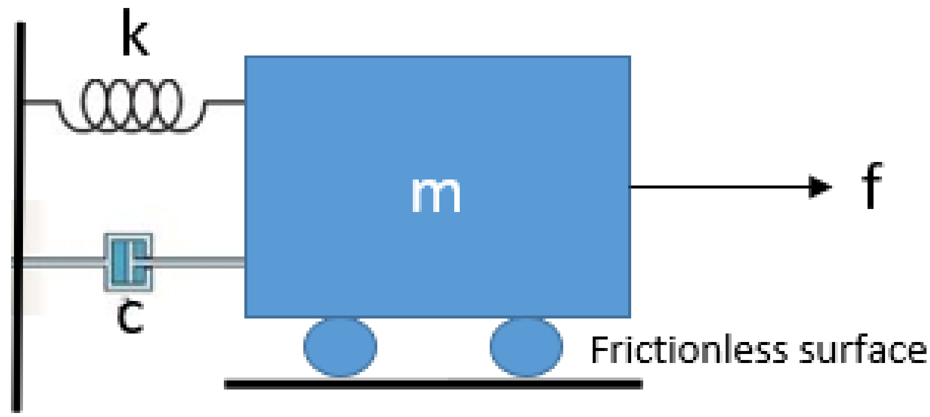

FIGURE 8 – Lumper mass system SDOF

An imbalanced mass m_2 is introduced and the lumped mass as m_1 is assumed to be located at a distance e, which is termed as eccentricity. Figure 9 illustrates the system.

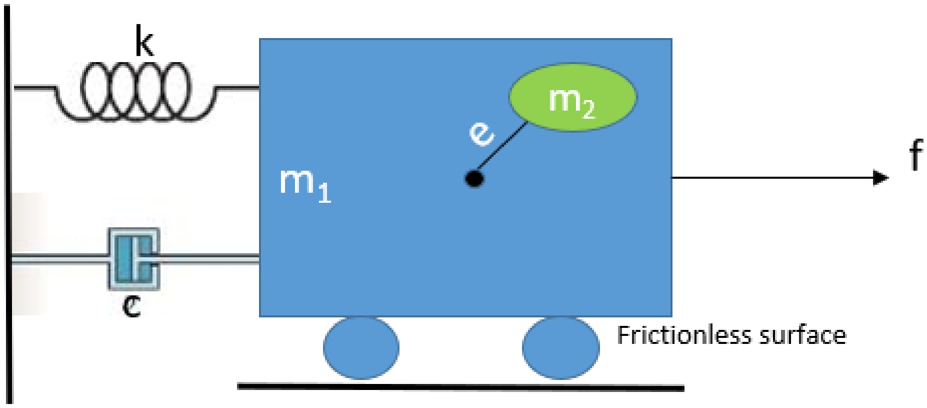

FIGURE 9 – SDOF System with imbalance mass m_2

Figure 10 shows the free body diagram of the system. From this system the equation of motion can be derived as the following,

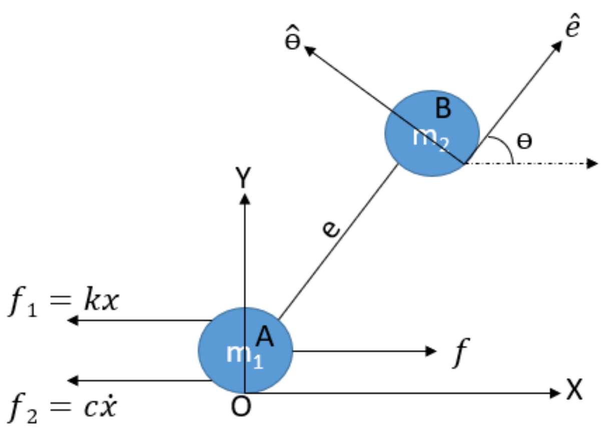

FIGURE 10 – Free Body Diagram resolved in X Direction

$$\sum F = m_2 * \overrightarrow{a_{B/O}} = m_2 * \overrightarrow{a_{A/O}} + m_2 * \overrightarrow{a_{B/A}}$$

(45)

$$=> \ m_2\ddot{x} + m_2[(\ddot{e} - e\dot{\theta}^2)\hat{e} + (e\ddot{\theta} + 2\dot{e}\dot{\theta})\hat{\theta}]$$

(46)

where $\dot{e} = \ddot{e} = 0$ since the arm length does not change over time and $\ddot{\theta} = \omega$ which is a constant.

$$=> \ m_2\ddot{x}\hat{\imath} - m_2e\dot{\theta}^2\hat{e} => \ \hat{e} = Cos\omega t\ \hat{\imath} + Sin\omega t\ \hat{\jmath}$$

(47)

$$=> \ m_2\ddot{x}\hat{\imath} - m_2e\omega^2(Cos\omega t\ \hat{\imath} + Sin\omega t\ \hat{\jmath} + m_2g\ \hat{\jmath}$$

(48)

Resolving into X and Y components,

$$\sum F_{m_{2_x}} = \ m_2\ddot{x} - \ m_2e\omega^2Cos\omega t = \ \sum F_{m_{1_x}}$$

(49)

$$\sum F_{m_{2_y}} = \ -m_2e\omega^2Sin\omega t + m_2g$$

(50)

Since we are interested only in the X direction this thesis, this can further reduced to

$$\sum F_{m_{1_x}} = \ m_1\ddot{x} = \ -\sum F_{m_{2_x}} = -m_2\ddot{x} + \ m_2e\omega^2Cos\omega t$$

(51)

Which gives,

$$(m_1 + m_2)\ddot{x} = \ m_2e\omega^2Cos\omega t$$

(52)

Considering the forces due to the damper and spring from Figure 10, Equation (51) can be rewritten as

$$(m_1 + m_2)\ddot{x} = \ m_2e\omega^2Cos\omega t - kx - c\dot{x}$$

(53)

Note, $m_2e\omega^2Cos\omega t$ is the centrifugal force whose direction depends on the rotational direction of the imbalanced mass. In this thesis, it is used to provide counter force to the external force to reduce acceleration, velocity and displacement of the system.

CHAPTER FOUR

VIRTUAL MODEL DEVELOPMENT AND FORCE CANCELLATION SDOF SYSTEM

4.1 SDOF SYSTEM MODEL IN SIMULINK

In this section the single degree of freedom system is defined in a virtual Simulink model and its behavior under external force excitation is discussed. Force cancelation using the force actuator and the accelerations, velocities and displacements of an ideal system (no losses) are also illustrated. The equations and findings from the previous sections are used to define a virtual Simulink model consisting of a SDOF system with external force excitation and a DC motor with a PID controller to feed into a force actuator are used to cancel the external force in real time. Figure 11 shows a single degree of freedom representation in Simulink. Figure 11 shows, for a unit force excitation, the output displacement, velocity, and acceleration for the single degree of freedom system. To cancel this force excitation, an equal and opposite force is introduced into the system. Figure 12 shows the calculation of an equal and opposite force based on the output response from the single degree of freedom system, which is then fed back into the system to cancel the initial force. This is the most simplistic representation of force cancellation in theory. To this model a detailed DC motor representation has been added, illustrated by Figure 13. A PID controller has also been added to the DC motor to control the rotation of the shaft for a given load and voltage.

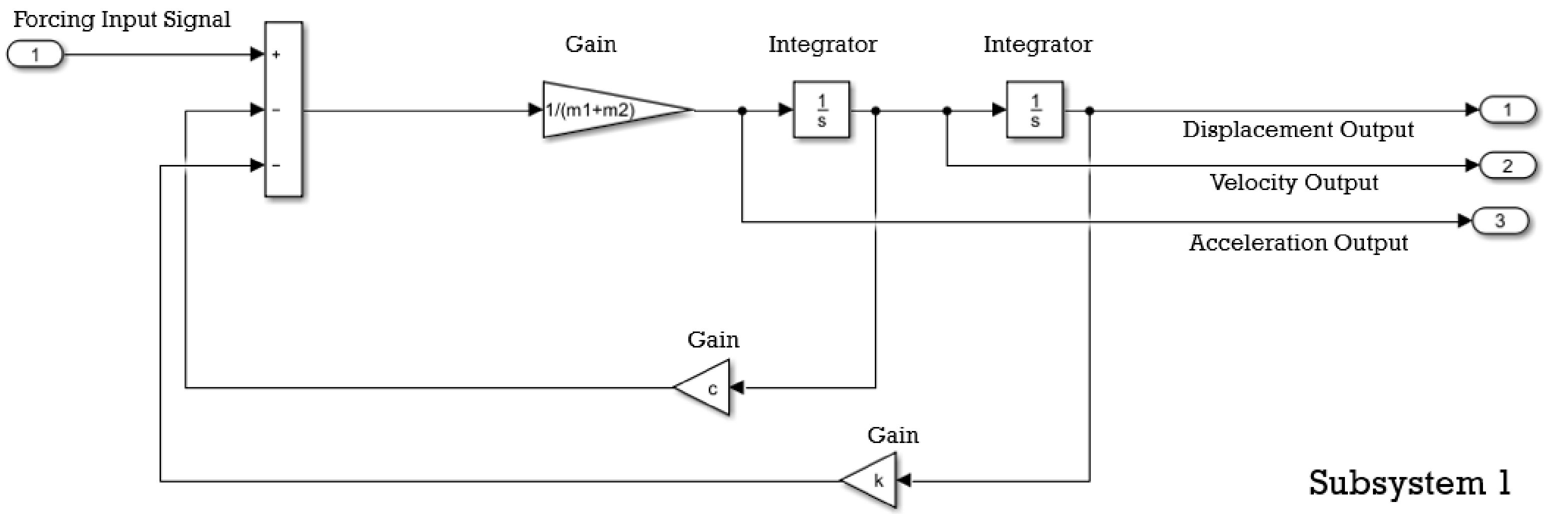

FIGURE 11 – SDOF Representation in Simulink

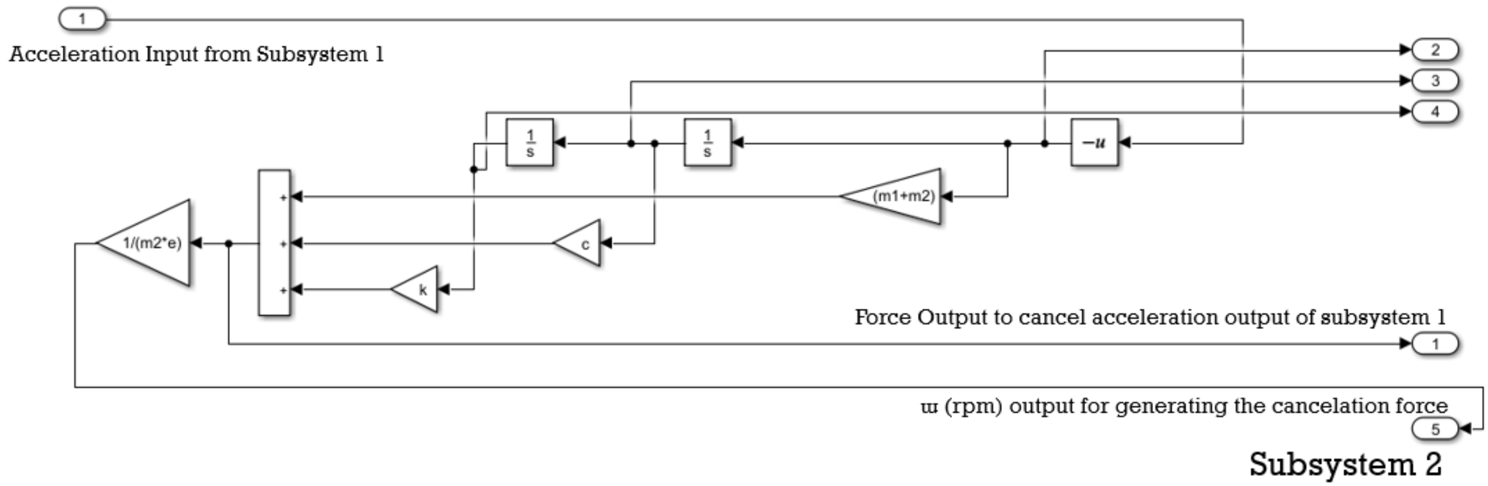

FIGURE 12 – Cancellation Force Representation in Simulink for SDOF System

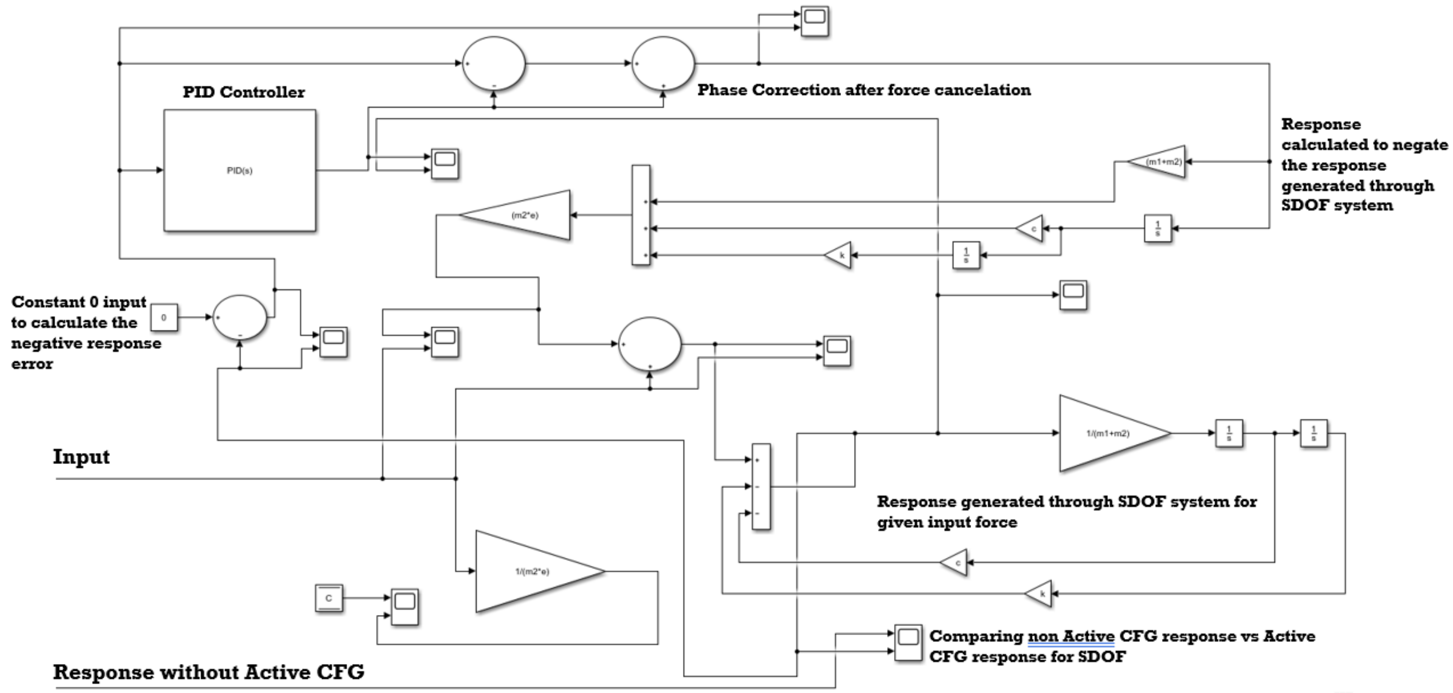

FIGURE 13 – Manual Force Cancellation using DC Motor to calculate

4.2 STATE SPACE MODEL

In this section the fundamentals of state space have been discussed and how the various mechanical systems illustrated in this research has been modelled in state space format using MATLAB, Nastran and Simulink. State Space is a form of representation of a system in terms of input and output states. In general, states are represented in the form of A, B, C and D matrices. The size of the matrices are determined by the number of inputs and outputs and the number of states of the system [35]. The following block diagram can help understand the size requirements of a state space system.

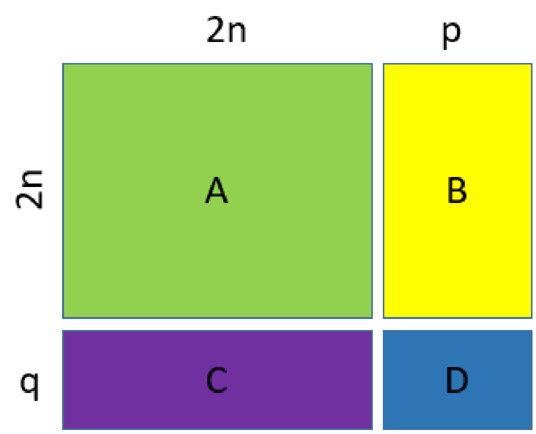

FIGURE 14 – State Space Dimensions Block Diagram

From Figure 14, it can be inferred that matrix A is of the dimension 2n x 2n, B is 2n x p, C is q x 2n and D is q x p. Here p is the number of inputs to the system, q is the number of outputs of the system and 2n represents the number of states of the system. For a simple mass spring damper system excited by only an external force represented by

Equation (43), it can be expressed in matrix format as the following (using G notation for damping to avoid confusion with C output matrix),

$$M\ddot{x} + G\dot{x} + Kx = F \tag{54}$$

Which gives,

$$\ddot{x} = -M^{-1}G\dot{x} - M^{-1}Kx + M^{-1}F \tag{55}$$

Therefore,

$$A = \begin{bmatrix} 0 & I \\ -M^{-1}K & -M^{-1}G \end{bmatrix};\ B = \begin{bmatrix} 0 \\ M^{-1} \end{bmatrix};\ C = \begin{bmatrix} I & 0 \\ 0 & I \\ -M^{-1}K & -M^{-1}G \\ 0 & 0 \end{bmatrix};\ D = \begin{bmatrix} 0 \\ 0 \\ M^{-1} \\ I \end{bmatrix}; \tag{56}$$

Here, the number of inputs is 1 and there are 4 outputs. This can be referred as state space realization of the transfer function of the system.

The following equation is the general representation of the transfer function,

$$Y(s) = G(s)U(s)\ where, G(s) = \frac{b_1 s^{n-1} + b_2 s^{n-2} + \cdots + b_n s}{s^n + a_1 s^{n-1} + \cdots + a_{n-1}s + a_n} \tag{57}$$

4.2.1 CONTROLLABLE CANONICAL FORM

Based on Equation (57), a state space representation of a system has been defined as following,

$$\dot{x}_c = A_c x_c + B_c u\ ; y = C_c x_c + D_c u \tag{58}$$

Here $\dot{x}$ is a 4x1 matrix, A is 4x4 matrix, x is 4x1 matrix, B is 4x1 matrix, u is 1x1 matrix, y is 1x1 matrix, C is 1x4 and D = 0. The controllable canonical form realization of the state space system can be defined using Equation (57) as,

$$x_c = \begin{bmatrix} x_{1c} \\ x_{2c} \\ x_{3c} \\ x_{4c} \end{bmatrix}, A_c = \begin{bmatrix} -a_1 - a_2 - a_3 - a_4 \\ 1 \quad 0 \quad 0 \quad 0 \\ 0 \quad 1 \quad 0 \quad 0 \\ 0 \quad 0 \quad 1 \quad 0 \end{bmatrix}, B_c = \begin{bmatrix} 1 \\ 0 \\ 0 \\ 0 \end{bmatrix}, C_c = [b_1 b_2 b_3 b_4] \ and \ D_c = 0$$

(59)

4.2.2 OBSERVABLE CANONICAL FORM

Based on Equation (57), assuming a state space representation of a system as following,

$$\dot{x}_o = A_o x_o + B_o u \, ; y = C_o x_o + D_o u$$

(60)

Here $\dot{x}$ is a 4x1 matrix, A is 4x4 matrix, x is 4x1 matrix, B is 4x1 matrix, u is 1x1 matrix, y is 1x1 matrix, C is 1x4 and D = 0. The observable canonical form realization of the state space system can be defined using Equation (57) as,

$$x_o = \begin{bmatrix} x_{1o} \\ x_{2o} \\ x_{3o} \\ x_{4o} \end{bmatrix}, A_o = \begin{bmatrix} -a_1 & 1 & 0 & 0 \\ -a_2 & 0 & 1 & 0 \\ -a_3 & 0 & 0 & 1 \\ -a_4 & 0 & 0 & 1 \end{bmatrix}, B_o = \begin{bmatrix} b_1 \\ b_2 \\ b_3 \\ b_4 \end{bmatrix}, C_o = [1\ 0\ 0\ 0] \ and \ D_o = 0$$

(61)

The controllable and observable canonical forms are helpful in determining a state space form if the system has been represented in a transfer function form. At that point, the controllability and observability of a system can be checked. This representation is particularly useful in order to perform calculations in a more efficient and faster manner.

4.3 ANALYTICAL SOLUTION FOR SDOF SYSTEM

In this section, the solution to a SDOF system has been described. As a first step, the SDOF system shown in Figure 8 has been solved. The solution has then been verified using MATLAB and Simulink to show the state space system used in Simulink is correct and can be used for more complicated systems. Following that, the system shown in

Figure 9 with an unbalanced mass has also been illustrated. The objective of this section is to show that solving the system with higher degrees of freedom analytically increases the complexity of the solution and therefore using Simulink is necessary for further progress into the virtual tool development for force cancellation of SDOF systems with mass imbalances. This example is followed by a simple beam example and a finite element model of a truck frame.

As shown by Katsuhiko Ogata [36], the following differential equations can be derived for the SDOF system shown in Figure 8,

$$\ddot{y} + \frac{c}{m}\dot{y} + \frac{k}{m}y = \frac{c}{m}\dot{u} + \frac{k}{m}u \tag{62}$$

Referencing Equation 57, the following standard form can be shown,

$$\ddot{y} + a_1\dot{y} + a_2 y = b_1\dot{u} + b_2 u \tag{63}$$

Therefore,

$$a_1 = \frac{c}{m}, \qquad a_2 = \frac{k}{m}, \qquad b_1 = \frac{c}{m}, \qquad b_2 = \frac{k}{m}$$

As shown in [31],

$$\beta_1 = b_1 - a_1\beta_0 = \frac{c}{m}$$

$$\beta_2 = b_2 - a_1\beta_1 - a_2\beta_2 = \frac{k}{m} - (\frac{c}{m})^2 \tag{64}$$

$$x_1 = y - \beta_0 u = y$$

$$x_2 = \dot{x_1} - \beta_1 u = \dot{x_1} - \frac{c}{m}u \tag{65}$$

$$\dot{x}_1 = x_2 + \beta_1 u = x_2 + \frac{c}{m}u$$

$$\dot{x}_2 = -a_2x_1 - a_1x_2 + \beta_2 u = -\frac{k}{m}x_1 - \frac{c}{m}x_2 + \left[\frac{k}{m} - \left(\frac{c}{m}\right)^2\right]u$$

(66)

The output equation is given in state space for as,

$$\begin{bmatrix} \dot{x}_1 \\ \dot{x}_2 \end{bmatrix} = \begin{bmatrix} 0 & 1 \\ -\frac{k}{m} & -\frac{c}{m} \end{bmatrix} \begin{bmatrix} x_1 \\ x_2 \end{bmatrix} + \begin{bmatrix} \frac{c}{m} \\ \frac{k}{m} - \left(\frac{c}{m}\right)^2 \end{bmatrix} u$$

And,

$$y = [1 \quad 0] \begin{bmatrix} x_1 \\ x_2 \end{bmatrix}$$

(67)

From Equations 36 and 37,

$$A = \begin{bmatrix} 0 & 1 \\ -\frac{k}{m} & -\frac{c}{m} \end{bmatrix}, B = \begin{bmatrix} \frac{c}{m} \\ \frac{k}{m} - \left(\frac{c}{m}\right)^2 \end{bmatrix}, C = [1 \quad 0] \; and \; D = 0$$

(68)

Assuming the following parameters,

$m = 200\ Kgs, k = \frac{1000N}{mm}, c = 3.8\frac{Ns}{mm}, u = 20000Sin(2\pi ft)$

$where\ f = 10\ Hz.$

$$\dot{X}(t) = \begin{bmatrix} 0 & 1 \\ -\frac{1000}{200} & -\frac{3.8}{200} \end{bmatrix} X(t) + \begin{bmatrix} \frac{3.8}{200} \\ \frac{1000}{200} - \left(\frac{3.8}{200}\right)^2 \end{bmatrix} * 20000Sin(20\pi t)$$

Taking the Laplace transform of the state equation,

$$sX(s) - X(0) = AX(s) + BU(s)$$

$$sX(s) - X(0) = \begin{bmatrix} 0 & 1 \\ -\frac{1000}{200} & -\frac{3.8}{200} \end{bmatrix} X(s) + \begin{bmatrix} \frac{3.8}{200} \\ \frac{1000}{200} - \left(\frac{3.8}{200}\right)^2 \end{bmatrix} * \frac{20000 * 2\pi * 10}{s^2 + (2\pi * 10)^2}$$

$$(sI - A)X(s) = X(0) + BU(s)$$

(69)

$$Y(t) = [1 \quad 0]\, X(t) + 0$$

Taking the Laplace transform of the state equation,

$$Y(s) = [1 \quad 0]\, X(s) + 0 \tag{70}$$

Substituting into the output equation, $U(s)\ and\ X(s)$,

$$Y(s) = [1 \quad 0] \left((sI - A)^{-1} \begin{bmatrix} \frac{3.8}{200} \\ \frac{1000}{200} - \left(\frac{3.8}{200}\right)^2 \end{bmatrix} * \frac{20000 * 2\pi * 10}{s^2 + (2\pi * 10)^2} \right) + 0 \tag{71}$$

In this example, MATLAB has been used to do the arithmetic calculation and the result has been compared with output from Simulink.

Following is the MATLAB code for the arithmetic calculation setup,

```
syms s t m k c f

% Given parameters
m_val = 200;
k_val = 1000;
c_val = 3.8;
f_val = 10;

% State-space matrices
A = [0 1; -k/m -c/m];
B = [c/m; ((k/(m) - ((c/m))^2))];
C = [1 0];
D = 0;

% Substitute values
A = subs(A, [m, k, c], [m_val, k_val, c_val]);
B = subs(B, [m, k, c], [m_val, k_val, c_val]);
C = subs(C, [m, k, c], [m_val, k_val, c_val]);

% Input force Laplace transform
U_s = laplace(20000*sin(2*pi*10*t), t, s);

% State and output Laplace transforms
X_s = inv(s * eye(size(A)) - A) * B * U_s;
Y_s = C * X_s + D * U_s;
t = 0:0.2:2;
```

```
% Inverse Laplace transform
y_t = ilaplace(Y_s, s, t);

% Display the result
disp(y_t);
plot(t,y_t);
hold on
plot(simout.time,simout.signals.values)
```

Following FIGURE 15 shows the overlay of the analytical solution for this example compared with the output from Simulink for the same setup. A good correlation can be observed.

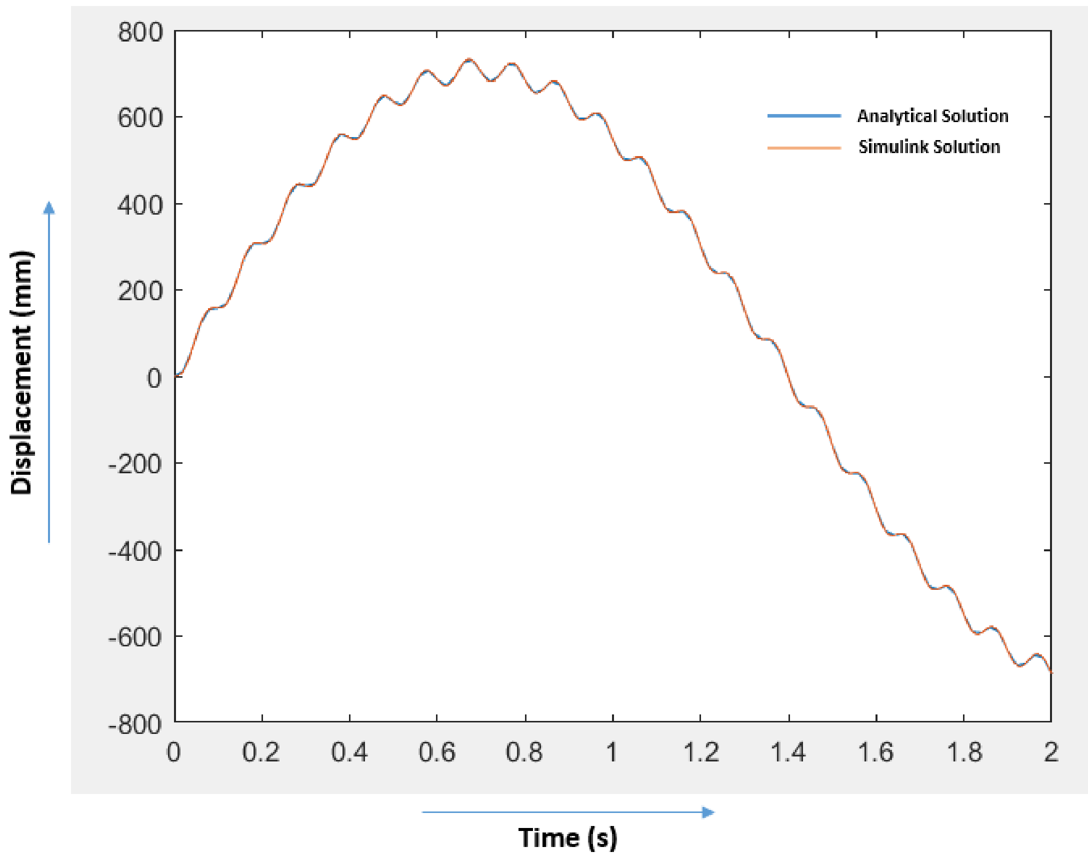

FIGURE 15 – Analytical Solution Comparison with Simulink

As a next step, to show the complexity of solving for higher degree of freedom structures an additional imbalance mass has been added to the system described earlier.

$$m_1 = 200\ Kgs, m_2 = 2\ Kgs, k = \frac{1000N}{mm}, c = 3.8\frac{Ns}{mm}, u = 2000Sin(2 * ft)$$

$where\ f = 10\ Hz\ and\ \omega = 10\ Hz.$

Using the same principle as shown earlier, the output equation can be written as,

$$A = \begin{bmatrix} 0 & 1 \\ -\dfrac{k}{m_1 + m_2} & -\dfrac{c}{m_1 + m_2} \end{bmatrix}, B = \begin{bmatrix} 0 \\ \dfrac{m_2 e\omega^2}{m_1 + m_2} \end{bmatrix}, C = \begin{bmatrix} 1 & 0 \\ 0 & 1 \end{bmatrix}\ and\ D = \begin{bmatrix} 0 \\ \dfrac{1}{m_1 + m_2} \end{bmatrix} \tag{72}$$

Taking the Laplace transform and solving for $(sI - A)X(s) = BU(s)$

$$\begin{bmatrix} s & -1 \\ \dfrac{k}{m_1 + m_2} & s + \dfrac{c}{m_1 + m_2} \end{bmatrix} \begin{bmatrix} X_1(s) \\ X_2(s) \end{bmatrix} = \begin{bmatrix} 0 \\ \dfrac{m_2 e\omega^2}{m_1 + m_2} . \dfrac{1}{s^2 + 400} \end{bmatrix} . \frac{2000}{m_1 + m_2} \tag{73}$$

$$\begin{bmatrix} X_1(s) \\ X_2(s) \end{bmatrix} = \begin{bmatrix} s & -1 \\ \dfrac{k}{m_1 + m_2} & s + \dfrac{c}{m_1 + m_2} \end{bmatrix}^{-1} \begin{bmatrix} 0 \\ \dfrac{m_2 e\omega^2}{m_1 + m_2} . \dfrac{1}{s^2 + 400} \end{bmatrix} . \frac{2000}{m_1 + m_2} \tag{74}$$

Now calculating the inverse,

$$\begin{bmatrix} s & -1 \\ \dfrac{k}{m_1 + m_2} & s + \dfrac{c}{m_1 + m_2} \end{bmatrix}^{-1} = \frac{1}{s^2 + \dfrac{c}{m_1 + m_2}s + \dfrac{k(m_1 + m_2)}{(m_1 + m_2)^2}} \begin{bmatrix} s + \dfrac{c}{m_1 + m_2} & 1 \\ \dfrac{-k}{m_1 + m_2} & s \end{bmatrix} \tag{75}$$

Substituting this back into Equation (74) gives,

$$\begin{bmatrix} X_1(s) \\ X_2(s) \end{bmatrix} = \frac{1}{s^2 + \dfrac{c}{m_1 + m_2}s + \dfrac{k(m_1 + m_2)}{(m_1 + m_2)^2}} \begin{bmatrix} s + \dfrac{c}{m_1 + m_2} & 1 \\ \dfrac{-k}{m_1 + m_2} & s \end{bmatrix} \begin{bmatrix} 0 \\ \dfrac{m_2 e\omega^2}{m_1 + m_2} . \dfrac{1}{s^2 + 400} \end{bmatrix} . \frac{2000}{m_1 + m_2}$$

(76)

As it can be seen, the size and complexity of the system has increased, therefore MATLAB is used to perform the arithmetic operations and is compared to the simulation for the same using the state space block in Simulink to validate the block result. Following is the MATLAB code used and Figures 16 and 17 show the overlay of the plots.

```
syms s t m1 m2 k c

%Given parameters
m1_val = 200;
m2_val = 2;
k_val = 1000;
c_val = 3.8;
f_val = 10;
e = 250;
w = 10;
f = 2000*sin(2*f_val*t);
% State-space matrices
AA = [0 1; -k/(m1+m2) -c/(m1+m2)];
BB = [0; m2*e*(w^2)/(m1+m2)];
CC = [1 0;0 1];
DD = [0; 1/(m1+m2)];
a21 = -k/(m1_val+m2_val);
a2 = -c/(m1_val+m2_val);
% Substitute values
AA = subs(AA, [m1, m2, k, c], [m1_val, m2_val, k_val,
c_val]);
BB = subs(BB, [m1, m2, k, c], [m1_val, m2_val, k_val,
c_val]);
CC = subs(CC, [m1, m2, k, c], [m1_val, m2_val, k_val,
c_val]);
DD = subs(DD, [m1, m2, k, c], [m1_val, m2_val, k_val,
c_val]);
% Input force Laplace transform
U_s = laplace([0;f/(m1_val+m2_val)], t, s);

% State and output Laplace transforms
X_s = inv(s * eye(size(AA)) - AA) * (BB .* U_s);
Y_s = CC * X_s + DD .* U_s;
t = [0:0.05:2];
```

```
% Inverse Laplace transform
y_t1 = ilaplace(Y_s(1,1), s, t);
y_t2 = ilaplace(Y_s(2,1), s, t);

% Display the result
disp(y_t1);
disp(y_t2);
plot(t,y_t1)
hold on
plot(simout.time,simout.signals.values)
figure
plot(t,y_t2)
hold on
plot(simout.time,simout1.signals.values)
```

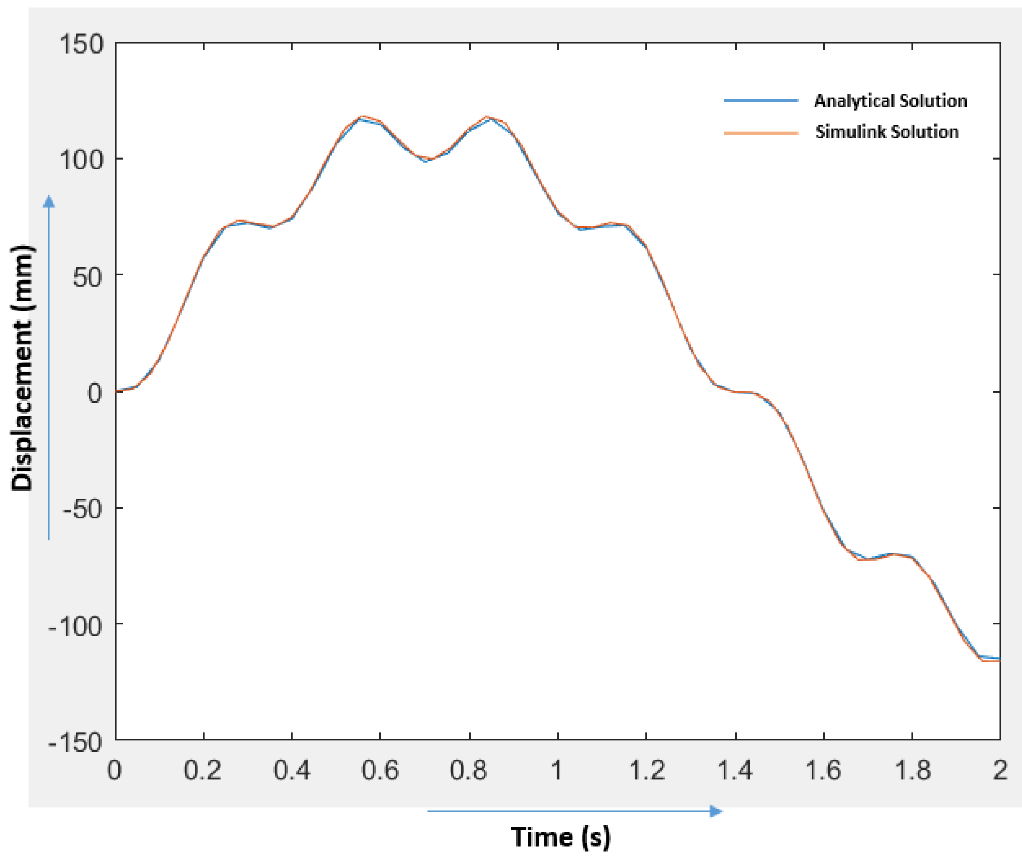

FIGURE 16 – Analytical Solution Comparison with Simulink Mass (m_1)

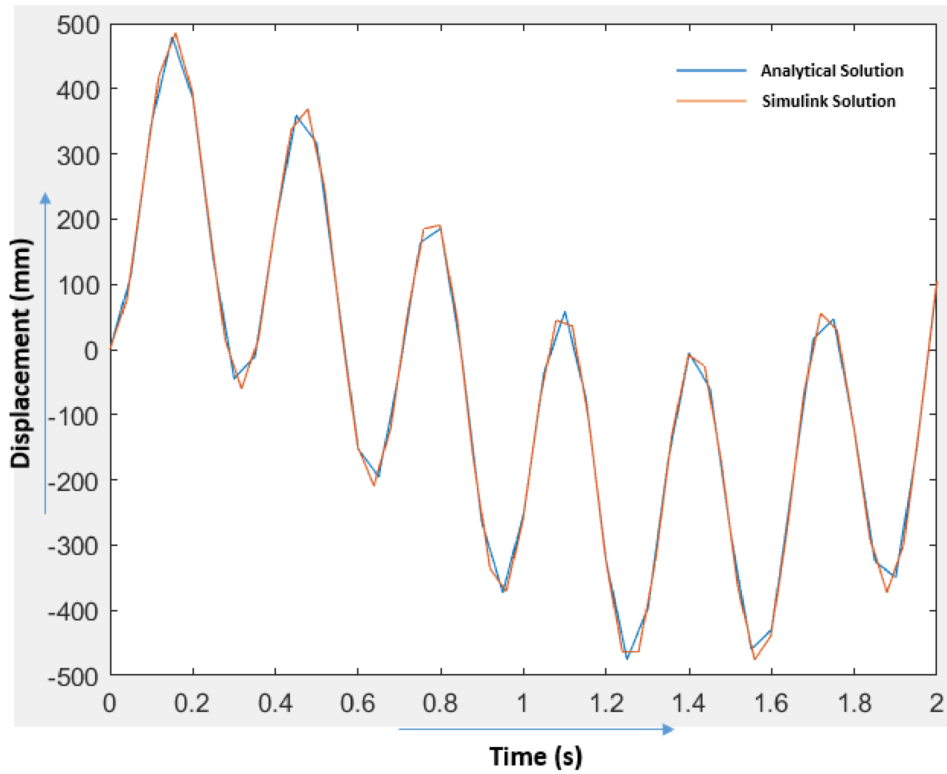

FIGURE 17 – Analytical Solution Comparison with Simulink Mass (m_2)

4.4 VIRTUAL TOOL FOR SDOF SYSTEM FORCE CANCELLATION

In this section the details of the virtual tool created using Simulink and MATLAB to simulate response of a SDOF system under forced excitation and the generation of cancellation forces using a DC motor and an actuator has been illustrated. The actuator represents the physics of centrifugal force generation using an imbalanced mass. The difference in response output measured in terms of acceleration when the actuator is switched off, and the response output when it is switched on, has been compared. Results from previous sections have been applied in this section to develop this virtual tool. Some of the key differences between what is represented in this section vs the model described in section 2.3 is the use of a DC motor to generate the angular velocity used by the centrifugal force actuator to generate the cancellation force, and the creation of a closed loop system which helps in reducing the response output for a given force excitation to a SDOF system. Using the results from section 2.2.2, 2.3 and 2.4, one can represent the SDOF system with the mass imbalance in state space form as following,

Assuming the same system described in Figure 9 for which the equation of motion is described in Equation (53). Therefore, in state space form,

$$\dot{x} = Ax + Bu\,; y = Cx + Du \tag{62}$$

Where,

$$A = \begin{bmatrix} 0 & 1 \\ \dfrac{-k}{m_1 + m_2} & \dfrac{-c}{m_1 + m_2} \end{bmatrix}; B = \begin{bmatrix} 0 & 0 \\ \dfrac{1}{m_1 + m_2} & \dfrac{1}{m_1 + m_2} \end{bmatrix}; C$$

$$= \begin{bmatrix} 1 & 0 \\ 0 & 1 \\ \dfrac{-k}{m_1 + m_2} & \dfrac{-c}{m_1 + m_2} \\ 0 & 0 \end{bmatrix};$$

$$D = \begin{bmatrix} 0 & 0 \\ 0 & 0 \\ \frac{1}{m_1+m_2} & \frac{1}{m_1+m_2} \\ 1 & 1 \end{bmatrix}; \tag{63}$$

This can be represented in Simulink using the state space block and filling the A, B, C and D matrices from Equation (63) as shown in figure below.

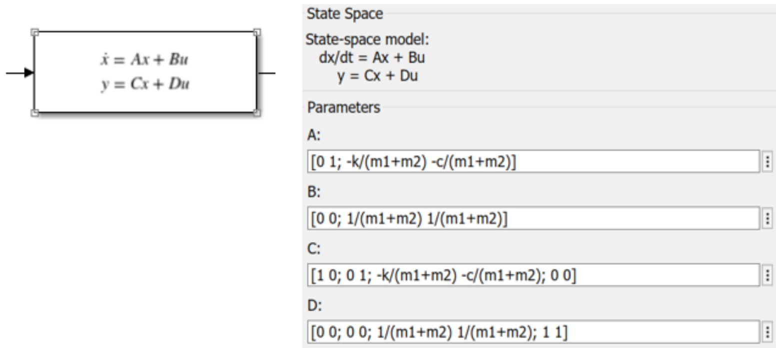

FIGURE 18 – State Space Simulink Definition of SDOF System

Next, an input to the system has been defined. This will represent the external excitation of the force into the SDOF system defined in state space. Referencing the fundamentals of state space system from section 2.4.1, it can clearly be seen that from the system defined in Equation (62), the B matrix is of dimension 2x2 which means that 2 inputs to the system are required. Out of the 2 inputs, one will be the external excitation force and the other will be the actuation force coming from the centrifugal force generator, which will be defined shortly. This is the cancellation force used to cancel the external force in order to reduce the response of the system. Prior to this, the state space system excited by an external force has been tested to see if it correctly generated the desired output. For now, the second input has been kept as zero and the state space system has been excited with a sinusoidal input of 10 Hz and amplitude of 1000 N. For this test, mass m_1 = 200 Kgs, m_2 = 0.2 Kgs, k = 1000 N/mm and c = 3.8 Ns/mm have been assumed. For an external force excitation, an unit impulse load has been used. Figure 19 shows the setup for the test of the state space system defined in Equation (63).

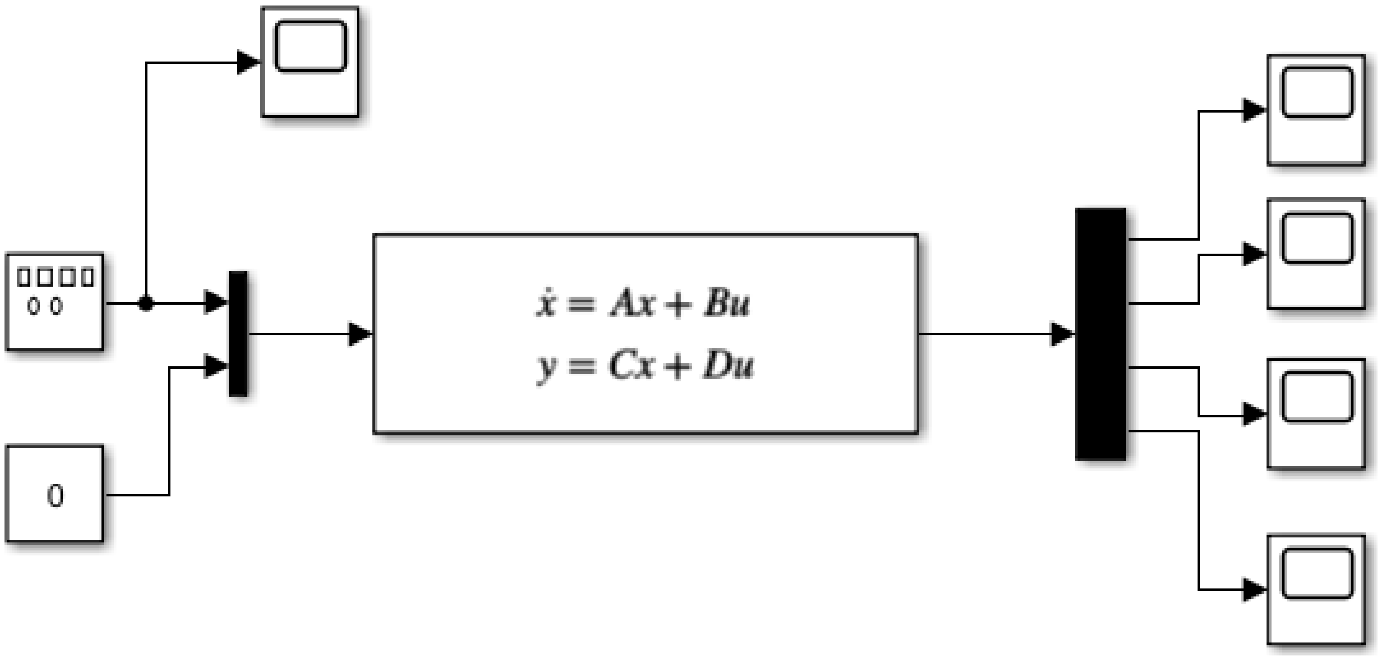

FIGURE 19 – Setup to test State Space System (Eq 63)

Following set of Figures 20, 21 and 22 show the external excitation simulated over 5 seconds, the responses (displacement, velocity and acceleration) and the force output respectively. The force output should match the force input in this case since the second force(cancellation) for this test is 0.

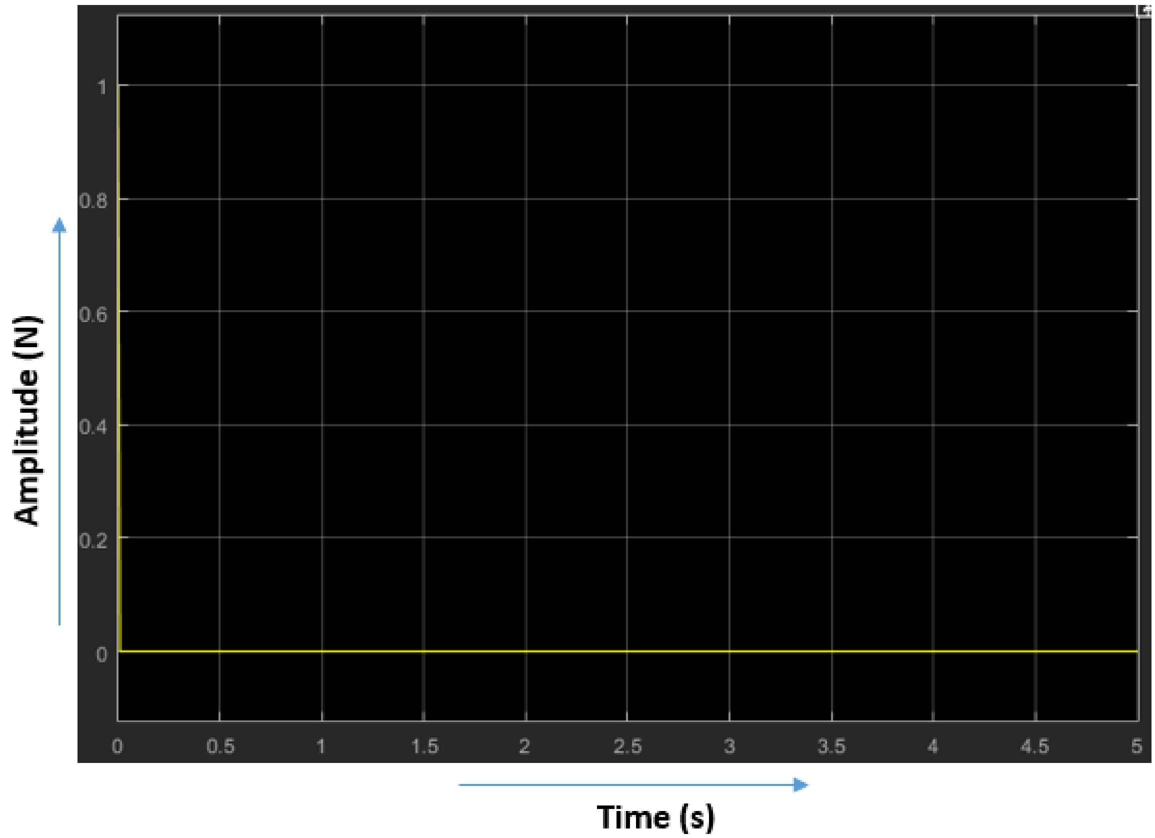

FIGURE 20 – External Force excitation

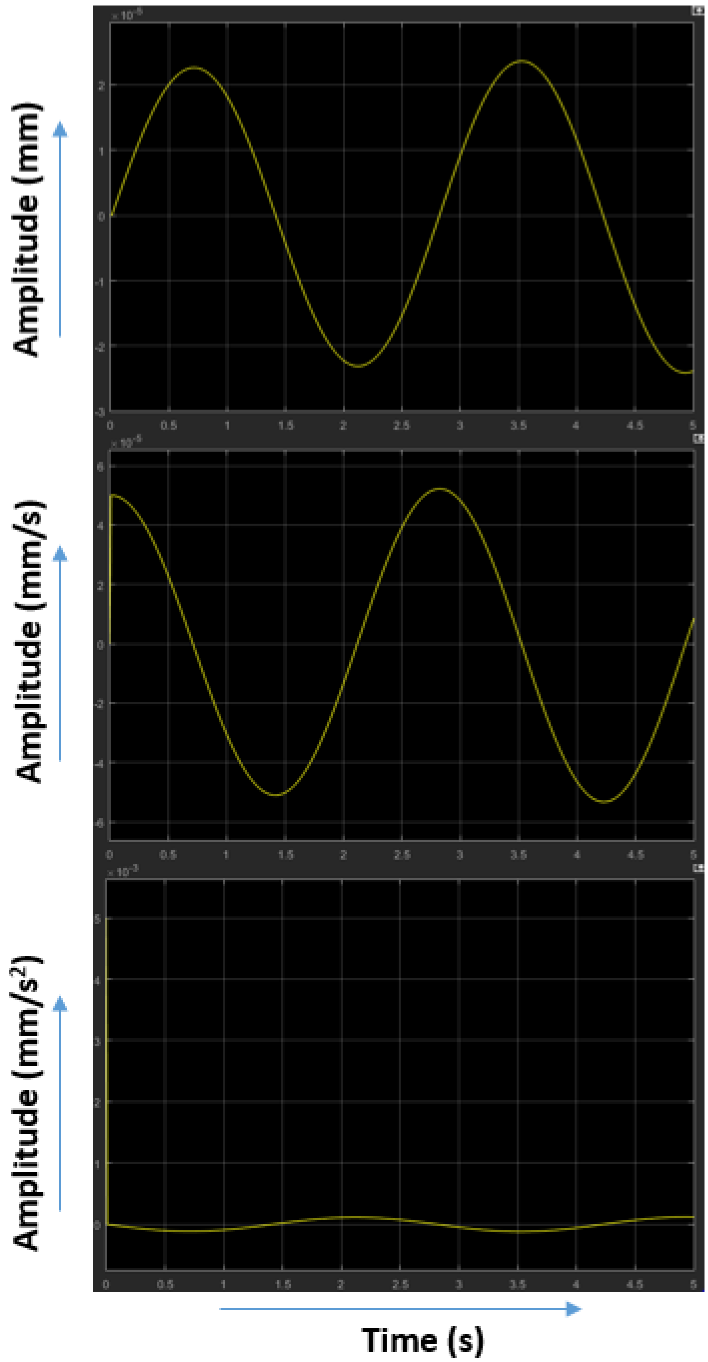

FIGURE 21 – Displacement, Velocity and Acceleration

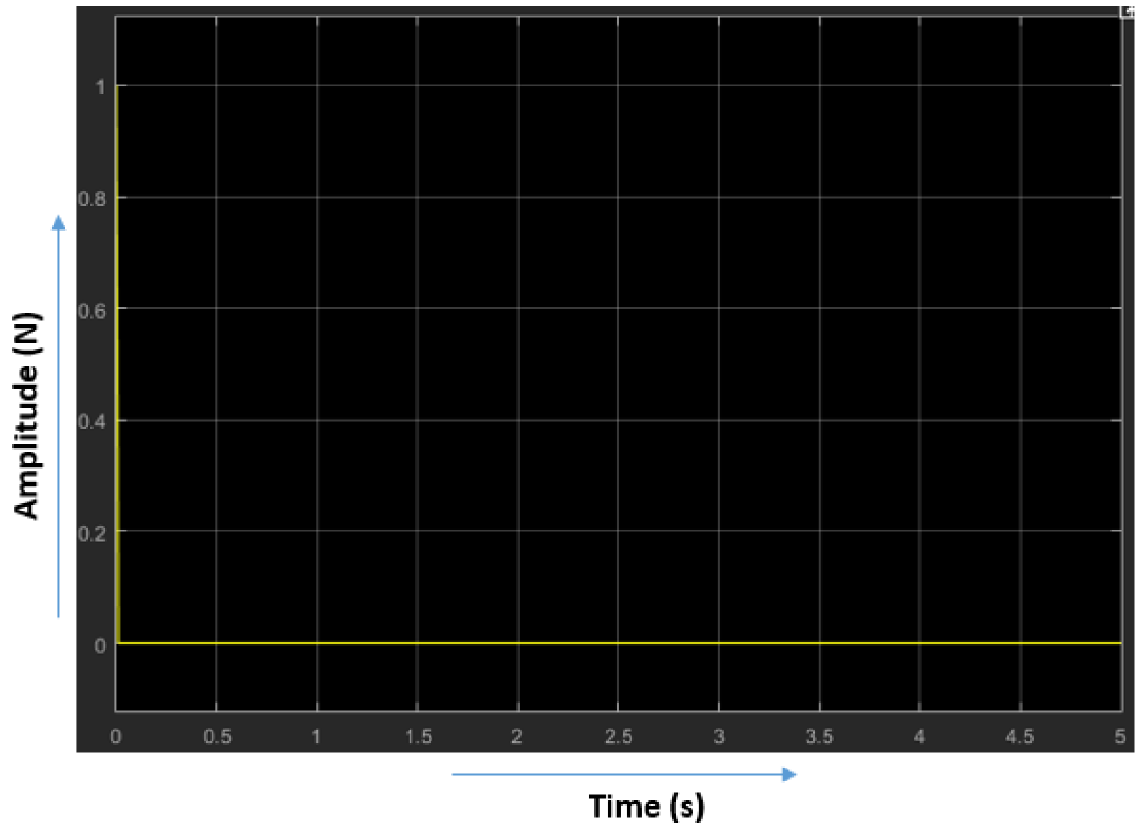

FIGURE 22 – Force Output from the State Space System (Eq 63)

Following this, a MATLAB code has been created to verify if the state space system conversion to a transfer function using the ss2tf function, and the same external force excitation to run the ODE simulation results in the same response output as the response output from the Simulink setup. Figure 23 shows the response from the MATLAB code, which matches with the system definition in Simulink, therefore validating the definition.

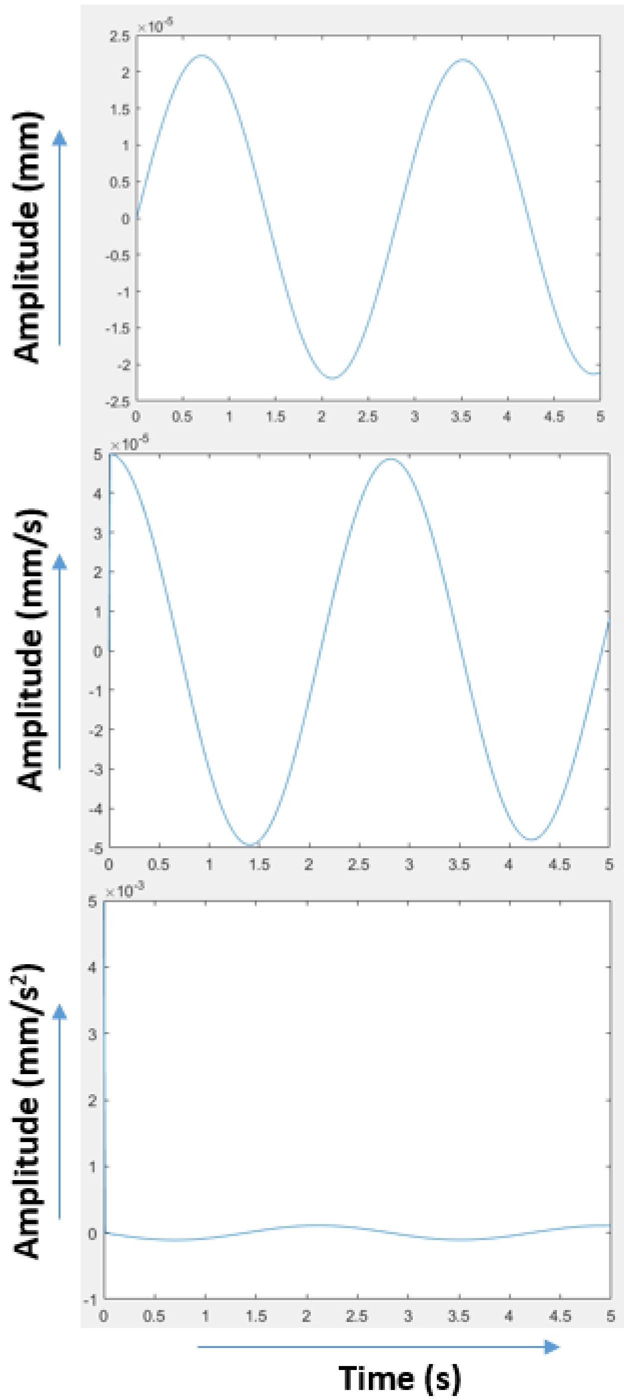

FIGURE 23 – Displacement, Velocity and Acceleration from MATLAB

After validating the system, the next step is to define a block to measure the frequency of excitation and a DC motor as described in Section 2.1.1. In addition, an actuator has also been defined which will take the angular velocity generated from the DC motor output shaft to then generate a force which will eventually become the cancellation force. The PID controller inside the DC motor will help control the angular velocity of the shaft based on input voltage and load torque.

A PID controller could have been used directly to control the output response from the system and generate a signal to cancel the excitation but that would not serve the practical purpose since an external motor with an actuator is needed to generate the force that can reduce the response from the system. Figure 24, shows the system with DC motor, CFG actuator and frequency counter added to the system.

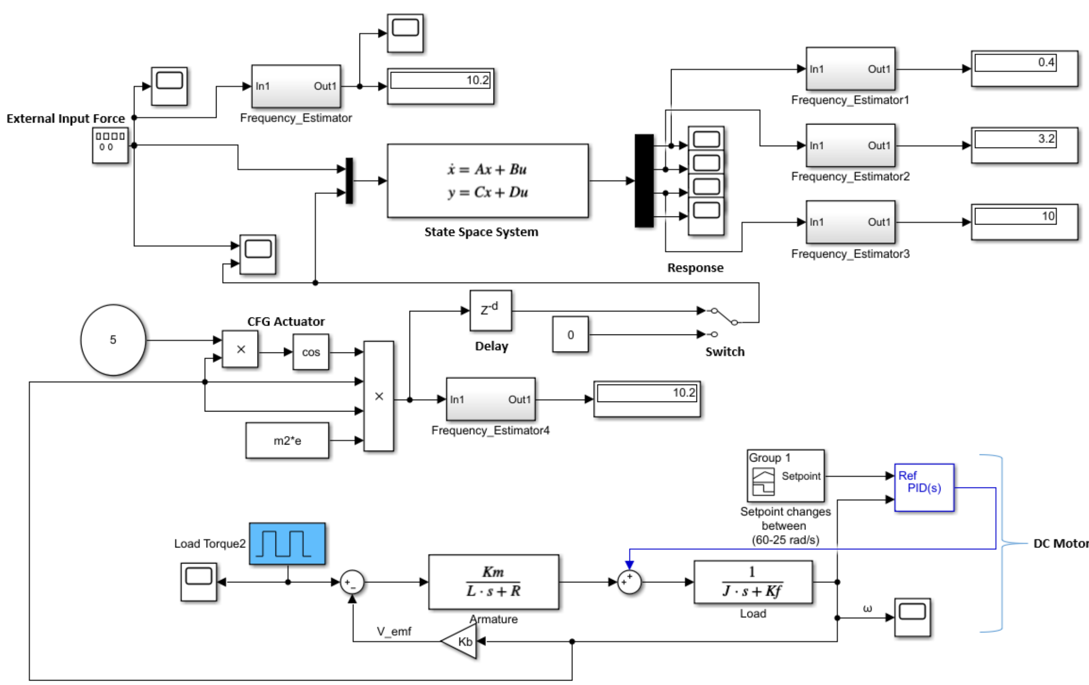

FIGURE 24 – Virtual Tool for CFG Force Cancellation for SDOF System

The tool also includes a switch to see the response with and without the cancellation force coming through the CFG actuator. For a test of the system, an external force excitation has been added in form of a sinusoidal wave of amplitude 20 kN and frequency of 10 Hz. First the switch is turned off and the force through the actuator is not fed back into the system. Figures 25, 26 and 27 show the excitation force, acceleration response and output force from the system without cancellation respectively. The simulation is run for 1 second and since for a given motor torque is proportional to current and back emf is proportional to rpm, a standard DC motor has been used with following numerical values of the coefficients: L = 0.5 Henrys, R = 2 Ohms, Kf = 0.2 Nms, Kb = 0.1, J = 0.02 Kgm2/s2 and Km = 0.1.

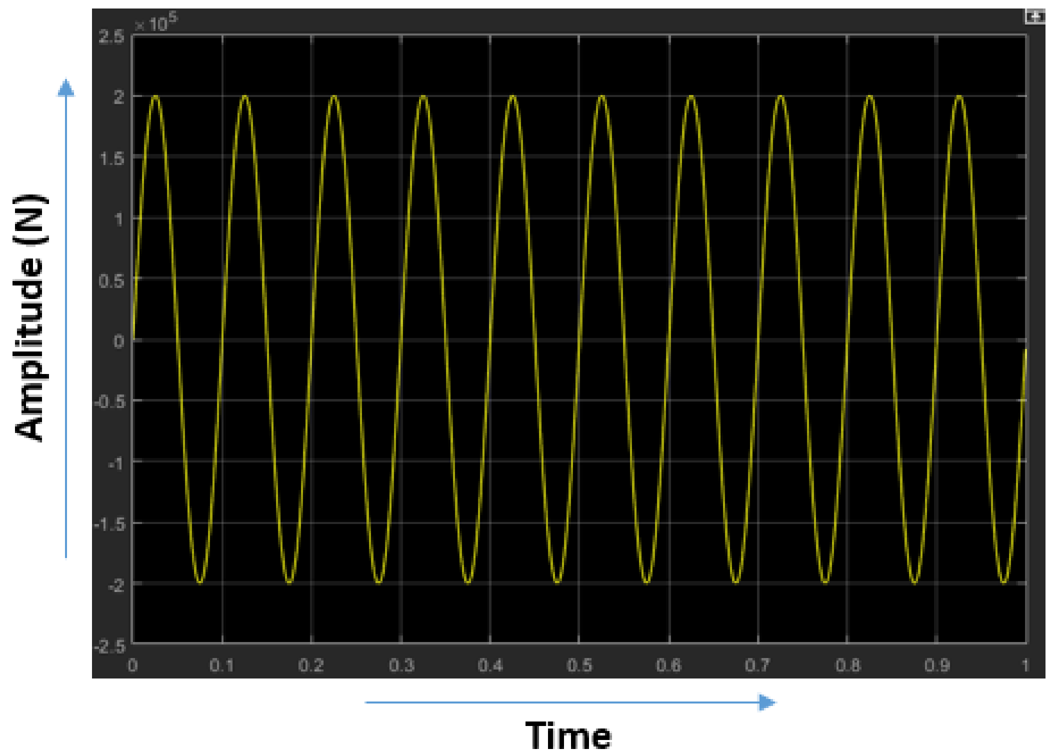

FIGURE 25 – Excitation Force

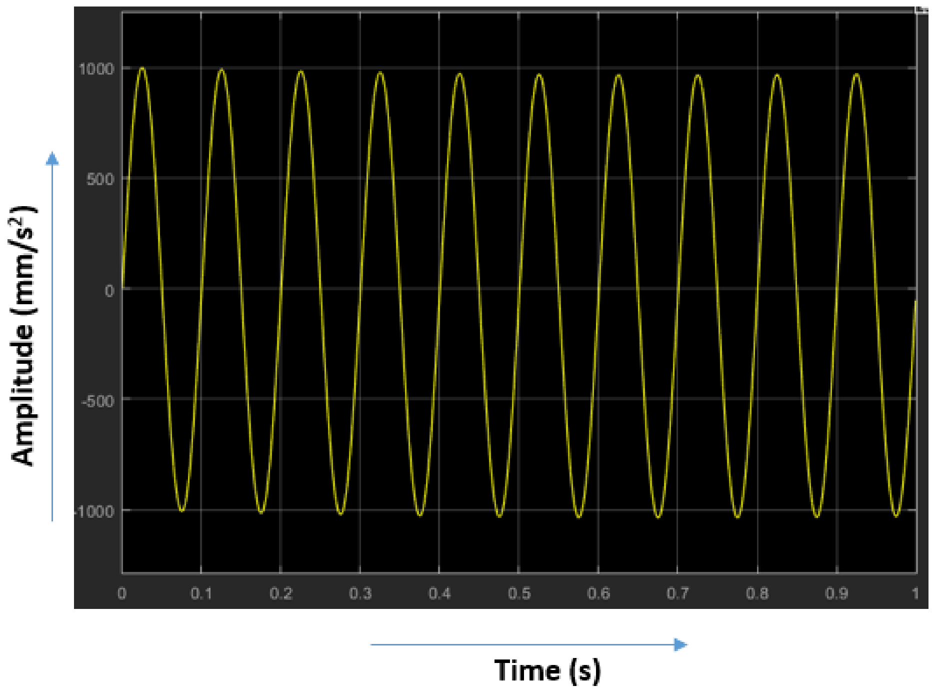

FIGURE 26 – Acceleration Response

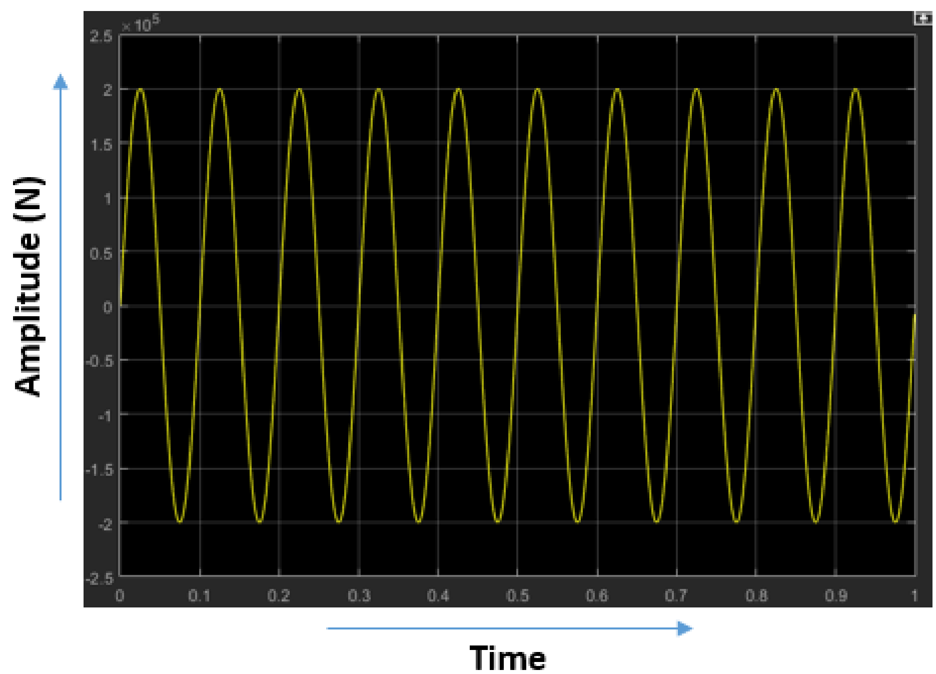

FIGURE 27 – Output Force from the System

Next the switch is turned on and the actuator supplies the cancellation force generated from the DC motor used. Figure 28 shows the time taken by the DC motor to achieve 10 Hz speed, which is equivalent to 600 rpm. It takes about 0.13 seconds to achieve a steady state of the velocity. The maximum centrifugal force generated for given mass and eccentricity and this angular velocity is about 20 kN. Due to the time taken by the DC motor to achieve steady state, there is a slight difference in frequency of the CFG force and the external force, and since this is a transient analysis, some cancellation to reduce the acceleration response is expected but IS not expected to be complete. A reduction of the forces from the force output through the system has also been observed.

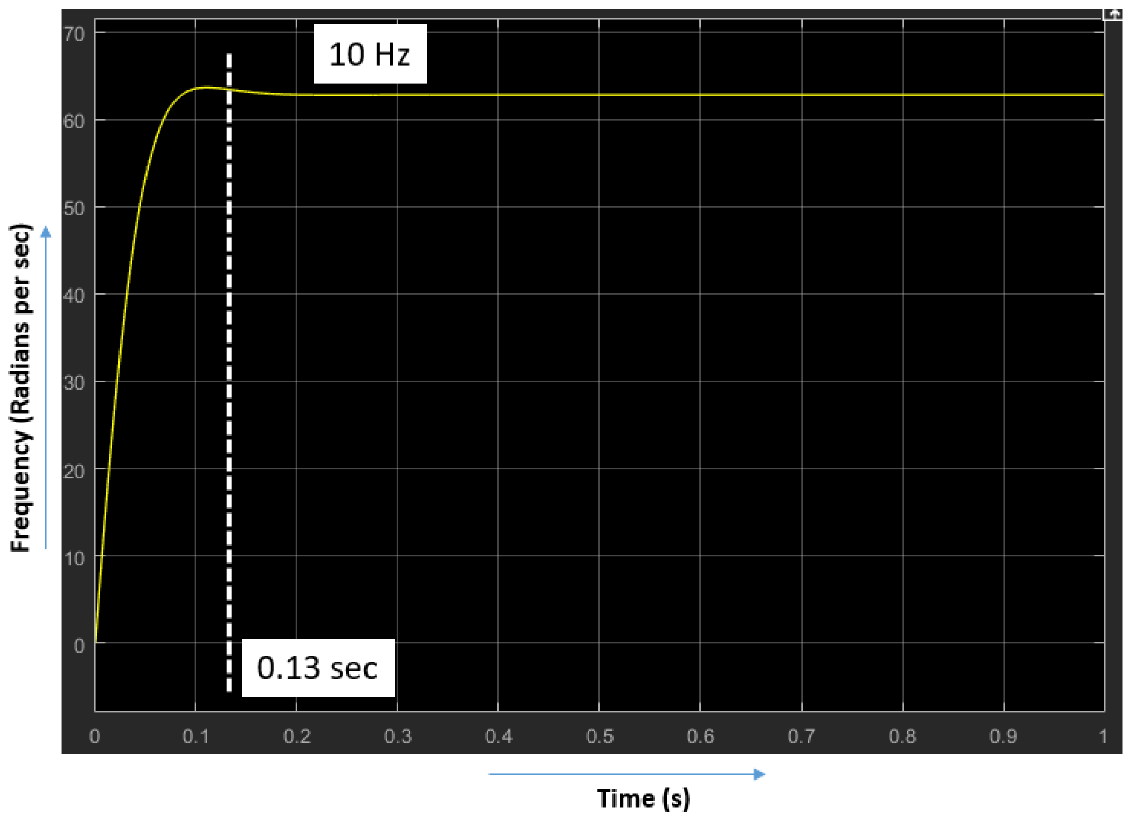

FIGURE 28 – Angular velocity of the DC motor shaft

Figure 29, shows a comparison of the external force with the CFG cancelation force which starts its maximum amplitude at about 0.13 seconds as it is proportional to the time taken by the DC motor to reach its steady state velocity of the shaft.

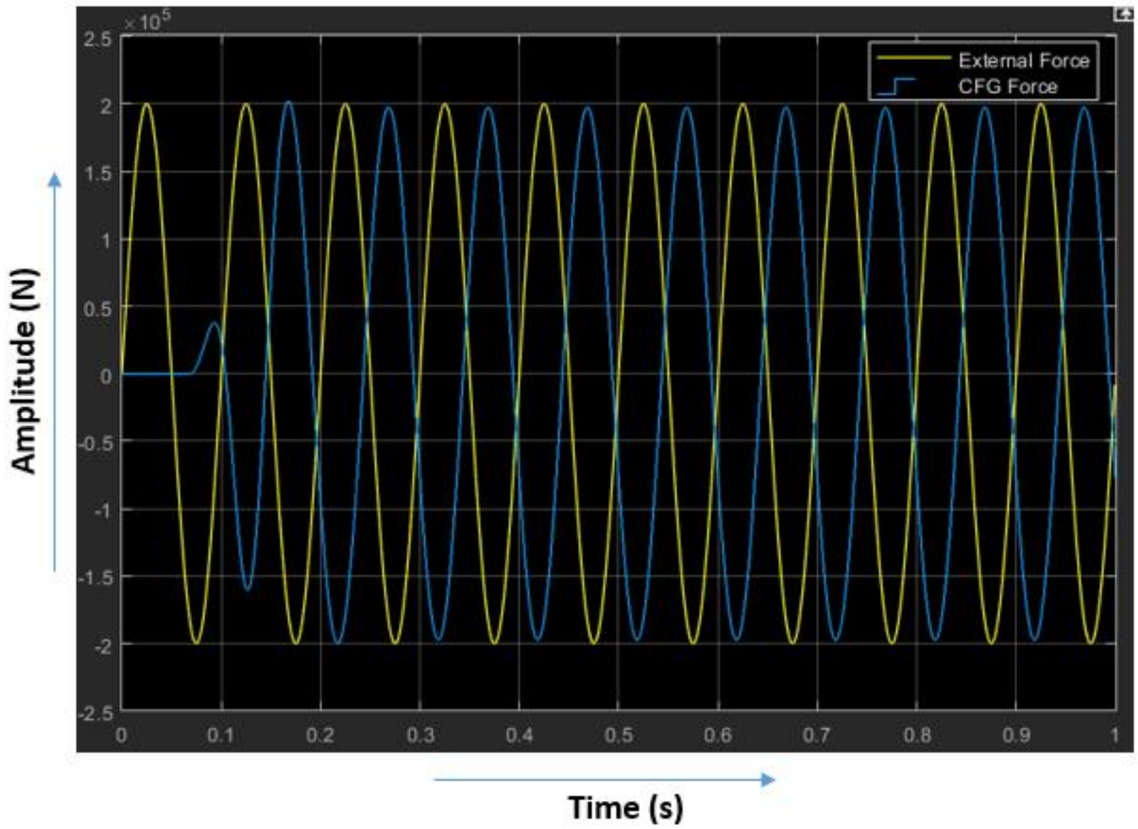

FIGURE 29 – Force Comparison

Figures 30 and 31, show the acceleration response and force output when the CFG is switched on. A reduction in the response output and the force has been observed.

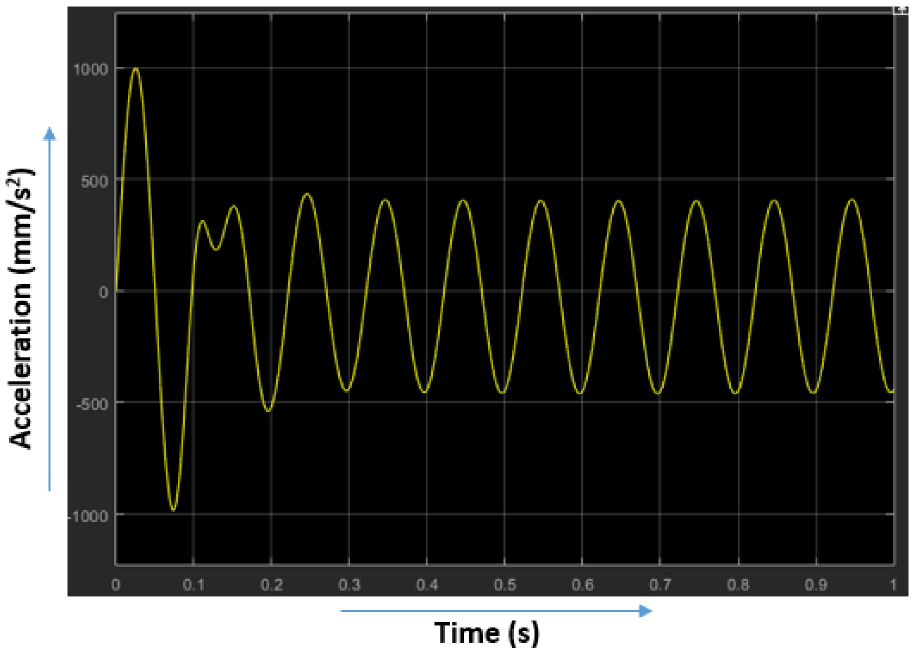

FIGURE 30 – Acceleration after CFG actuator is switched ON

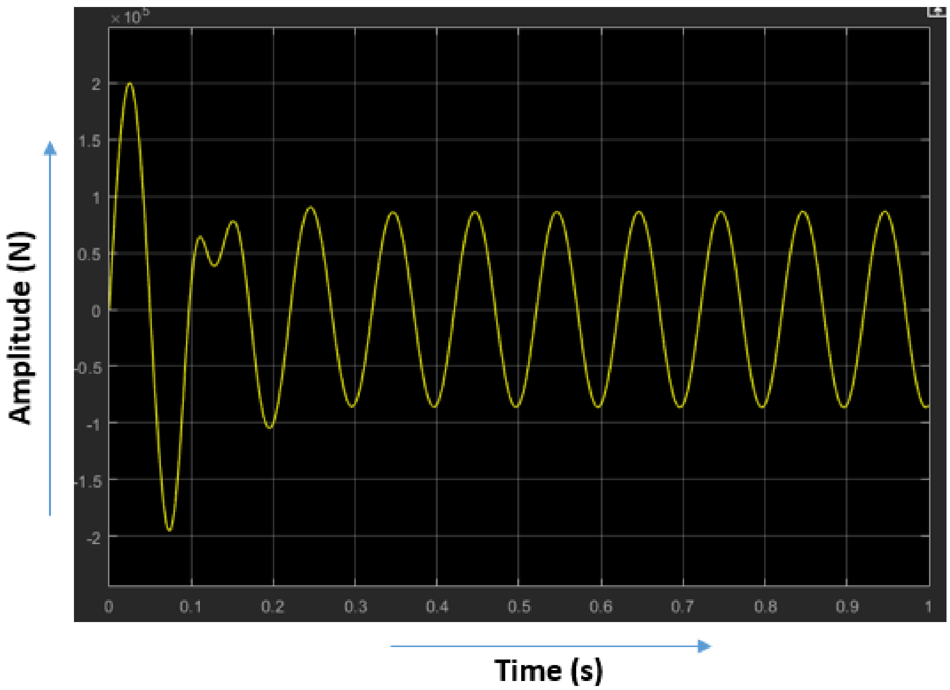

FIGURE 31 – Force Output after CFG actuator is switched ON

For complete cancellation, the time taken by the DC motor to achieve the steady state needs to be minimized, thereby reducing the difference in frequency between the excitation force and the CFG force. Theoretically, if the frequencies are identical then the cancellation will be 100% but in reality, there will be some loss due to time lag required for achieving steady state of the velocity. This can be optimized further to improve performance by better tuning the PID controller, but for this test it was not done as the objective was to see if the tool is performing the cancellation to reduce the output through the system, which was successful.

In the next sections, a deep dive into a MDOF system has been shown starting with defining a continuous beam and illustrating the state space model of the continuous beam using finite elements, MATLAB and Nastran. Modification of the virtual tool to simulate and cancel responses for this continuous beam has also been shown.

CHAPTER FIVE

VIRTUAL MODEL DEVELOPMENT AND FORCE CANCELLATION
CONTINUOUS BEAM

5.1 FINITE ELEMENT MODELLING AND ANALYSIS

In this section a DMAP has been illustrated to alter the Nastran code to extract a few matrices from a finite element model built using ANSA and then to generate a state space model. This section will help build and validate a continuous beam in finite elements and establish its state space formulation to be used in the Simulink virtual tool to validate the CFG force cancellation. Reduced order mass, stiffness, damping, eigenvalue, displacement, and force matrices have been extracted from the finite element model which have been discussed in detail in this section. The state space formulation using these matrices have also been described. The following flow chart shows the steps and the process followed to extract the state space form and run the virtual tool for force cancellation.

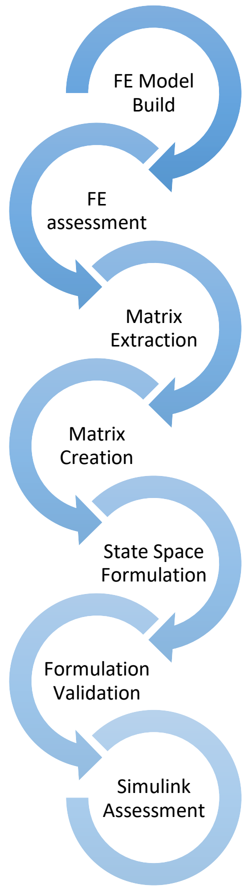

FLOW CHART – FE to SS Process Flow

In the following section every step shown in the flow chart above have been discussed.

This section includes the modeling done in finite element using ANSA pre-processor. For this section a simple beam model is represented using a 1D CBEAM element, which is then divided equally into 100 elements. Figure 32 shows the solid representation of the CBEAM element used for the analysis in this section.

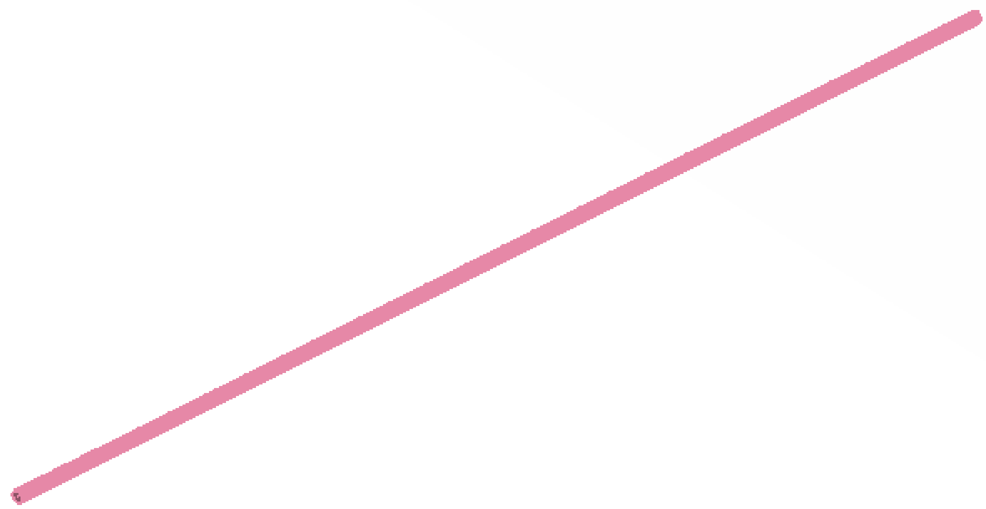

FIGURE 32 – Solid Representation of the CBEAM

The following assumptions were made with regards to the material and properties of the beam. The material was assumed to be steel with elastic modulus of 210 GPa, 0.3 Possion's ratio and density of 7.85e-9 Ton/mm^3 . The area of the beam cross section is 78.5 mm^2, the area moment of inertia for bending along the XY and XZ planes is 490.9 Ton-mm^2 and the torsional stiffness parameter is 981.75 Ton-mm^2. As mentioned previously, the CBEAM element is divided into 100 elements and Figure 33 shows four grids which are important for this analysis as they define the excitation point, the cancellation force actuator point and the response points. For this analysis, the same excitation which is to be used in the Simulink model has been used and the displacement and grid point forces have been requested as outputs.

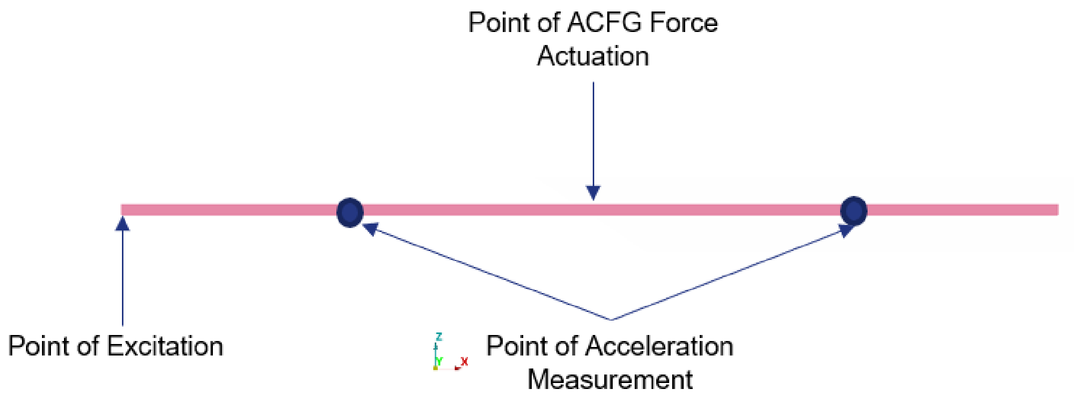

FIGURE 33 – Element and Grids of Concern for Analysis

5.2 MATRIX EXTRACTION AND STATE SPACE REPRESENTATION

In this section, a DMAP is written to identify the internal numbering sequence of Nastran and identify the grid number corresponding to the important nodes for the assessment mentioned in the previous section. Following this, another DMAP has been written to run solution 111, which is the Modal FRF in Nastran, to extract the reduced stiffness and mass matrices along with the proportional reduced damping matrix, the eigenvalues and the displacements. These matrices are important to define the state space matrices which will be discussed in the next section. At this point, one can also choose to extract the full mass, stiffness, damping, displacement, eigenvalue, and force matrices instead of the reduced model. The benefit of this is that, since this would be in the physical domain, it would be clear and easy to identify in the matrix where exactly the forces are being applied and responses are being computed, which can be used to propose an alternate methodology of force cancellation using internal matrix manipulation, but this has not been explored in this thesis. This is because it would be comparatively easy to do for a simple beam or a plate model with limited size of the matrices but at scale which done in next section, with a full vehicle frame model where size of the matrix would be huge, then working in the physical domain would be computationally very expensive. Therefore, eigenvalues are also extracted, and all matrices extracted are reduced matrices in the modal domain which makes it computationally cheaper and gives the ability to handle large models and matrices.

The extracted stiffness, mass, damping, displacement, eigenvalues and force matrices from the Nastran model are then used to formulate the A, B, C and D matrices for the state space representation of the simple beam. Figures 34, 35, 36, 37, 38 show the full KM (stiffness and mass) matrix, full damping matrix, eigenvalue matrix, displacement matrix and actuation force matrix respectively. To keep the figure size concise, only part of the matrices have been shown but the full matrices have been attached in the Appendix.

```
     606      606         6         1KXX      1P,5E16.9
       1        1       595
 3.298672440E+06 0.000000000E+00 0.000000000E+00 0.000000000E+00 0.000000000E+00
 0.000000000E+00-1.649336220E+06 0.000000000E+00 0.000000000E+00 0.000000000E+00
 0.000000000E+00 0.000000000E+00 0.000000000E+00 0.000000000E+00 0.000000000E+00
 0.000000000E+00 0.000000000E+00 0.000000000E+00 0.000000000E+00 0.000000000E+00
 0.000000000E+00 0.000000000E+00 0.000000000E+00 0.000000000E+00 0.000000000E+00
 0.000000000E+00 0.000000000E+00 0.000000000E+00 0.000000000E+00 0.000000000E+00

 .......
 .......

     606      590        17
-1.908330626E-06 6.310887242E-30 0.000000000E+00 1.262177448E-29-4.403839907E-06
 0.000000000E+00 0.000000000E+00 0.000000000E+00 0.000000000E+00 0.000000000E+00
 0.000000000E+00 0.000000000E+00-3.229482599E-06 0.000000000E+00 0.000000000E+00
 0.000000000E+00 5.871786543E-06
     607        1         1
 1.000000000E+00
```

FIGURE 34 – KM (Stiffness and Mass Matrix)

```
     606       606         6          1CFIN     1P,5E16.9
       1         1       595
1.649336220E+04 0.000000000E+00 0.000000000E+00 0.000000000E+00 0.000000000E+00
0.000000000E+00-8.246681100E+03 0.000000000E+00 0.000000000E+00 0.000000000E+00
0.000000000E+00 0.000000000E+00 0.000000000E+00 0.000000000E+00 0.000000000E+00
0.000000000E+00 0.000000000E+00 0.000000000E+00 0.000000000E+00 0.000000000E+00
0.000000000E+00 0.000000000E+00 0.000000000E+00 0.000000000E+00 0.000000000E+00
0.000000000E+00 0.000000000E+00 0.000000000E+00 0.000000000E+00 0.000000000E+00
0.000000000E+00 0.000000000E+00 0.000000000E+00 0.000000000E+00 0.000000000E+00
 .......
 .......

     606       590        17
1.048306938E+04 3.155443621E-32 0.000000000E+00 6.310887242E-32 8.735873795E+02
0.000000000E+00 0.000000000E+00 0.000000000E+00 0.000000000E+00 0.000000000E+00
0.000000000E+00 0.000000000E+00-1.048306938E+04 0.000000000E+00 0.000000000E+00
2.775557562E-19 1.039571064E+05
     607         1         1
1.000000000E+00
```

FIGURE 35 – Damping Matrix

```
       5       606         2          1LMAT     1P,5E16.9
       1         1       606
-2.605468035E-05-8.374452591E-06-7.938593626E-06-6.057322025E-06-5.766749382E-06
 1.043081284E-06 8.367628885E+04 8.367628885E+04 6.354664363E+05 6.354664363E+05
 2.440112235E+06 2.440112235E+06 6.659957114E+06 6.659957114E+06 1.483967705E+07
 1.483967705E+07 2.889636212E+07 2.889636212E+07 5.111120245E+07 5.111120245E+07
 8.411913620E+07 8.411913620E+07 1.015574319E+08 1.308971096E+08 1.308971096E+08
 1.947510288E+08 1.947510288E+08 2.640493498E+08 2.793015559E+08 2.793015559E+08
 3.884689047E+08 3.884689047E+08 4.063299689E+08 5.264568017E+08 5.264568017E+08
 6.977357786E+08 6.977357786E+08 9.070259682E+08 9.070259682E+08 9.146184341E+08
    .......
    .......

 1.245206390E+13 1.245206390E+13 1.264696059E+13 1.264696059E+13 1.283518342E+13
 1.283518342E+13 1.301582037E+13 1.301582037E+13 1.318794535E+13 1.318794535E+13
 1.335062811E+13 1.335062811E+13 1.350294507E+13 1.350294507E+13 1.364399125E+13
 1.364399125E+13 1.377289294E+13 1.377289294E+13 1.388882080E+13 1.388882080E+13
 1.399100322E+13 1.399100322E+13 1.407873937E+13 1.407873937E+13 1.415141175E+13
 1.415141175E+13 1.420849763E+13 1.420849763E+13 1.424957921E+13 1.424957921E+13
 1.427435180E+13 1.427435180E+13 2.385509875E+13 2.385509875E+13 2.385509875E+13
 2.385509875E+13
       6         1         1
 1.000000000E+00
```

FIGURE 36 – Eigenvalue Matrix

```
   606       18        2         1DISPS    1P,5E16.9
     1        1       18
 4.027345758E+01-8.641905006E-02-4.308871932E-02 4.027345758E+01-6.994842631E-02
-6.706214234E-02 4.027345758E+01-6.960528831E-02-6.756158866E-02 4.027345758E+01
-5.279152653E-02-9.203445792E-02 4.027345758E+01-8.676218806E-02-4.258927301E-02
 4.027345758E+01-5.244838853E-02-9.253390423E-02
     2        1       18
 6.526814643E-02 5.478906163E+01-2.977185061E+00 6.526814643E-02 3.942180384E+01
-2.754700213E+00 6.526814643E-02 3.910165264E+01-2.750065112E+00 6.526814643E-02
 2.341424364E+01-2.522945162E+00 6.526814643E-02 5.510921283E+01-2.981820162E+00
 6.526814643E-02 2.309409243E+01-2.518310061E+00
   .......
   .......
 4.571735120E-16-1.906670584E-04 3.789045113E-05-1.823805353E-15 2.606113267E-09
-3.409333984E-10-9.172554255E-16-8.306867538E-09 1.086710764E-09-6.934527050E-16
-1.309363130E+02-1.466619317E+02 1.359843575E-15-1.093162570E-03 2.172385990E-04
-1.130658718E-15-7.506953453E+02-8.408548162E+02
   607        1        1
 1.000000000E+00
```

FIGURE 37 – Displacement Matrix

```
     2      606        2         1ACTTRA   1P,5E16.9
     1        1      606
 2.397342302E-02-2.224848483E-01-4.935491661E+00 5.164424481E-01-6.678089117E+01
 1.866422724E-01 4.893144227E+00 1.255935153E+02-1.143472260E+01-7.771437652E+01
-1.324233907E+01-6.430150616E+00-9.997093229E+00 6.026796534E+01 1.228547054E+01
 1.220723964E+02-1.407303219E+00-7.559090833E+01 4.781065553E-01-6.104357817E+00
-3.813989343E+01-2.184603725E+01 1.607526970E-12-4.408186215E+01-1.017882440E+02
 4.034099264E+01-6.014101547E+01 4.170995967E-13-2.999430763E-01-1.824129868E+00
 2.238263221E+01 1.536130271E+01 2.444577925E-12-9.549028389E+01 2.385837900E+01
 6.218565533E+01 3.013542576E+01 4.322636744E+00-7.687489438E+00-8.925926277E-13
   .......
   .......
 8.500235116E-01 9.180157348E-01-1.480353174E+01-2.109461215E+01 7.030814531E+00
-4.691551975E+01 6.152710699E-02 2.290660365E+01-1.094528444E+00-6.198249155E-01
-1.800302301E+01-8.246677500E+00 4.051033238E+00-3.496605709E+01-1.095327928E+01
 1.232744382E+01-5.118679879E-01-8.208472774E-01-2.466065147E+00 1.277189219E+01
 1.408205267E+00 2.162512024E+01 5.360766270E-01 9.374295135E+00 1.598527172E-01
-4.921113058E-01-5.214050190E+00-2.236355375E+00-3.604020646E+00 6.369573283E+00
-1.897337001E+00-4.098585561E-02 4.109687947E-04-2.343173972E-04-1.309363130E+02
 1.466619317E+02
     3        1        1
 1.000000000E+00
```

FIGURE 38 – Actuation Force Matrix

These matrices are then used to formulate the A, B, C and D matrices that define the simple beam state space form. Figures 39, 40, 41, 42 show the A, B, C and D matrices respectively. To keep the figure size concise, only part of the matrices have been shown.

1212x1212 double

	1	2	3	4	5	6	7	8	9	10
606	0	0	0	0	0	0	0	0	0	0
607	2.6055e-05	0	0	0	0	0	0	0	0	0
608	0	8.3745e-06	0	0	0	0	0	0	0	0
609	0	0	7.9386e-06	0	0	0	0	0	0	0
610	0	0	0	6.0573e-06	0	0	0	0	0	0
611	0	0	0	0	5.7667e-06	0	0	0	0	0
612	0	0	0	0	0	-1.0431e-06	0	0	0	0
613	0	0	0	0	0	0	-8.3676e+04	0	0	0
614	0	0	0	0	0	0	0	-8.3676e+04	0	0
615	0	0	0	0	0	0	0	0	-6.3547e+05	0
616	0	0	0	0	0	0	0	0	0	-6.3547e+05
617	0	0	0	0	0	0	0	0	0	0

FIGURE 39 – A Matrix

1212x2 double

	1	2
609	5.5403e+08	-1.3707e-18
610	0	0
611	6.2244e+08	2.3204e-18
612	1.6842e-14	2.1542e-39
613	0	0
614	-2.7046e-15	5.0146e-39
615	1.3708e+08	-5.7059e-18
616	0	0
617	1.6738e+08	7.1748e-18
618	1.5192e-15	6.4592e-39
619	0	0
620	-3.0149e-16	1.7524e-38
621	3.8545e+07	-2.0369e-17
622	0	0
623	4.7289e+07	2.5045e-17

.
.
.
.
.

FIGURE 40 – B Matrix

18x1212 double

	1	2	3	4	5	6	7	8	9	10	11
1	0.0010	5.4658e-07	-5.6289e-07	-4.1003e-08	1.1195e-07	5.9186e-09	-3.0910e-07	8.3968e-07	-1.9603e-07	-2.7125e-07	-1.2397e-06
2	-2.2516e-06	4.5883e-04	-3.1393e-05	3.4677e-04	3.1833e-06	1.5169e-07	6.4215e+06	-2.5018e+05	4.6653e+07	-6.8644e+06	-7.6389e+07
3	-1.1227e-06	-2.4932e-05	-3.5809e-04	2.1948e-06	-3.7601e-04	-9.8194e-08	-2.5018e+05	-6.4215e+06	6.8644e+06	4.6653e+07	1.5732e+08
4	0.0010	5.4658e-07	-5.6289e-07	-4.1003e-08	1.1195e-07	5.9186e-09	-3.1006e-07	8.3637e-07	-1.9712e-07	-2.6347e-07	-1.2633e-06
5	-1.8225e-06	3.3014e-04	-2.1214e-05	-4.7947e-05	2.5703e-08	1.7155e-07	-4.0877e+06	1.5926e+05	-2.7321e+06	4.0199e+05	-6.0699e+07
6	-1.7473e-06	-2.3069e-05	-3.1891e-04	-9.3350e-07	9.0980e-06	9.6489e-08	1.5926e+05	4.0877e+06	-4.0199e+05	-2.7321e+06	1.2500e+08
7	0.0010	5.4658e-07	-5.6289e-07	-4.1003e-08	1.1195e-07	5.9186e-09	-3.0986e-07	8.3641e-07	-1.9609e-07	-2.6539e-07	-1.2560e-06
8	-1.8135e-06	3.2745e-04	-2.1002e-05	-5.6170e-05	-4.0081e-08	1.7196e-07	-4.0937e+06	1.5949e+05	2.6262e-05	-7.9285e-06	-6.1063e+07
9	-1.7603e-06	-2.3030e-05	-3.1809e-04	-9.9868e-07	1.7121e-05	1.0055e-07	1.5949e+05	4.0937e+06	3.4346e-06	1.3074e-05	1.2575e+08
10	0.0010	5.4658e-07	-5.6289e-07	-4.1003e-08	1.1195e-07	5.9186e-09	-3.0870e-07	8.3957e-07	-2.0056e-07	-2.6668e-07	-1.2166e-06
11	-1.3755e-06	1.9608e-04	-1.0610e-05	-4.5911e-04	-3.2635e-06	1.9224e-07	6.4215e+06	-2.5018e+05	-4.6653e+07	6.8644e+06	-7.6389e+07
12	-2.3979e-06	-2.1128e-05	-2.7810e-04	-4.1921e-06	4.1025e-04	2.9928e-07	-2.5018e+05	-6.4215e+06	-6.8644e+06	-4.6653e+07	1.5732e+08
13	0.0010	5.4658e-07	-5.6289e-07	-4.1003e-08	1.1195e-07	5.9186e-09	-3.0916e-07	8.3968e-07	-1.9623e-07	-2.6966e-07	-1.2531e-06
14	-2.2606e-06	4.6151e-04	-3.1605e-05	3.5499e-04	3.2491e-06	1.5127e-07	6.7344e+06	-2.6237e+05	5.0630e+07	-7.4496e+06	-8.5817e+07

.
.
.
.

FIGURE 41 – C Matrix

18x2 double

	1	2
1	-4.3408e+07	-7.9792e+06
2	-1.3054e+10	-2.3798e+09
3	-1.0530e+11	-2.5445e+09
4	-9.9993e+06	-5.3518e+07
5	-5.8901e+09	1.3401e+09
6	-3.4455e+10	-9.2853e+08
7	-9.8542e+06	-1.0782e+08
8	-8.1975e+09	-2.4337e+09
9	-3.6724e+10	-1.0333e+09
10	-4.5618e+07	1.3247e+08
11	4.4487e+10	1.0192e+09
12	5.9884e+10	2.3809e+09
13	-4.3438e+07	1.8953e+08
14	-1.5415e+10	2.6987e+09
15	-1.4208e+11	2.8198e+09

FIGURE 42 – D Matrix

The validation and assessment will be covered in the next section along with the results. In this next section the reduced matrices and the A, B, C and D matrices used for the simple beam have also been shared.

5.3 VIRTUAL TOOL MODIFICATION AND RESULTS FOR BEAMS

In this section, all the results from the previous sections have been used along with the tool shown in Figure 43 to simulate the state space created in the previous section and excited by an external force. The responses at multiple points have been measured and the CFG cancellation actuator has been switched on to run the DC motor and generate the cancellation force for the given mass imbalance. The imbalanced mass m_2 is assumed to be 2 kg with eccentricity for the imbalanced mass as 250mm. All the motor assumptions and beam assumptions are the same as defined in Section 4.4 and 5.1, respectively. The simulation time is taken to be 4 seconds. Figures 44, 45, 46 47 and 48 show the reduced KM matrix, damping matrix, eigenvalue matrix, displacement matrix, actuation force matrix, respectively. Figures 49, 50 show the A and C matrices and Figures 51 show the B and D matrices.

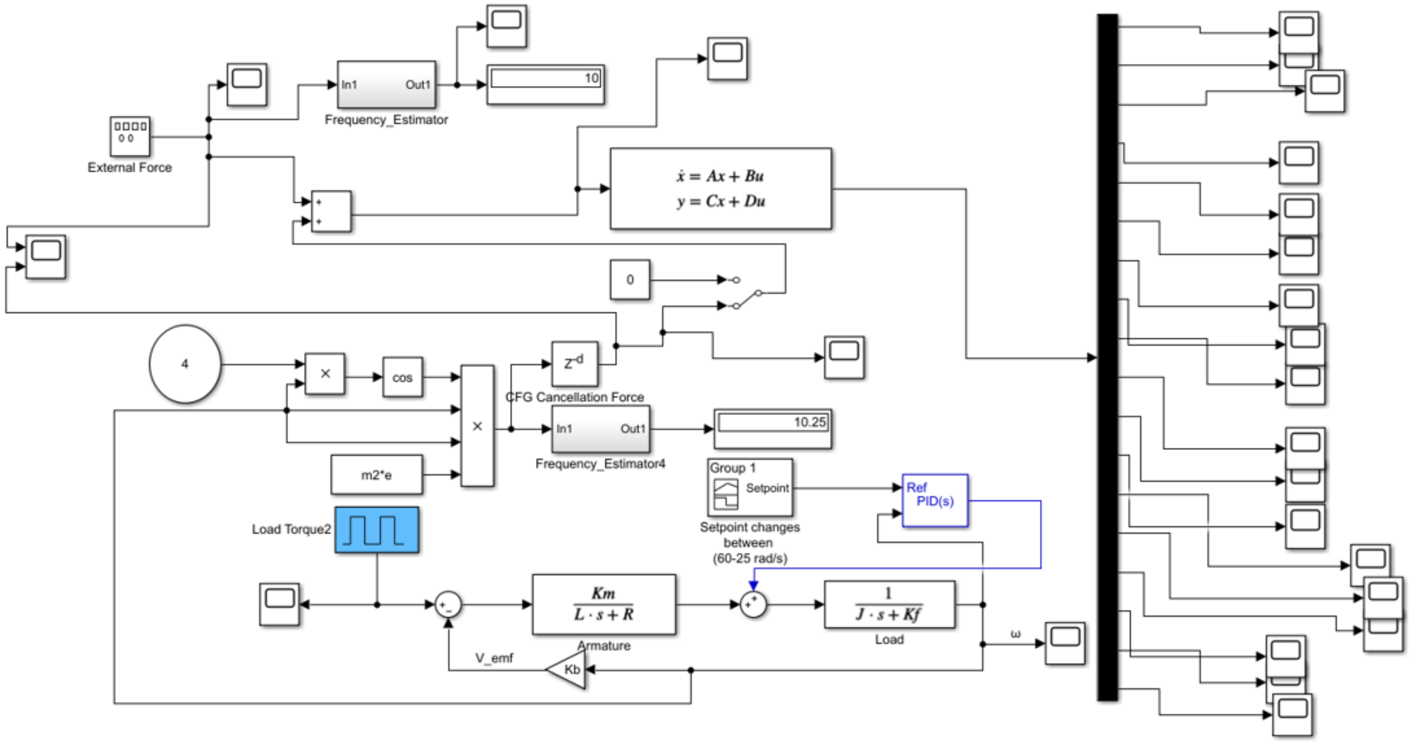

FIGURE 43 – Virtual Tool for Simple Continuous Beam

To keep the figure size concise, only part of the matrices have been.

```
      10        10         6          1MYK       1P,5E16.9
       1         1        10
-1.200486367E-06 1.445243803E-09 7.608073228E-08-2.945812669E-09 6.155900161E-10
-5.351522595E-11-6.115866671E-07 8.904987173E-09 1.059562125E-06 5.716827172E-09
       2         1        10
-2.864379309E-09-4.431501628E-07-1.890152846E-08-4.813427360E-07 6.824016059E-10
 1.827319909E-11 7.393636184E-09 1.196720670E-06-6.406906593E-09 1.742352988E-06
       3         1        10
 3.605827441E-07 2.406144739E-09 8.975159708E-07-3.108681797E-09-1.101321338E-10
-5.001479484E-11 1.223116995E-06 1.320049406E-08-6.165879961E-08 7.859250556E-09
       4         1        10
 2.200890043E-09 4.332520247E-07-9.017848234E-10-6.709662705E-07-1.534195452E-10
 1.406669814E-11-7.048299492E-09-2.052422995E-07-4.128603503E-09 4.251415314E-07
       5         1        10
 5.215091824E-11 1.522406884E-10 8.231722080E-11-2.046804595E-10-3.360163123E-08
 7.554461150E-10-1.987124622E-09 4.778444743E-09 6.042055114E-10 3.650962125E-10
       6         1        10
 1.486719292E-10-7.048732476E-11-8.085861467E-11 7.895255413E-12 3.328779282E-09
-9.578365926E-07 3.541134001E-09-2.090190724E-10 1.334674510E-09 1.913928939E-09
       7         1        10
-1.245651220E-06 1.184901066E-09 1.085962140E-06-1.014500128E-08-2.068027971E-09
 3.535663762E-09 8.367628885E+04-6.887090205E-09-5.521178537E-08 4.746411264E-09
       8         1        10
 4.990795333E-09-2.170963853E-07-8.555502973E-09 1.733787940E-07 4.737306103E-09
-1.446228692E-10-7.810957685E-09 8.367628885E+04-4.375198870E-09-5.195397534E-08
       9         1        10
 6.339978427E-07-8.511733540E-09-2.296037565E-07 3.794582426E-10 6.220410853E-10
 1.235415326E-09-3.304157872E-07-1.893099011E-09 6.354664363E+05-8.346762764E-09
      10         1        10
 9.117684385E-10-1.652224455E-07-1.984517439E-09-1.912048901E-07 1.589413046E-10
 1.953136763E-09 4.697213285E-09 9.697687346E-07-7.891434256E-09 6.354664363E+05
      11         1         1
 1.000000000E+00
```

FIGURE 44 – Reduced KM (Stiffness and Mass Matrix)

```
      10        10         6         1MYC      1P,5E16.9
       1         1        10
 5.000071763E-03 3.873466149E-11-1.577540911E-09-2.148505227E-12 2.120272274E-11
 4.634663780E-12-5.998062267E-09 6.130234104E-11 8.114899100E-09 5.846266742E-11
       2         1        10
 3.822468555E-11 5.000072628E-03 1.108787270E-10 2.732089349E-09-2.476957804E-11
-1.624223367E-12 6.456415505E-11 7.543952525E-09-2.001631344E-11 3.074546016E-09
       3         1        10
 1.055043695E-09-3.524203864E-11 5.000072655E-03-1.676906058E-11 1.731248434E-11
-1.053791003E-11 6.508603409E-09 2.472930399E-11 1.107571167E-09 8.114109434E-11
       4         1        10
-1.797149974E-11 3.591259507E-09 4.340109256E-11 5.000072998E-03 2.847409067E-11
-2.749224305E-12-4.473315495E-11-1.885085110E-09-4.360177935E-11 3.343373995E-09
       5         1        10
 2.332813148E-11-2.848296745E-11 1.927747051E-11 3.324790549E-11 5.000239316E-03
 1.505794511E-10-9.713366096E-12 2.464587190E-11 1.966202192E-12 1.697017432E-12
       6         1        10
 4.140914619E-12-1.555458381E-12-1.144567846E-11-2.670895966E-12 1.315946619E-10
 4.999983799E-03 1.737415162E-11-7.106207060E-13 6.067877133E-12 9.644248614E-12
```

FIGURE 45 – Reduced Damping Matrix

```
       5        10         2         1LMAT     1P,5E16.9
       1         1        10
-9.059906006E-06-8.359551430E-06-8.076429367E-06-7.424503565E-06 1.440569758E-05
 2.641603351E-05 8.367628884E+04 8.367628884E+04 6.354664363E+05 6.354664363E+05
       2         1        10
 3.009967775E-03 2.891288887E-03 2.841905939E-03 2.724794224E-03 3.795483841E-03
 5.139653053E-03 2.892685411E+02 2.892685411E+02 7.971614870E+02 7.971614870E+02
       3         1        10
 4.790512499E-04 4.601629183E-04 4.523033780E-04 4.336644697E-04 6.040700147E-04
 8.180011892E-04 4.603851819E+01 4.603851819E+01 1.268721911E+02 1.268721911E+02
       4         1        10
 1.000000000E+00 1.000000000E+00 1.000000000E+00 1.000000000E+00 1.000000000E+00
 1.000000000E+00 1.000000000E+00 1.000000000E+00 1.000000000E+00 1.000000000E+00
       5         1        10
-9.059906006E-06-8.359551430E-06-8.076429367E-06-7.424503565E-06 1.440569758E-05
 2.641603351E-05 8.367628884E+04 8.367628884E+04 6.354664363E+05 6.354664363E+05
       6         1         1
 1.000000000E+00
```

FIGURE 46 – Eigenvalue Matrix

```
      10        18         2         1DISPS   1P,5E16.9
       1         1        18
-5.725273484E-03 4.897105021E+01 1.814914197E-01-5.725273440E-03-1.338469173E+01
 1.542014328E-03-5.725273441E-03-1.468376969E+01-2.206931641E-03-5.725273475E-03
-7.833858958E+01-1.859052830E-01-5.725273484E-03 5.027012817E+01 1.852403657E-01
-5.725273475E-03-7.963766754E+01-1.896542290E-01
       2         1        18
 6.878894106E-03-7.837770591E-01 4.500789335E+01 6.878894923E-03-3.709646856E-01
-1.571242670E+01 6.878894923E-03-3.623644276E-01-1.697743337E+01 6.878894076E-03
 5.904820352E-02-7.896276009E+01 6.878894106E-03-7.923773168E-01 4.627290002E+01
 6.878894075E-03 6.764846157E-02-8.022776676E+01
       3         1        18
-4.640478045E-03 6.242033030E+01 1.274265341E-01-4.640478083E-03 3.800752661E+01
-3.662169164E-01-4.640478083E-03 3.749892653E+01-3.765011549E-01-4.640478046E-03
 1.257752277E+01-8.804288440E-01-4.640478045E-03 6.292893037E+01 1.377107726E-01
-4.640478046E-03 1.206892269E+01-8.907130826E-01
       4         1        18
-8.151726126E-03-2.821312162E-01-6.534061104E+01-8.151726345E-03-2.185843793E-01
-3.710650867E+01-8.151726346E-03-2.172604869E-01-3.651829820E+01-8.151726104E-03
-1.523897576E-01-7.695985358E+00-8.151726125E-03-2.834551086E-01-6.592882151E+01
-8.151726104E-03-1.510658652E-01-7.107774892E+00
       5         1        18
-4.027356970E+01-1.422761787E-02 2.087187310E-02-4.027356970E+01-2.492583555E-03
 4.868075684E-03-4.027356970E+01-2.248104168E-03 4.534663849E-03-4.027356970E+01
 9.731410162E-03-1.180254616E-02-4.027356970E+01-1.447209797E-02 2.120528590E-02
-4.027356970E+01 9.975889396E-03-1.213595906E-02
       6         1        18
-2.330902251E-02-5.471316072E-03 1.204669488E-03-2.330902098E-02-5.440967243E-03
 1.448676822E-03-2.330902098E-02-5.440334561E-03 1.453759798E-03-2.330902254E-02
-5.409353544E-03 1.702850700E-03-2.330902251E-02-5.471948148E-03 1.199585699E-03
-2.330902254E-02-5.408720726E-03 1.707934541E-03
```

FIGURE 47 – Displacement Matrix

```
       2        10         2         1ACTTRA  1P,5E16.9
       1         1        10
 1.799494054E-01 6.072032005E+01 4.936434505E-01-2.823410238E+01 1.600379741E-02
-2.440073340E-04-6.140395001E-01-1.256872981E+02-4.666877889E-01 7.854972566E+01
       2         1        10
 1.836983514E-01 6.198532672E+01 5.039276891E-01-2.882231284E+01 1.633721001E-02
-2.490909015E-04 6.143890296E-01 1.257588431E+02-4.408696463E-01 7.420419088E+01
       3         1         1
 1.000000000E+00
```

FIGURE 48 – Actuation Force Matrix

20x20 double

		8	9	10	11	12	13	14	15	16	17
8	0	0	0	0	0	0	0	0	0	0	0
9	0	0	0	0	0	0	0	0	0	0	0
10	0	0	0	0	0	0	0	0	0	0	0
11	0	0	0	0	-0.0050	-3.8225e-11	-1.0550e-09	1.7972e-11	-2.3328e-11	-4.1409e-12	-8.0142e-10
12	0	0	0	0	-3.8735e-11	-0.0050	3.5242e-11	-3.5913e-09	2.8483e-11	1.5555e-12	3.0875e-11
13	0	0	0	0	1.5775e-09	-1.1088e-10	-0.0050	-4.3401e-11	-1.9277e-11	1.1446e-11	-5.0358e-09
14	0	0	0	0	2.1485e-12	-2.7321e-09	1.6769e-11	-0.0050	-3.3248e-11	2.6709e-12	2.6298e-11
15	0	0	0	0	-2.1203e-11	2.4770e-11	-1.7312e-11	-2.8474e-11	-0.0050	-1.3159e-10	1.1900e-11
16	0	0	0	0	-4.6347e-12	1.6242e-12	1.0538e-11	2.7492e-12	-1.5058e-10	-0.0050	-1.7848e-11
17	04	0	0	0	5.9981e-09	-6.4564e-11	-6.5086e-09	4.4733e-11	9.7134e-12	-1.7374e-11	-418.3864
18	0	-8.3676e+04	0	0	-6.1302e-11	-7.5440e-09	-2.4729e-11	1.8851e-09	-2.4646e-11	7.1062e-13	1.3910e-11
19	0	0	-6.3547e+05	0	-8.1149e-09	2.0016e-11	-1.1076e-09	4.3602e-11	-1.9662e-12	-6.0679e-12	-5.6755e-09
20	0	0	0	-6.3547e+05	-5.8463e-11	-3.0745e-09	-8.1141e-11	-3.3434e-09	-1.6970e-12	-9.6442e-12	-5.4836e-11

FIGURE 49 – A Matrix

18x20 double

	1	2	3	4	5	6	7	8	9	10
1	-5.1870e-08	5.7504e-08	-3.7478e-08	-6.0523e-08	5.8017e-04	6.1573e-07	2.8827e-05	-5.3735e-05	-3.2990e-05	-2.8771e-06
2	4.4367e-04	-6.5520e-06	5.0413e-04	-2.0947e-06	2.0496e-07	1.4453e-07	-6.4263e+06	3.1395e+04	-4.7154e+07	-2.8016e+05
3	1.6443e-06	3.7625e-04	1.0292e-06	-4.8512e-04	-3.0067e-07	-3.1823e-08	3.1395e+04	6.4263e+06	2.8016e+05	-4.7154e+07
4	-5.1870e-08	5.7504e-08	-3.7478e-08	-6.0523e-08	5.8017e-04	6.1573e-07	-2.8291e-05	5.3731e-05	3.4390e-05	3.2318e-06
5	-1.2126e-04	-3.1011e-06	3.0697e-04	-1.6229e-06	3.5907e-08	1.4373e-07	4.0907e+06	-1.9985e+04	2.7614e+06	1.6407e+04
6	1.3971e-08	-1.3135e-04	-2.9577e-06	-2.7550e-04	-7.0128e-08	-3.8268e-08	-1.9985e+04	-4.0907e+06	-1.6407e+04	2.7614e+06
7	-5.1870e-08	5.7504e-08	-3.7478e-08	-6.0523e-08	5.8017e-04	6.1573e-07	-2.8362e-05	5.3722e-05	3.4198e-05	3.2616e-06
8	-1.3303e-04	-3.0292e-06	3.0286e-04	-1.6131e-06	3.2386e-08	1.4371e-07	4.0967e+06	-2.0014e+04	3.3577e-05	1.9574e-06
9	-1.9995e-08	-1.4192e-04	-3.0408e-06	-2.7113e-04	-6.5325e-08	-3.8403e-08	-2.0014e+04	-4.0967e+06	-6.4755e-06	2.2514e-05
10	-5.1870e-08	5.7504e-08	-3.7478e-08	-6.0523e-08	5.8017e-04	6.1573e-07	3.1700e-05	-5.6992e-05	-3.2178e-05	-3.4960e-06
11	-7.0974e-04	4.9362e-07	1.0158e-04	-1.1314e-06	-1.4019e-07	1.4289e-07	-6.4263e+06	3.1395e+04	4.7154e+07	2.8016e+05
12	-1.6843e-06	-6.6009e-04	-7.1107e-06	-5.7139e-05	1.7002e-07	-4.4983e-08	3.1395e+04	6.4263e+06	-2.8016e+05	4.7154e+07
13	-5.1870e-08	5.7504e-08	-3.7478e-08	-6.0523e-08	5.8017e-04	6.1573e-07	2.8867e-05	-5.3804e-05	-3.3028e-05	-2.8796e-06
14	4.5544e-04	-6.6239e-06	5.0824e-04	-2.1045e-06	2.0848e-07	1.4455e-07	-6.7395e+06	3.2925e+04	-5.1175e+07	-3.0404e+05
15	1.6783e-06	3.8682e-04	1.1122e-06	-4.8949e-04	-3.0548e-07	-3.1688e-08	3.2925e+04	6.7395e+06	3.0404e+05	-5.1175e+07

FIGURE 50 – C Matrix

20x1 double

	1
1	0
2	0
3	0
4	0
5	0
6	0
7	0
8	0
9	0
10	0
11	185.2404
12	4.6273e+04
13	137.7108
14	-6.5929e+04
15	21.2053

18x1 double

	1
1	-9.1716e-05
2	-3.2005e-06
3	1.8552e+07
4	6.2981e-05
5	3.1000e-06
6	-2.5683e+06
7	6.3034e-05
8	4.6906e-05
9	-2.3214e+06
10	-9.7596e-05
11	2.1648e-05
12	-2.9368e+06
13	-9.1848e-05
14	7.7335e-06
15	1.9460e+07

FIGURE 51 – B and D Matrices

The results for the tool validation for the simple beam have been shown. Figure 52 shows the excitation force used for this simulation. A sinusoidal excitation of frequency 10 Hz (62.83 rad/s) has been applied. Figure 53 shows the the shaft rotation of the DC motor. The time taken by the PID controller to achieve 10 Hz (62.83 rad/s) stabilization is also shown. Figure 54 shows the parameters for the PID controller tuning to achieve this stabilization for the DC motor. Equation (64) defines the PID equation used to tune the controller.

$$P(b.r - y) + I\frac{1}{s}\,(r - y) + D\frac{N}{1+N\frac{1}{s}}\,(c.r - y)$$

(64)

Where P is the proportional coefficient, I is the integral coefficient, D is the derivative coefficient, N is the filter coefficients, b and c are the setpoint weights, r and y are the tuning variables.

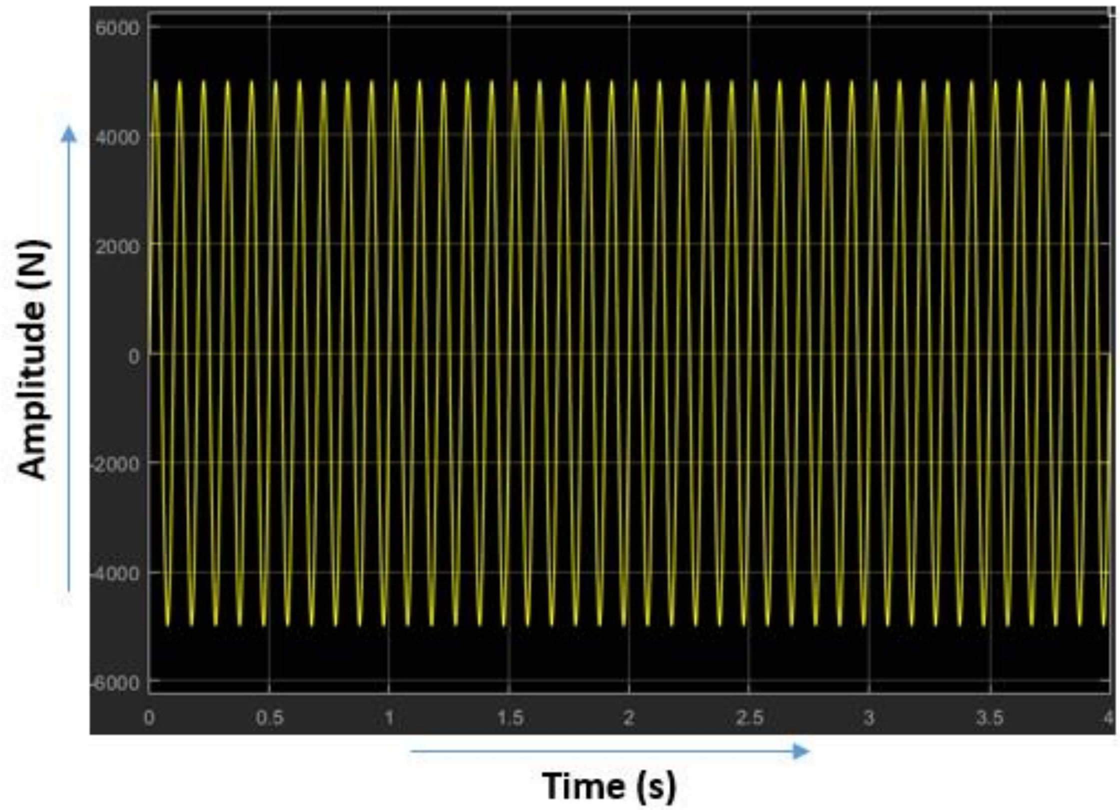

FIGURE 52 – Excitation Force

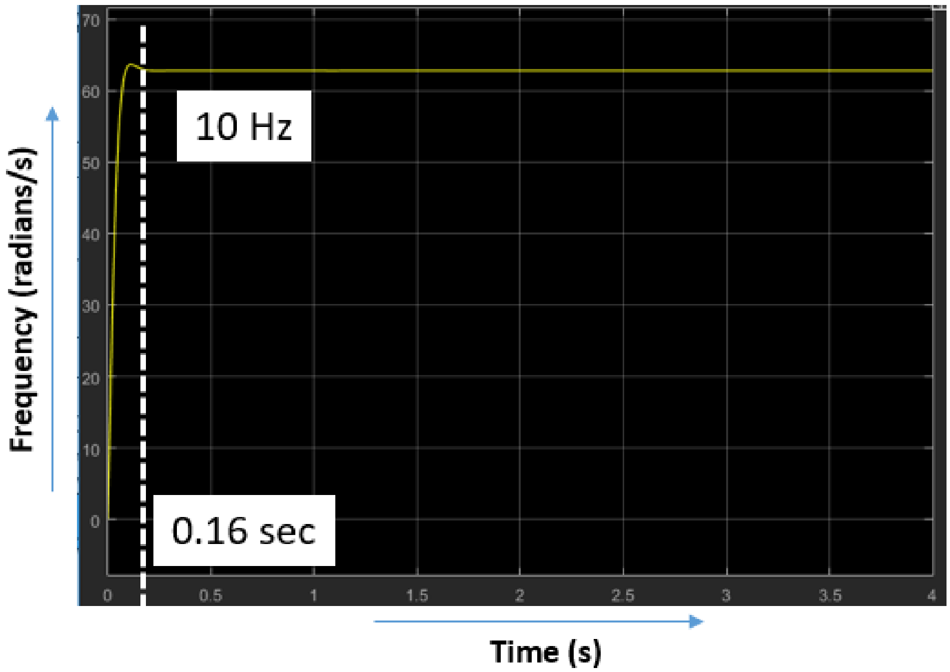

FIGURE 53 – Angular Velocity from DC motor shaft

Proportional (P):	1.74
Integral (I):	54.36
Derivative (D):	0.005
Filter coefficient (N):	120.70
Setpoint weight (b):	0.29
Setpoint weight (c):	0.0019

FIGURE 54 – PID Controller Parameters after tuning.

Figure 55 shows the acceleration response when the actuator is switched off. The actuator is then switched on after 0.5 seconds. Figure 56 shows an overlay of the excitation force and actuation force. A zoomed image is also shown in Figure 56 to show the equal and opposite forces with same phase. The amplitude of the force is governed by the imbalanced mass and eccentricity. Figure 57 shows the acceleration response after the actuator is switched on after 0.5 seconds.

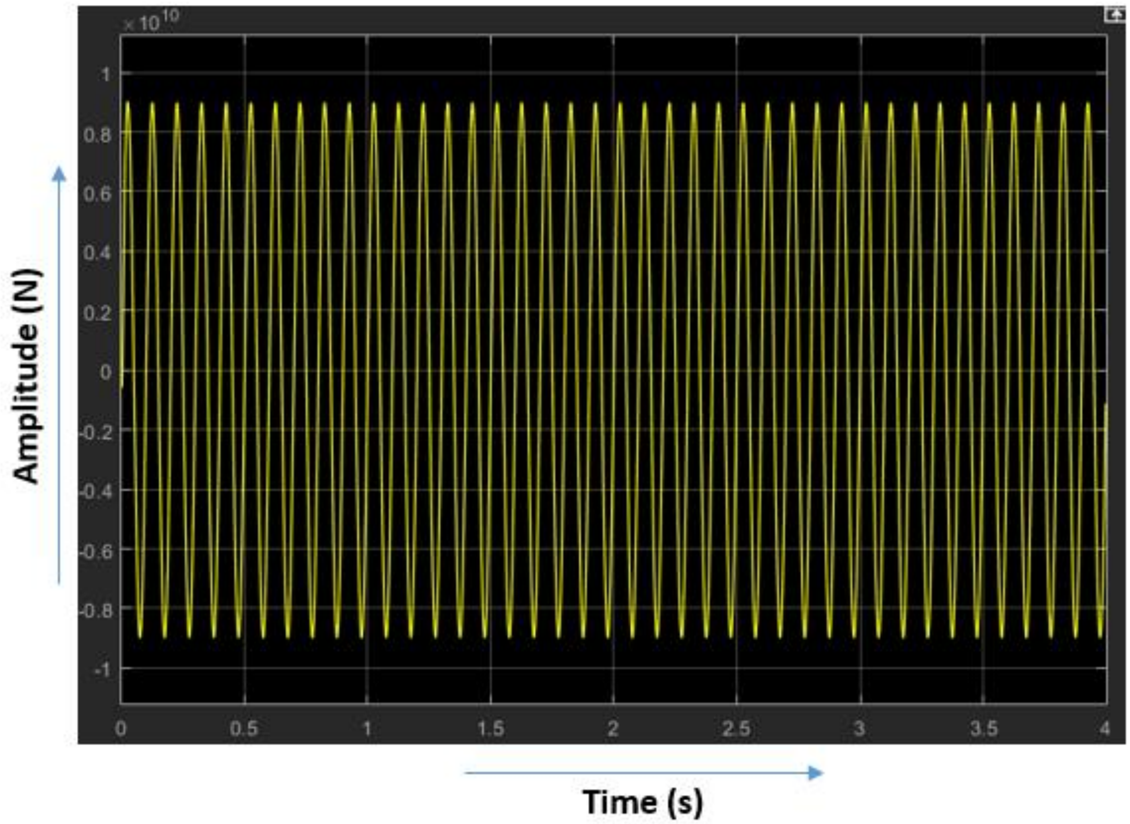

FIGURE 55 – Acceleration Response for Simple continuous beam

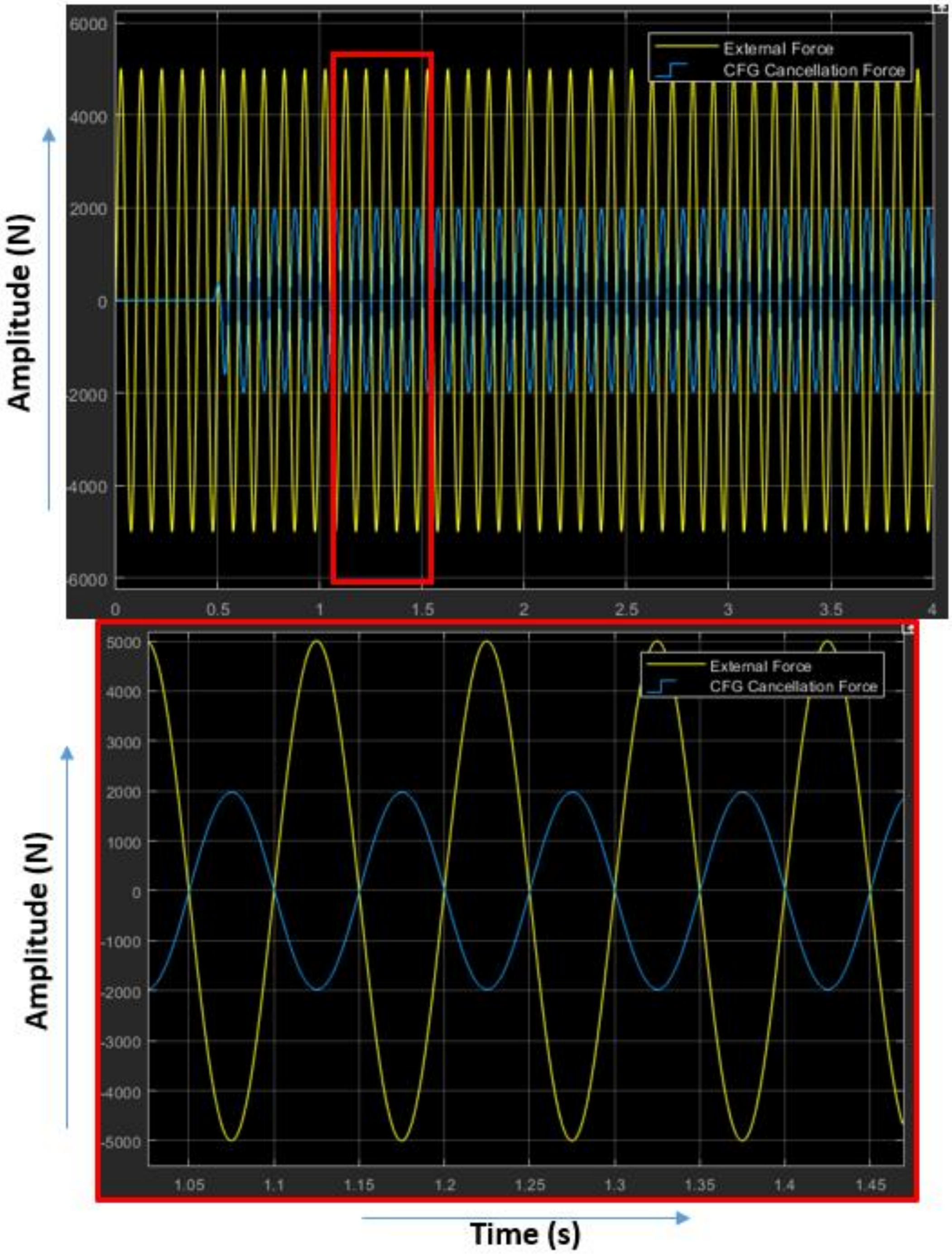

FIGURE 54 – Excitation Force and Actuation Force Overlay

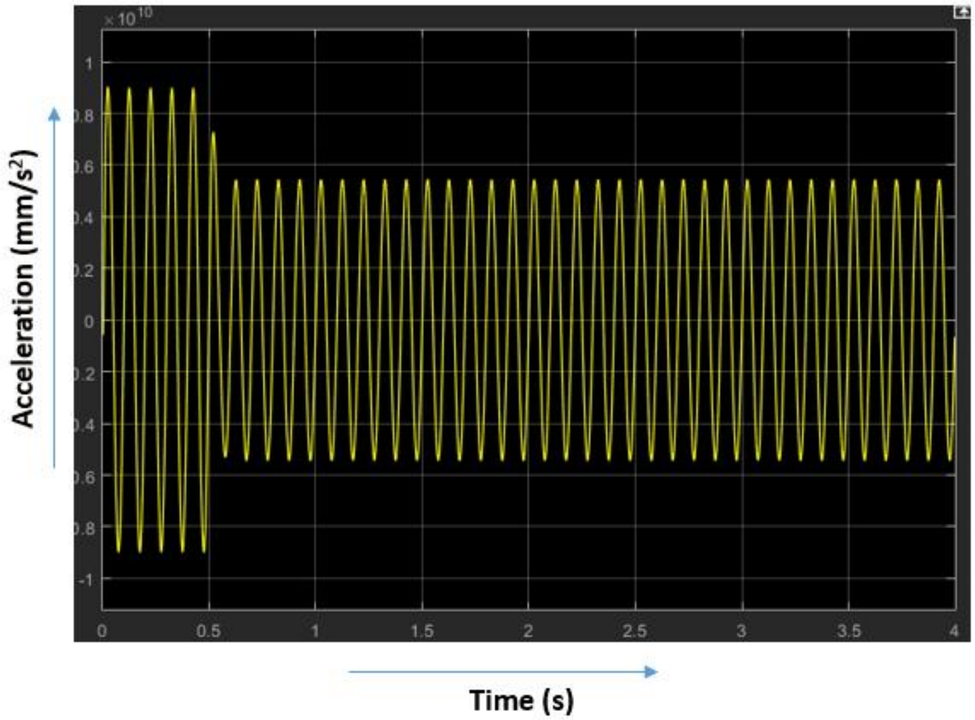

FIGURE 57 – Acceleration Response after CFG Actuator switched ON at 0.5 seconds

This validates that the virtual tool is working to cancel external forces for the simple beam system. This example has its limitations, which will be discussed later in the thesis.

In the next section a finite element model will be created to represent a truck frame and a state space system will be described for the truck frame and the virtual tool will be applied to attempt to cancel the external force excitation for the truck frame. A modal analysis will also be performed to compute the natural frequencies of the frame. The response excitation will be shown due to an external force that excites the frame natural modes , and the virtual tool will be applied to reduce the amplitudes for the response at the frequency of excitation.

CHAPTER SIX

VIRTUAL MODEL DEVELOPMENT AND FORCE CANCELLATION TRUCK FRAME

6.1 FINITE ELEMENT MODELLING AND ANALYSIS

With the results from all the previous sections, a state space model for a full vehicle truck frame with multiple degree of freedom has been defined in this section. The first step in this is to model a finite element model of a 169-inch wheelbase truck frame. Figure 58 shows the finite element model of the truck frame. After standard model validation, the first step is to run the normal mode analysis to determine the first bending mode of the frame. An beaming issue has been identified in this particular vehicle, which has been observed at around 8 Hz at a full vehicle level. This is primarily due to high acceleration amplitudes due to the vertical bending mode of the frame. Therefore the objective has been defined to reduce the output acceleration amplitude at the affected node of the first bending mode of the frame. To work with this problem without making it computationally expensive, the full vehicle model has been stripped down to its frame level without any trims. The reduced finite element model has a total of 156271 elements. Total mass of the frame is 295 kg. The frame is excited at the front suspension location and the CFG is placed at the center node of the frame to cancel and/or reduce the maximum amplitude for the bending mode. Figure 58 shows the bending mode shape and frequency of the frame.

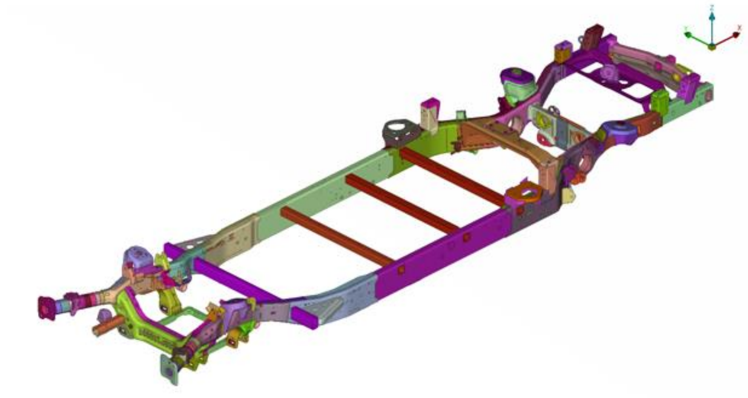

FIGURE 58 – Finite Element Model of a Truck Frame

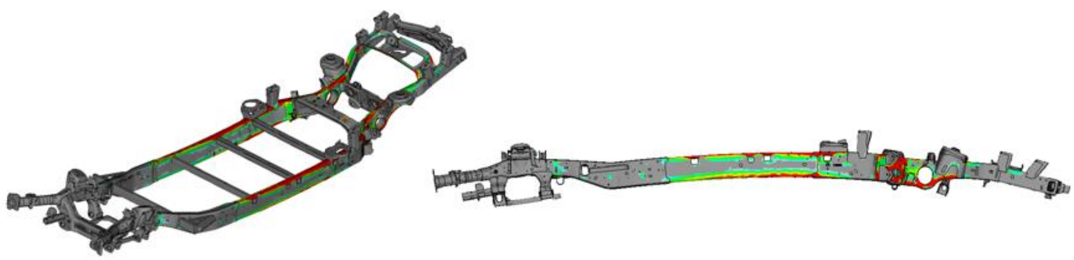

FIGURE 59 – Bending Mode Shape at 19.75 Hz

6.2 MATRIX EXTRACTION AND STATE SPACE REPRESENTATION

In this section a portion of the stiffness, mass, damping, displacement, eigenvalue and force matrices have been shown. To keep the problem computationally less expensive the matrices have been converted into modal matrices using DMAP in NASTRAN. Figures 60-64 show all the matrices.

```
     278      278        6        1MYK      1P,5E16.9
       1        1      278
-8.491387116E-06-1.843903162E-06-5.163452545E-07 6.678707066E-07-4.479374972E-07
-7.084593442E-07-1.113203069E-08 2.394374595E-07-2.661882467E-07 3.117213224E-06
 9.335967139E-07 1.890258074E-06-8.379242063E-08-7.153259441E-08-7.095484370E-08
-1.269963490E-06 7.662137921E-07-5.895559963E-07-8.984253298E-07-4.768185441E-06
-8.020251206E-08 1.063794436E-06-1.456155460E-07 4.476349312E-07-6.748886275E-07
-1.106078881E-06-4.000921453E-07-2.939130033E-06 5.716981187E-07-4.535771872E-08

  ......

  ......

-1.658592708E-11 1.807943031E-11-1.147576131E-11 1.709250103E-11-1.232163677E-12
 2.078642813E-12-2.637736383E-12-2.254319669E-12 8.807954366E-13-6.388500839E-13
 1.212904777E-12 1.277625575E-12 5.075037612E-13 3.076715965E-12 6.597986046E-13
 1.262080718E-13 4.755328076E-13 1.000000000E+00
     279        1        1
 1.000000000E+00
```

FIGURE 60 – KM (Stiffness and Mass Matrix)

```
     278      278        6        1MYC      1P,5E16.9
       1        1      278
 5.000014055E-03 5.331461676E-09 1.699219551E-10-2.556746674E-09-3.907736093E-10
 2.951687061E-10 2.919640590E-10-1.272769114E-09-1.177811455E-09-1.385867336E-08
-2.790232872E-09-4.466826515E-09 8.574267680E-10-7.006057220E-11 5.285873034E-10
 3.067630600E-09-1.365021039E-08-1.727096143E-09 1.667767058E-09 1.363149331E-08
-3.945084020E-10 1.353938813E-09 2.536320425E-10 2.064140725E-10 1.763442048E-09
 7.772496583E-10 4.419470336E-09 1.481761386E-08-8.567396273E-10 3.627613466E-11

  ......

  ......

-1.176148999E-06 1.269154950E-06-8.163829079E-07 1.200284714E-06-8.836201459E-08
 1.461462489E-07-1.767076583E-07-1.512053984E-07 4.653702490E-08-5.659967428E-08
 8.164761311E-08 7.696871762E-08 4.658977559E-08 2.210824732E-07 5.649417290E-08
 9.424638847E-09 3.317222763E-08 7.053469807E+04
     279        1        1
 1.000000000E+00
```

FIGURE 61 – Damping Matrix

```
       5      278        2        1LMAT     1P,5E16.9
       1        1      278
-1.651728255E-06 6.339479341E-08 1.974950834E-07 7.130137476E-07 2.535221611E-06
 5.960586677E-06 7.197598948E+03 1.503524092E+04 1.653043141E+04 2.005061310E+04
 2.969384490E+04 3.544102778E+04 4.111527833E+04 4.757893026E+04 5.327709248E+04
 7.489438401E+04 8.385213039E+04 9.528387930E+04 1.060145386E+05 1.230012490E+05
 1.965234444E+05 2.022024341E+05 2.181947769E+05 2.194281196E+05 2.362790765E+05
 2.604722732E+05 2.897276930E+05 2.990302586E+05 3.208645499E+05 3.737766382E+05

 ......

 ......

 1.299688090E+07 1.312208743E+07 1.323322727E+07 1.325448338E+07 1.327266043E+07
 1.337740922E+07 1.358670038E+07 1.365324628E+07 1.372579423E+07 1.376412320E+07
 1.383790022E+07 1.389313520E+07 1.398044116E+07 1.398267770E+07 1.399973460E+07
 1.404874634E+07 1.408585815E+07 1.410693861E+07
       6        1        1
 1.000000000E+00
```

FIGURE 62 – Eigenvalue Matrix

```
     278       45        2        1DISPS    1P,5E16.9
       1        1       45
-1.182248964E-03-1.686710983E+00-8.542601288E-02-2.205202427E-03-1.018845764E+00
-1.041595235E-01-1.587003925E-02-5.523371093E-01-1.477323202E-01-7.813003560E-03
-1.678171201E-01-1.381638287E-01 3.272399391E-02 3.397305572E-01-5.513900965E-02
 1.673417132E-02 5.969288135E-01-9.906885414E-02 4.746703422E-03 1.200531697E+00
-1.420439567E-01 1.265073539E-02 1.457289572E+00-1.297126464E-01 1.576260325E-02
-2.398193904E+00-2.814332526E-02 1.995694450E+00 2.910827314E-01 1.677818287E-01

 ......

 ......

 4.118306811E-01-6.163663539E-01-5.745217392E-02-9.322973636E-01 6.595175500E-01
 2.064053159E-02-3.261788917E-01-3.724149969E-01-3.898246216E-02 1.441127735E-01
-1.696242983E-01 2.411002073E-02 2.958345071E-02 1.500341532E-01 4.366021743E-02
-3.160740485E-02 2.885880726E-01 4.567341930E-02 2.187078730E-03 4.045010967E-01
     279        1        1
 1.000000000E+00
```

FIGURE 63 – Displacement Matrix

```
      14      278        2        1PGTRA    1P,5E16.9
       1        1      278
 1.677818287E-01-5.603842069E-01-6.049041976E-01 1.108087523E+00-5.951833876E-01
-2.974475040E+00-1.130413091E-01 8.650261589E-01-1.432239705E+00-1.867805192E+00
-1.962910082E-01 9.291476055E-01-3.152341158E-01-5.017655843E-01-1.168094543E-01
 6.603508087E-01-9.488826438E-01-1.222823466E-02-5.606369014E-01-6.602867020E-02
-1.046414379E-01 8.038181528E-01-2.113438024E-01 5.965542746E-01 6.360684611E-01
-1.011844826E-01-5.853414685E-02 9.307005154E-02 5.000766389E-01 8.581914701E-02

 ......

 ......
-1.702707243E-01-5.559979072E-01-4.752665581E-01-3.355056854E-01-2.435850482E-01
-7.317580741E-02 3.619760924E-01 7.028364959E-01-6.987459571E-02 2.675298222E-01
-8.364191765E-02 8.057920682E-03 7.398210757E-02 6.065660858E-02 1.745957113E-01
 9.439927817E-02-1.159997353E-01-6.163663539E-01
      15        1        1
 1.000000000E+00
```

FIGURE 64 – Force Matrix

These matrices are then used to formulate the A, B, C and D matrices to form out simple beam state space form. Figures 65-68 show the A, B, C and D matrices, respectively. To keep the figure size concise, only part of the matrices have been shown. In this section, modal superposition has been used to solve for the final solution, therefore another state space system is defined which uses the A, C matrices from before but new B2 and D2 matrices have been created to represent the cancellation forces. The B and D matrices include force columns and as modal superposition requires the new state space system to be combined with the first state space system for the final solution. Figures 69 and 70 show a portion of the B2 and D2 matrices. Full matrices have been included in the Appendix

556x556 double

	1	2	3	4	5	6	7	8	9	10
278	0	0	0	0	0	0	0	0	0	0
279	1.6517e-06	0	0	0	0	0	0	0	0	0
280	0	-6.3395e-08	0	0	0	0	0	0	0	0
281	0	0	-1.9750e-07	0	0	0	0	0	0	0
282	0	0	0	-7.1301e-07	0	0	0	0	0	0
283	0	0	0	0	-2.5352e-06	0	0	0	0	0
284	0	0	0	0	0	-5.9606e-06	0	0	0	0
285	0	0	0	0	0	0	-7.1976e+03	0	0	0
286	0	0	0	0	0	0	0	-1.5035e+04	0	0
287	0	0	0	0	0	0	0	0	-1.6530e+04	0
288	0	0	0	0	0	0	0	0	0	-2.0051e+04

FIGURE 65 – A Matrix

556x1 double

	1
279	-0.0281
280	0.2225
281	0.0998
282	-0.7193
283	-0.0092
284	-2.7555
285	-0.1733
286	1.4073
287	0.0060
288	0.0299
289	-0.1760

.
.
.
.
.

FIGURE 66 – B Matrix

45x556 double

	1	2	3	4	5	6	7	8	9	10
1	-1.9528e-09	-5.4626e-09	1.0849e-08	2.5993e-07	3.7841e-06	-9.2951e-08	-1.2746e+03	-5.7660e+03	-159.3434	-328.4674
2	-2.7860e-06	6.5758e-08	7.1150e-08	-6.9730e-07	7.6925e-07	1.9856e-06	18.4175	200.4047	9.0315e+03	-366.4612
3	-1.4110e-07	-2.0504e-08	-8.4898e-08	3.0841e-07	7.1686e-08	1.2864e-05	435.0808	-667.3921	-1.1436e+03	-2.2648e+03
4	-3.6424e-09	-5.6002e-09	9.3869e-09	2.5307e-07	3.7867e-06	-1.8162e-07	-1.3356e+03	-3.4484e+03	-175.3868	-369.1596
5	-1.6829e-06	7.8722e-08	-7.0659e-09	-3.9888e-07	5.5296e-07	1.3906e-06	-9.1063	111.7218	-3.4760e+03	5.2254e+03
6	-1.7204e-07	-2.6544e-08	-1.5895e-07	-8.5910e-09	1.8662e-07	8.5626e-06	-405.9824	1.8244e+04	-849.8473	-1.1994e+03
7	-2.6213e-08	-5.8765e-09	1.0824e-08	2.4807e-07	3.7902e-06	-1.7142e-07	-1.3797e+03	-2.1460e+03	-294.2333	-454.5600
8	-9.1231e-07	8.8185e-08	-5.5707e-08	-2.2715e-07	4.3296e-07	1.0639e-06	-28.6914	66.2080	-1.1317e+04	1.0617e+04
9	-2.4401e-07	-3.1713e-08	-2.1260e-07	-1.8332e-07	2.3096e-07	5.6134e-06	-761.7431	2.3906e+04	-443.8762	-85.3315
10	-1.2905e-08	-5.7121e-09	9.9969e-09	2.5110e-07	3.7881e-06	-1.7628e-07	-1.4572e+03	-928.5457	-213.8763	-494.3441

.
.
.

FIGURE 67 – C Matrix

45x1 double

	1
1	-0.7200
2	-0.3601
3	0.2960
4	-0.1618
5	0.5856
6	-0.3240
7	-0.5029
8	0.2479
9	-0.4632
10	-0.4244

FIGURE 68 – D Matrix

556x1 double

	1
279	0.1678
280	-0.5604
281	-0.6049
282	1.1081
283	-0.5952
284	-2.9745
285	-0.1130
286	0.8650
287	-1.4322
288	-1.8678

FIGURE 69 – B2 Matrix

45x1 double

	1
1	0.4484
2	4.0739
3	0.6597
4	-1.0593
5	0.8808
6	-0.1825
7	0.6128
8	-2.1205
9	1.2848
10	0.6747

.
.
.
.
.

FIGURE 70 – D2 Matrix

6.3 VIRTUAL TOOL MODIFICATION AND RESULTS FOR TRUCK FRAME

In this section the virtual tool modification for the truck frame will be presented. All the results generated for this model will also be presented along with the Simulink model. This section will also include the application of the virtual tool to cancel external excitation forces.

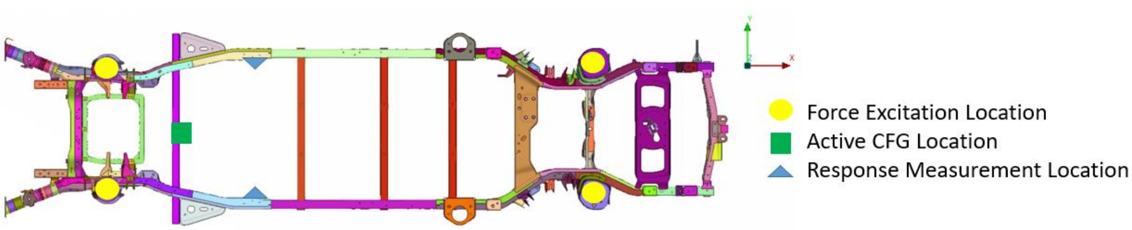

FIGURE 71 – Excitation, Response and ACFG Locations

Based on the characteristics of the truck frame under consideration, initially the point highlighted with the green square in Figure 71 has been selected as the location to place the ACFG tool. The yellow circular points have been selected as the points of road input or external force excitation. The triangular blue points have been selected as the output measurement points due to ease of accessibility to place accelerometers on the frame. All matrix calculations and extractions shown in the previous section to form the state space representation of this frame have been done with these points as the locations for cancellation force actuation using the Active CFG principle, output response measurement and external force excitation.

As mentioned in the previous section for the frame Simulink model, the principle of modal superposition has been implemented to reduce the matrix calculation complexity and thereby reduce the computational time. In this scenario, the state space representation of the frame without the ACFG cancellation force actuation is solved using the external excitation force and the output response is generated. In parallel the state space representation of the frame with the ACFG cancellation force actuation is solved to generate the output response and then the results are combined/superimposed to calculate the final output response. Figure 72 shows the modified Simulink model representing the truck frame.

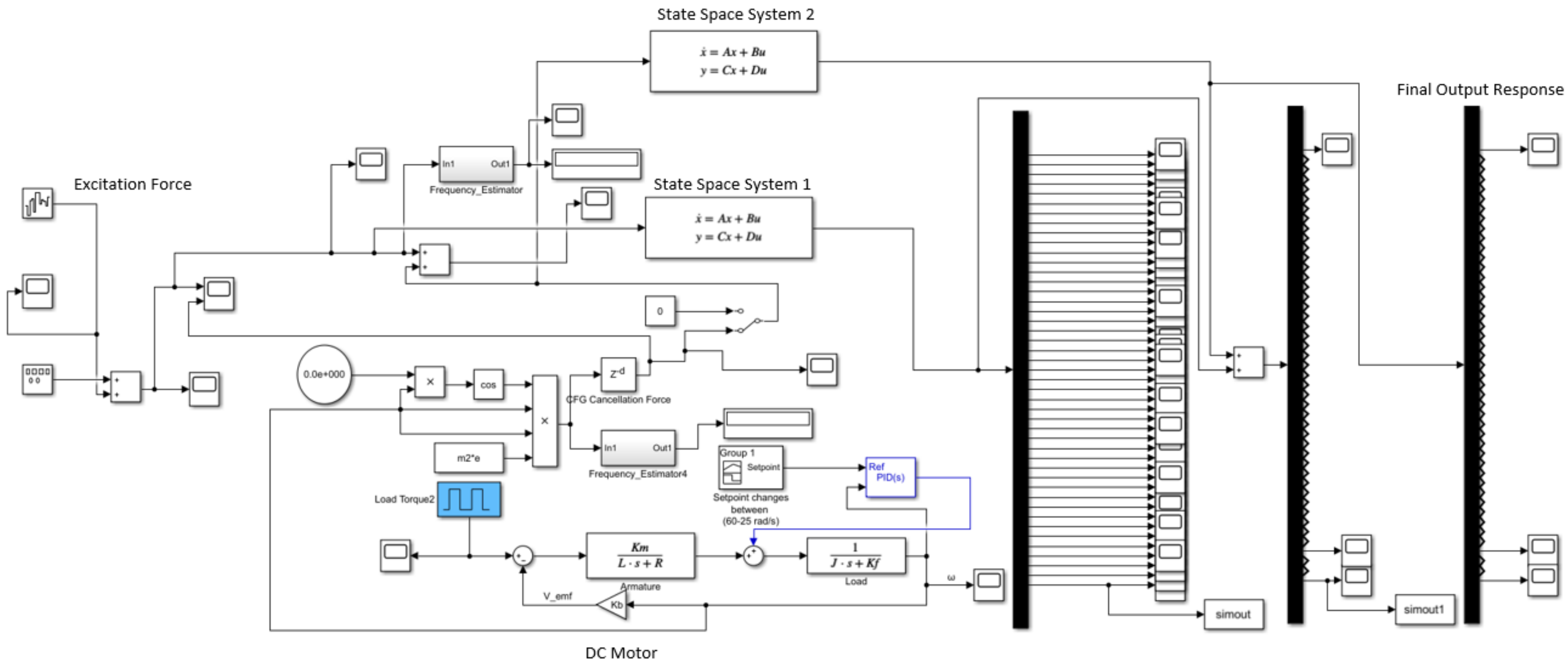

FIGURE 72 – Simulink Model for the Truck Frame

As stated in an earlier section, the frequency of the dominant amplitude at frame level for this truck has been identified as 19.4 Hz. The objective is to reduce the amplitude of this dominant peak using the ACFG tool, which include an imbalanced mass and DC motor with properties defined in Sections 5.3 and 4.4, respectively.

Figure 73 shows the external excitation force introduced to the model and Figure 74 shows the output from the DC motor for the angular velocity of the shaft and time taken by the controller to achieve steady state. These responses are used to calculate the actuation force used for cancellation.

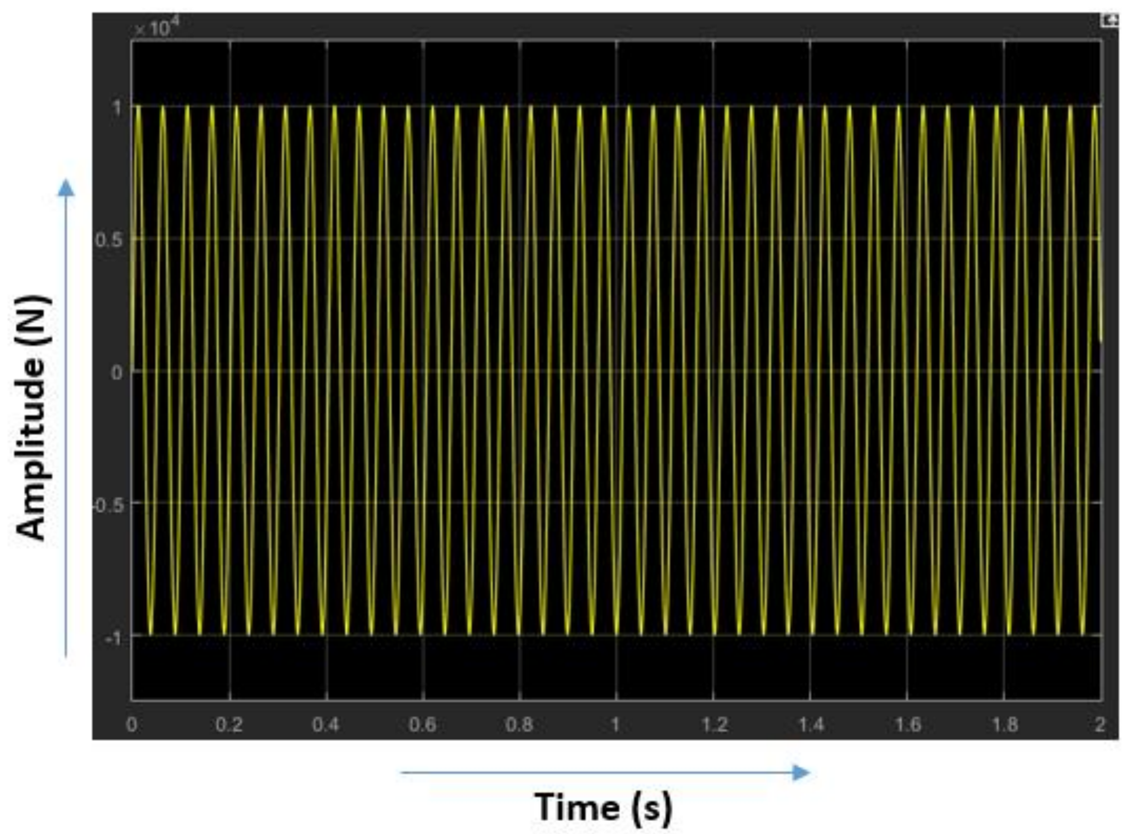

FIGURE 73 – External Excitation Force for the Truck Frame

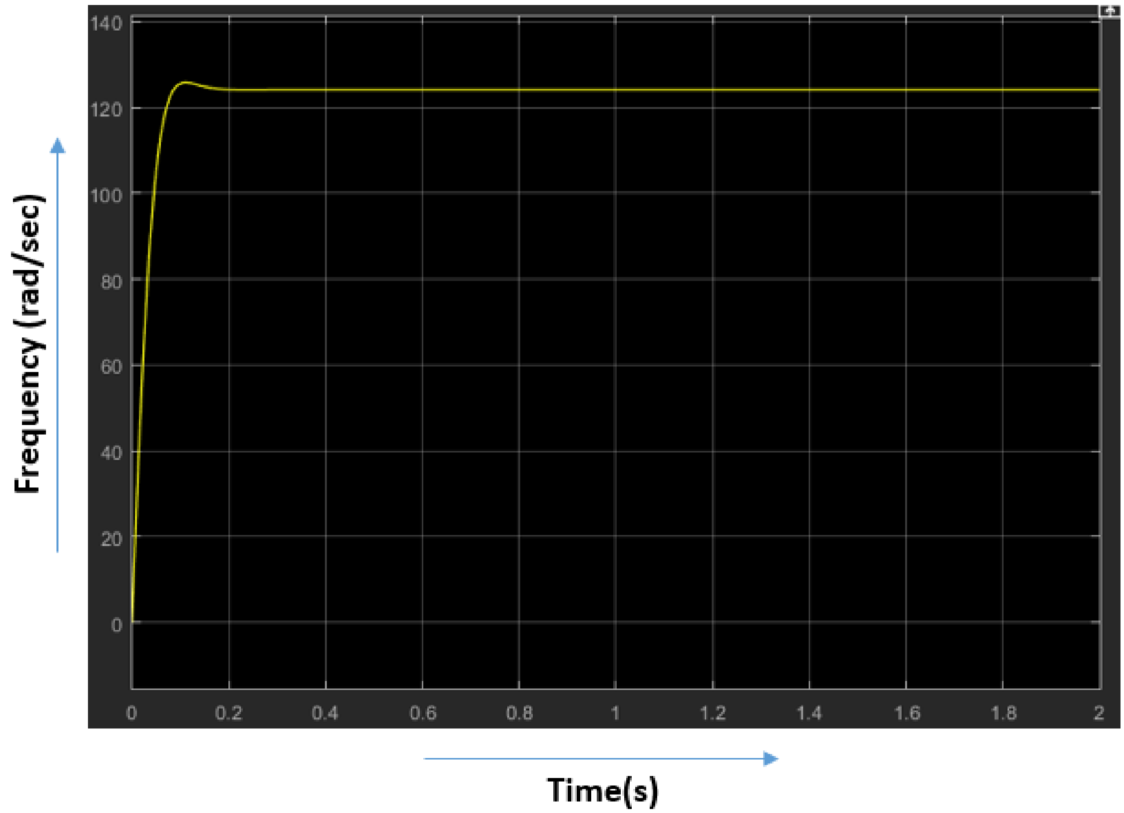

FIGURE 74 – Angular Velocity Output from DC Motor

Figure 75 shows the excitation and cancellation forces overlaid when the ACFG is switched ON and Figure 76 shows the final output response, with amplitude reduction, for the truck frame under the given external excitation as the ACF is switched ON. The time stamp of about 0.45 seconds shows the before and after effect of the ACFG on the amplitude reduction of the output response for this model. For the location shown in Figure 71, the tool with given imbalanced mass and DC motor properties shows an improvement of about 55%, with the control taking about 0.213 seconds to achieve the steady state angular velocity for the DC motor shaft.

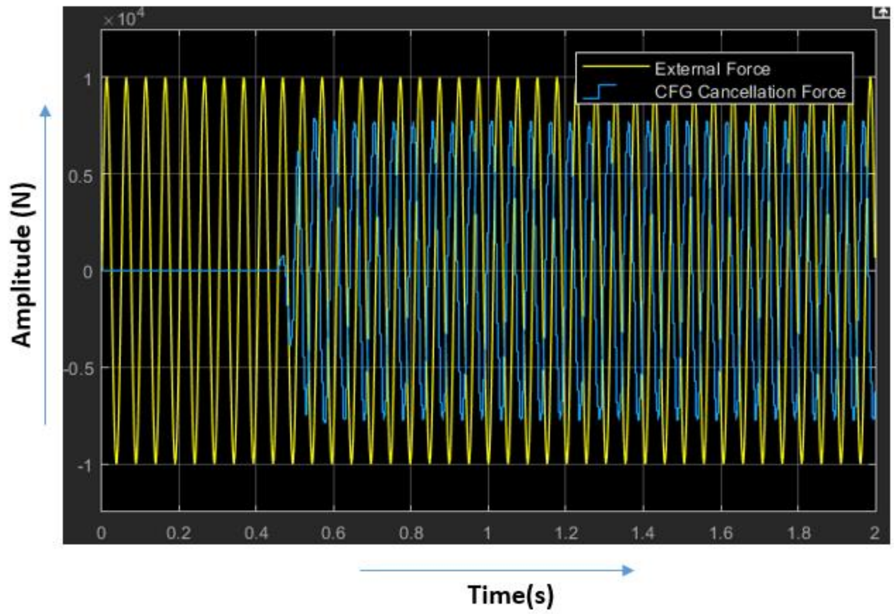

FIGURE 75 – External force and Cancellation force overlay

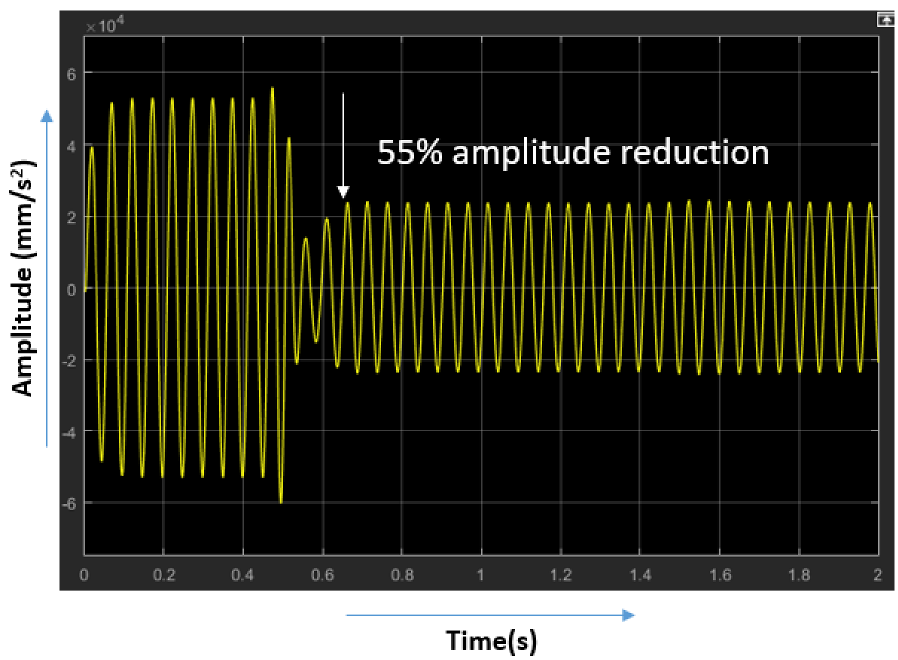

FIGURE 76 – Final output response with amplitude reduction

Following this, the robustness of the Simulink model developed for the truck frame was tested by perturbing the external force excitation with random white noise. The objective of this study was to see if the tool still reduces the concerning frequency of excitation. Figure 77 shows the external force excitation after the white noise was introduced and combined with the original excitation force. Figure 78 shows the overlay of the excitation force and the cancellation force from the actuator. It has been noted that the excitation force is random due to the white noise and the actuation force is steady state as it is an output from the angular velocity of the DC motor. The amplitude of the cancellation force is only dependent on the mass, the fixed eccentricity and the steady angular velocity.

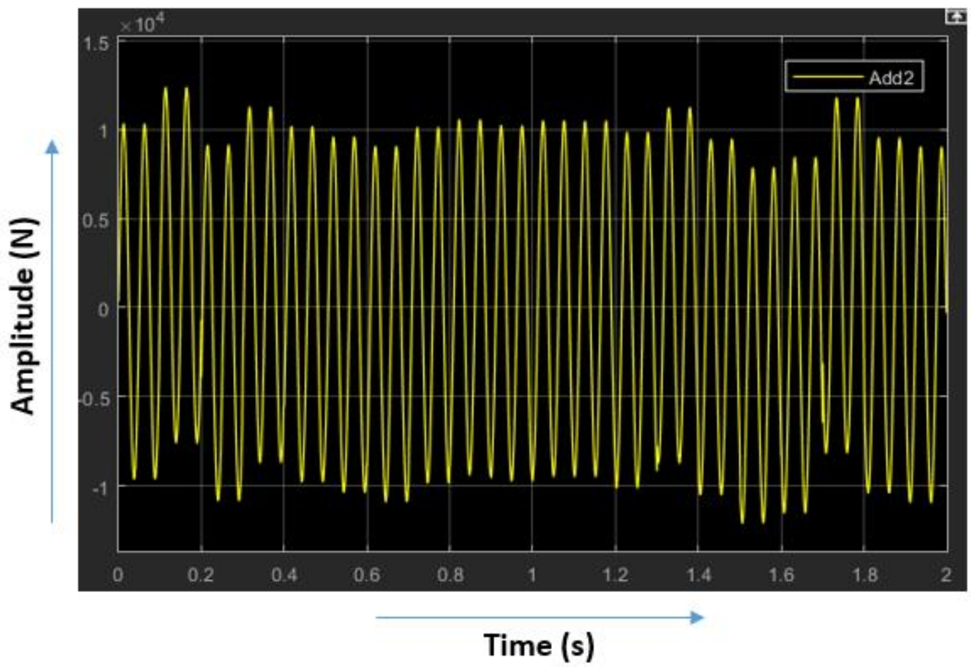

FIGURE 77 – External Force excitation combined with random white noise

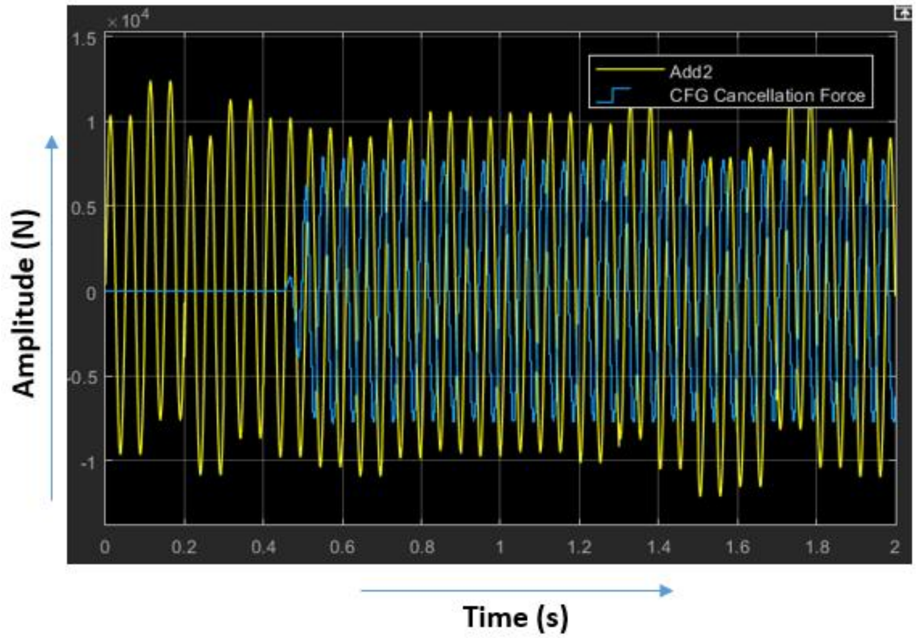

FIGURE 78 – Excitation force and Cancellation force overlay

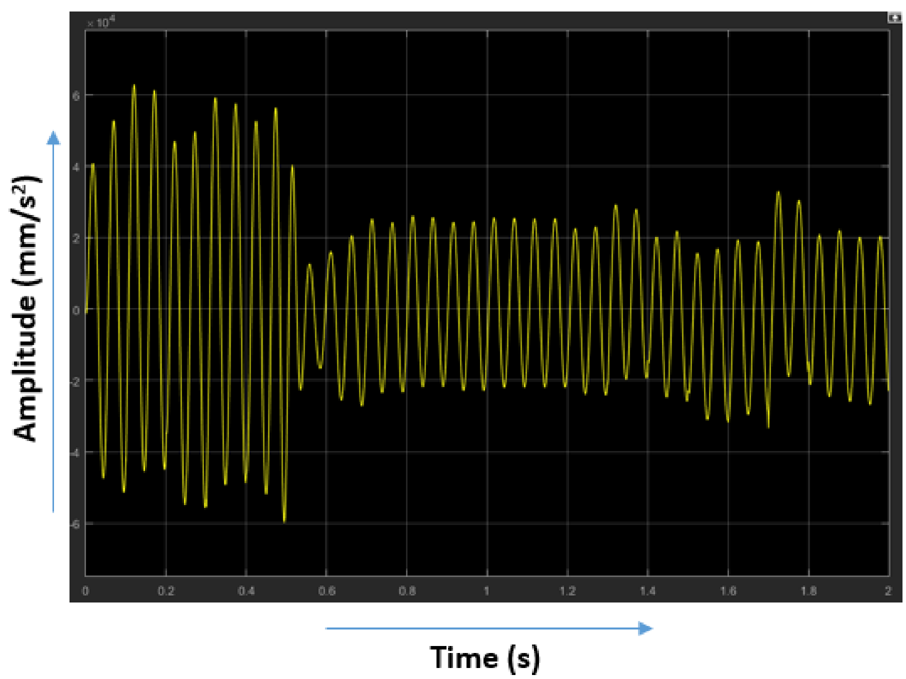

FIGURE 79 – Final output response with amplitude reduction

Figure 79 shows the final response output. It has been observed that the tool successfully reduced the overall amplitude with some frequency amplitudes going higher and lower due to the randomness of the excitation force, at level which are acceptable. This helps confirm the effectiveness of the tool to identify percentage amplitude reduction for any external force excitation at the frequency of concern.

6.4 OPTIMIZED LOCATION FOR ACFG ON TRUCK FRAME

In this section a location identification study has been executed. The objective of this study is to identify, from a set of pre-determined locations the best location to place the ACFG tool to get maximum amplitude reduction and also the corresponding controller time to achieve steady state for the fixed angular velocity. The pre-determination of locations was based on the probable feasible locations on the frame where this tool can be placed. This resulted in 9 locations as shown in Figure 80. The stiffness, mass, damping, displacement, eigenvalue and force matrices for each of these locations were extracted using DMAP in NASTRAN and then the Simulink model was simulated to capture the final output performance for all the locations.

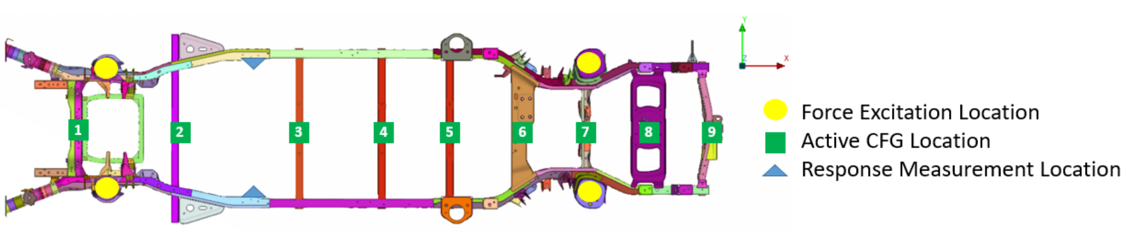

FIGURE 80 – Additional Possible Excitation Locations

Figure 81 shows the summary of the amplitude reduction achieved for all the locations and the time taken by the controller to achieve steady state angular velocity of the DC motor.

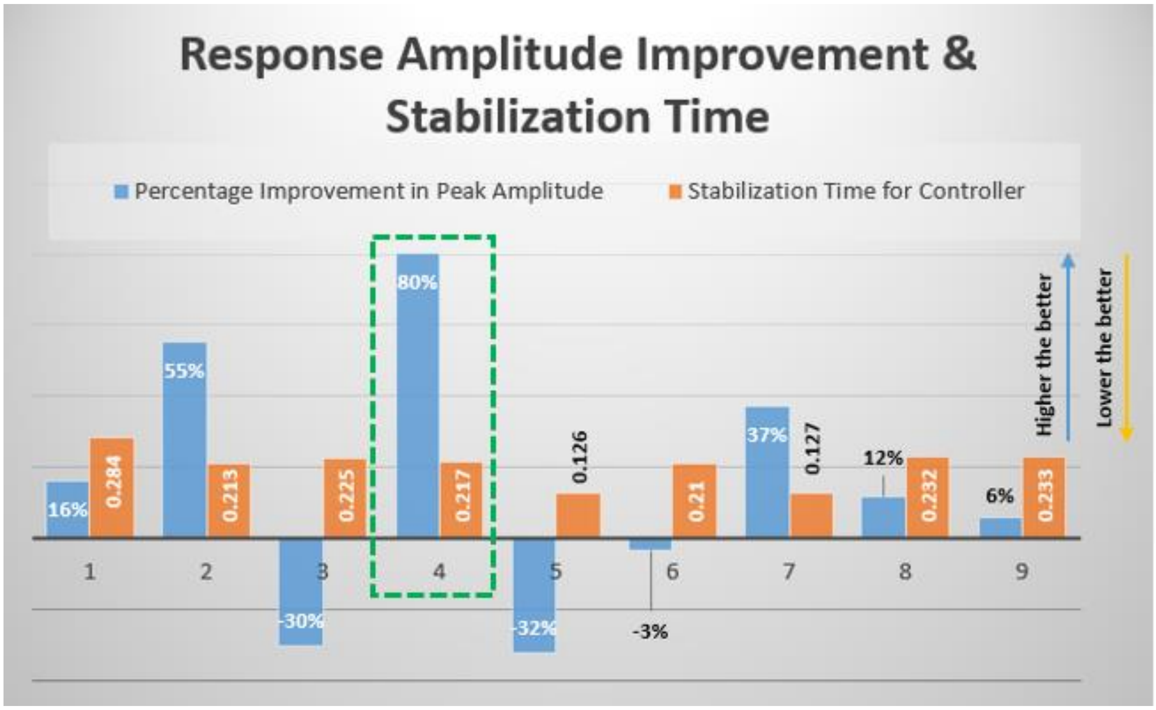

FIGURE 81 – Result Summary for all the probable tool placement location

As seen from the results, not all locations positively affect the final output response. Locations 3, 5 and 6 adversely affect the response, and instead of an amplitude reduction an increase in amplitude has been observed. This may be due to the mode shape and load path at the target frequency of the frame, 19.75 Hz. It can also be seen that location 7 shows the minimum time (0.127 seconds) for the controller to achieve the DC motor output steady state angular velocity for positive amplitude reduction, but the reduction is limited to only 37% improvement. The maximum improvement has been identified at location 4, which achieves about 80% amplitude reduction, with the time taken to achieve steady state angular velocity to be 0.217 seconds. Since this location shows maximum potential benefit for amplitude reduction, therefore it was identified to be the best location for tool placement. The controller time can be further optimized by investigating different control techniques which has not been scope of this dissertation but can be researched in the future. Figure 82 shows the final output response for location 4 when the ACFG is switched ON.

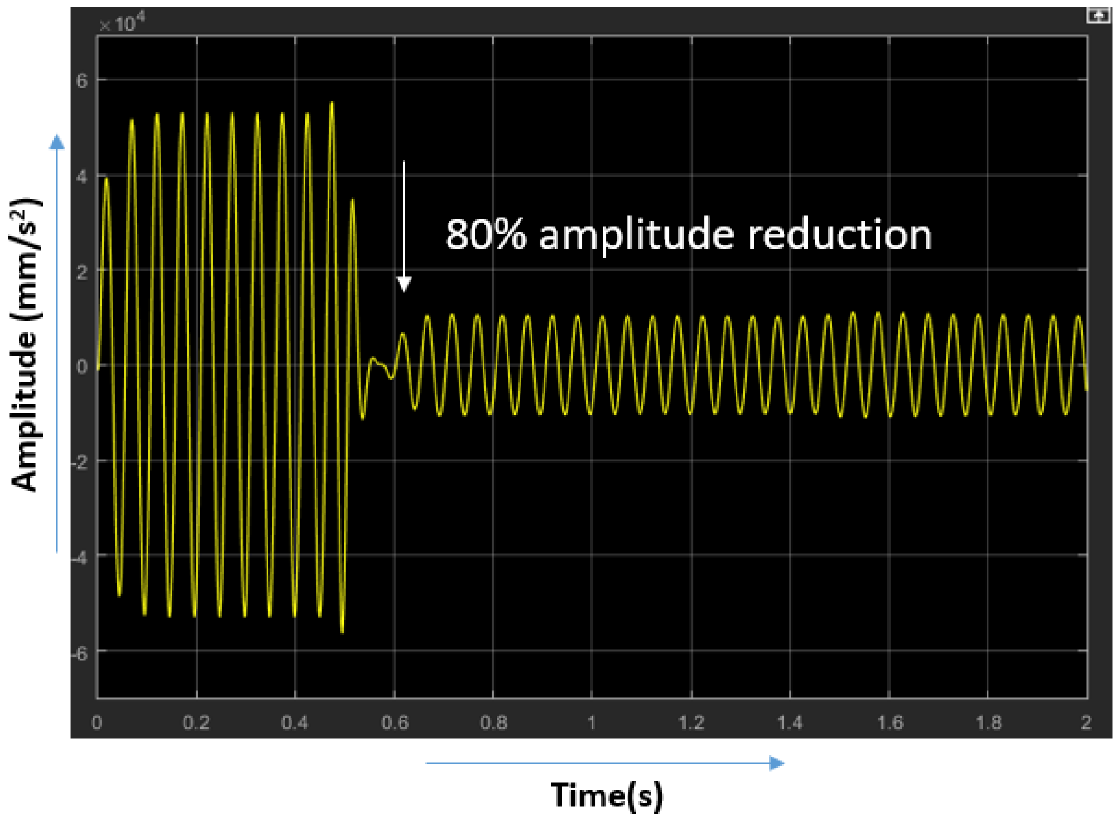

FIGURE 82 – Final output response with amplitude reduction for location 6

CHAPTER SEVEN

CONTRIBUTIONS AND FUTURE WORK

7.1 DISSERTATION CONTRIBUTIONS

The main contributions for this dissertation are listed below.

- Derived the working principle of a DC motor and investigated the efficiencies of different types of DC motor. Formulated the equations pertaining to the brushed DC motor with friction losses and represented it in a Simulink model.
- Derived and illustrated the dynamic behavior of a single degree of freedom structure with a mass imbalance and calculated the centrifugal force generated due to the imbalanced mass.
- Developed a Simulink model to represent a single degree of freedom structure and calculated the equal and opposite force required to cancel the output response based on the response of the system excited by an external force.
- Validated the single degree of freedom Simulink model by correlating the results with MATLAB using an ordinary differential equation technique.
- Developed the representation of force actuation based on centrifugal force generation principle using a DC motor and PID controller to perform virtual reduction of the output response for the single degree of freedom structure with an imbalanced mass in Simulink.
- Analytically solved the system of equations and correlated with the Simulink model to validate the developed virtual tool of force cancellation in a single degree of freedom model with a mass imbalance.

- Developed a finite element model of a continuous beam (multiple degree of freedom structure) and extracted the reduced mass, stiffness, damping, displacement, eigenvalue, and force matrices to represent a state space system for the continuous beam.
- Developed and modified the virtual tool to solve and calculate the amplitude reduction for multiple degree of freedom structures and implemented it to show the results for a continuous beam.
- Developed a finite element model for a truck frame. Identified a vehicle level issue and derived the concerning frequency of issue a frame level. Extracted the reduced mass, stiffness, damping, displacement, eigenvalue, and force matrices to represent the finite element truck frame in state space form and validated the functionality of the state space model with MATLAB.
- Developed and modified the virtual active CFG tool to simulate the truck frame model in Simulink and showed the amplitude reduction for the output response at the concerning frequency.
- Further demonstrated use of random white noise to combine with the external force excitation and still capture the amplitude reduction for the concerning frequency with the developed ACFG virtual tool.
- Identified the optimum location for a physical ACFG prototype on the frame using virtual simulation in Simulink and illustrated the results of the best and worst locations on the frame for maximum amplitude reduction and minimum time taken by the controller to achieve steady state angular velocity output from the DC motor.

7.2 FUTURE WORK

Based on the research of this dissertation the following is the list of recommendation for future work.

- Research alternate controllers or to optimize the current controller to improve the time taken between cancelling force generation and steady state. Although theoretically this tool can cancel any frequency of force application, reduction of the time by ten times of the current scenario would be beneficial for force cancellation at higher velocities and therefore improve the capability of the tool to cancel higher frequency content in practical applications.
- The current research presents the application of the tool developed on a truck frame but modification of the tool to simulate unibody vehicle would also increase the practical capabilities of the tool. Determination of the environment to package the tool in a unibody or a body on frame vehicle at different angles and building a physical prototype of the tool can also be investigated.
- Methodology to capture and optimize live video processing capability to determine an oncoming bump or pothole on the road through a front camera to pre-calculate the forcing function that the system will observe, based on the dynamic characteristics of the suspension, in order to apply the ACFG tool to simulate force cancellation, would be a highly beneficial ADAS feature that can be added to a future vehicle.

REFERENCES

1. Connor, Jerome J. , “Intro to Structural Motion Control”. *Tuned Mass Damper Systems*, Prentice Hall; First Edition (January 1, 2002): pp. 217-285

2. Smith, Emma, “Analysis and simulation of centrifugal pendulum vibration absorbers” Master’s Thesis. Royal Institute of Technology, KTH Stockholm, Sweden. 2015.

3. Alsuwaiyan, A and Shaw, S “Performance and dynamic stability of general-path centrifugal pendulum vibration absorbers.” *Journal of Sound and Vibration* Vol. 252, No.5 (2002): pp. 791-815.

4. Ferreira, Fernando. Moutinho, Carlos. Cunha, Alvaro and Caetano, Elsa “Use of semi-active tuned mass dampers to control footbridges subjected to synchronous lateral excitation”, *Journal of Sound and Vibration* Vol. 446 (2019): pp. 176-194.

5. Scheller, Jorn and Starossek, Uwe “A versatile active mass damper for structural vibration control”, *Proceedings of the 8th International Conference on Structural Dynamics*, EURODYN 2011. Leuven, Belgium, July 4-6 2011.

6. Yang, Don-Ho. Shin, Ji-Hwan, Lee. HyunWook, Kim. Seoug-Ki and Kwak, Moon K. “Active vibration control of structure by Active Mass Damper and Multi-Modal Negative Acceleration Feedback control algorithm”, *Journal of Sound and Vibration* Vol. 392 (2017): pp. 18-30.

7. Talib, Ezdiani. Shin, Ji-Hwan. and Kwak, Moon K. “Designing multi-input multi-output modal-space negative acceleration feedback control for vibration suppression of structures using active mass dampers”, *Journal of Sound and Vibration* Vol. 439 (2019): pp. 77-98.

8. Chang, C.C. and Yang, H.T.Y, “Control of buildings using active tuned mass damper”, *Journal of Engineering Mechanics* Vol. 121, No. 3 (1995), pp: 355-366.

9. Samali, B. and Al-Dawod, M. “Performance of a five-storey benchmanrk model using active tuned mass damper and fuzzy controller”, *Engineering Structures* Vol. 25 (2003): pp. 1597-1610. DOI:10.1016/S0141-0296(03)00132-9.

10. Christenson, R.E. Spencer Jr., B.F. Hori, N. and Seto, K. “Coupled building control using acceleration feedback”, *Computer-Aided Civil and Infrastructure Engineering* Vol. 18 (2003): pp. 4-18.

11. Zhang, Y. Li, L. Cheng, B. and Zhang, X. “An active mass damper using rotating actuator for structural vibration control”, *Advances in Mechanical Engineering* Vol. 8, No. 7 (2016). DOI:10.1177/1687814016657730

12. Young-Moon, Kim. Ki-Pyo, You. Jang-Youl, You. Sun-Young, Paek and Byung-Hee, Nam, “LQG Control of Along-Wind Responses of Tall Building Using Composite Tuned Mass Dampers”, *Key Engineering Materials* Vol. 723, (2017): pp. 753-759.

13. Nassim Djedoui. Abdelhafid Ounis. and Mahdi Abdeddaim. “Active Vibration Control for Base-Isolated Structures Using a PID Controller Against Earthquakes”, *International Journal of Engineering Research in Africa*, Vol. 26, (2016): pp. 99-110.

14. Ge, S. Hou, S. Yang, Y. Zhang, Z. et al., "Active Vibration Control of Electric Drive System in Electric Vehicles Based on Active Disturbance Rejection Current Compensation under Impact Conditions" *SAE Int. J. Veh. Dyn., Stab., and NVH,* Vol. 7, No. 4, (2023): pp. 513-531. https://doi.org/10.4271/10-07-04-0033

15. Roessler, S. and Baier, H., "Car Body Influence on the Perceived Driving Dynamics due to Feelable Structure Vibrations," *SAE Int. J. Veh. Dyn., Stab., and NVH,* Vol. 6, No. 3, (2022): pp. 311-331.

16. Derrix, D. and Prokop, G., "Experimental Analysis of the Influence of Body Stiffness on Drivability and Dynamic Body Behavior with On-Road Experiments," *SAE Int. J. Veh. Dyn., Stab., and NVH,* Vol. 6, No. 3, (2022): pp. 283-296.

17. Wang, Liuping. Chai, Shan. Yoo, Dae. Gan, Lu. and Ng, Ki. *PID And Predictive Control Of Electrical Drives And Power Converters Using Matlab/Simulink,* John Wiley & Sons, Singapore (2015).

18. Karl J. Astrom and Tore Hagglund, *PID Controllers, 2nd Edition*, ISA: The Instrumentation, Systems, and Automation Society, USA (1995).

19. Janpan, I. Chaisricharoen, R. Boonyanant, P. “Control of the Brushless DC Motor in Combine Mode”, *Procedia Engineering*, Vol. 32, (2012): pp. 279-285. https://doi.org/10.1016/j.proeng.2012.01.1268.

20. Zaccarian, L. “Dynamic model and control techniques.” *DC Motors*. Roma Italy, 2012.

21. Rani, B. Indu. And Tom, Ashly Mary. "Dynamic simulation of brushless DC drive considering phase commutation and backemf waveform for

electromechanical actuator", *TENCON 2008 - 2008 IEEE Region 10 Conference*: pp. 1-6, 2008.

22. Yedamale, Padmaraja. “Brushless DC (BLDC) Motor Fundamentals” *AN885*: pp. 1-20. Microchip Technology Inc, (2003).

23. Condit, Reston. “Brushed DC Motor Fundamentals” *AN905*: pp. 1-10. Microchip Technology Inc, (2003).

24. Taut, Marius Alexandru. Chindris, Gabriel. Taut, Adrian Catalin and Pitica, Dan. "Model-in-the-Loop for Determining the Speed and Position of a DC Motor", *Electronics Technology (ISSE) 2018 41st International Spring Seminar*: pp. 1-7, Zlatibor, Serbia, May 16-20, 2018. DOI: 10.1109/ISSE.2018.8443767

25. Kreyszig, Erwin. *Advanced Engineering Mathematics, 9th Edition*. John Wiley & Sons, USA (2006).

26. Umez-Eronini, Eronini. *System Dynamics & Control*. PWS Publishing Company, (1999)

27. Bistritz, Y. "Bounded-Input Bounded-Output Stability Tests for Two-Dimensional Continuous-Time Systems," *IEEE Transactions on Circuits and Systems I: Regular Papers*, Vol. 68, No. 5 (2021): pp. 2134-2147, DOI: 10.1109/TCSI.2021.3059839.

28. Shahruz, S. M. "Bounded-input bounded-output stability of a damped nonlinear string," *IEEE Transactions on Automatic Control*, Vol. 41, No. 8: pp. 1179-1182, Aug (1996), DOI: 10.1109/9.533679.

29. Debeljković, Dragutin. Višnjić, Nemanja. and Pješćić, Milmir. “The Stability of Linear Continuous Singular Systems in the sense of Lyapunov: An Overview” *Scientific Technical Review*, Vol. 57, No.1 (2007): pp. 51-65.

30. Debeljković, Dragutin Lj. and Stojanović, Sreten. “The Stability of Linear Discrete Time Delay Systems in the Sense of Lyapunov: An Overview” *Scientific Technical Review*, Vol. 60, No.3-4 (2016): pp.67-81

31. Kreindler E. and Sarachik, P. "On the concepts of controllability and observability of linear systems," *IEEE Transactions on Automatic Control*, Vol. 9, No. 2: pp. 129-136, April (1964), DOI: 10.1109/TAC.1964.1105665.

32. Gilbert, Elmer G. “Controllability and Observability in Multivariable Control Systems”, *Journal of Society for Industrial and Applied Mathematics Series A control*, Vol. 1, No. 2, DOI: 10.1137/0301009.

33. Yasuda, Kazunori. Skelton, Robert E. "Assigning Controllability and Observability Gramians in Feedback Control" *Journal of Guidance, Control, and Dynamics*, Vol. 14, No. 5, September (1991): pp. 878-885.

34. Pederson, Jacob. "Model Based and Robust Control Techniques for Internal Combustion Engine Throttle Valves." PhD Thesis. University of East London, London, UK. 2013.

35. Geffroy, N. Brunetti, L. Bolzon, B. and Jeremie, A. "Creation of a State-Space Model from a Finite Element Model for the active control algorithm efficiency tests." Technical Report. EUROTeV 054. 2007.

36. Ogata, Katsuhiko. *Modern Control Engineering Fifth Edition*. Prentice Hall, New Jersey (2010).

APPENDIX A

CONTINUOUS BEAM MATRICES

KM Reduced Matrix

```
  10      10       6       1MYK     1P,5E16.9
       1       1      10
-1.200486367E-06     1.445243803E-09     7.608073228E-08-2.945812669E-09
6.155900161E-10
-5.351522595E-11-6.115866671E-07     8.904987173E-09     1.059562125E-06
5.716827172E-09
       2       1      10
-2.864379309E-09-4.431501628E-07-1.890152846E-08-4.813427360E-07
6.824016059E-10
 1.827319909E-11     7.393636184E-09     1.196720670E-06-6.406906593E-09
1.742352988E-06
       3       1      10
 3.605827441E-07     2.406144739E-09     8.975159708E-07-3.108681797E-09-
1.101321338E-10
-5.001479484E-11     1.223116995E-06     1.320049406E-08-6.165879961E-08
7.859250556E-09
       4       1      10
 2.200890043E-09          4.332520247E-07-9.017848234E-10-6.709662705E-07-
1.534195452E-10
 1.406669814E-11-7.048299492E-09-2.052422995E-07-4.128603503E-09
4.251415314E-07
       5       1      10
 5.215091824E-11     1.522406884E-10     8.231722080E-11-2.046804595E-10-
3.360163123E-08
 7.554461150E-10-1.987124622E-09     4.778444743E-09     6.042055114E-10
3.650962125E-10
       6       1      10
 1.486719292E-10-7.048732476E-11-8.085861467E-11          7.895255413E-12
3.328779282E-09
-9.578365926E-07     3.541134001E-09-2.090190724E-10     1.334674510E-09
1.913928939E-09
       7       1      10
-1.245651220E-06     1.184901066E-09     1.085962140E-06-1.014500128E-08-
2.068027971E-09
 3.535663762E-09          8.367628885E+04-6.887090205E-09-5.521178537E-08
4.746411264E-09
       8       1      10
```

4.990795333E-09-2.170963853E-07-8.555502973E-09 1.733787940E-07
4.737306103E-09
-1.446228692E-10-7.810957685E-09 8.367628885E+04-4.375198870E-09-
5.195397534E-08
9 1 10
6.339978427E-07-8.511733540E-09-2.296037565E-07 3.794582426E-10
6.220410853E-10
1.235415326E-09-3.304157872E-07-1.893099011E-09 6.354664363E+05-
8.346762764E-09
10 1 10
9.117684385E-10-1.652224455E-07-1.984517439E-09-1.912048901E-07
1.589413046E-10
1.953136763E-09 4.697213285E-09 9.697687346E-07-7.891434256E-09
6.354664363E+05
11 1 1
1.000000000E+00
10 10 6 1MYM 1P,5E16.9
1 1 10
1.000000000E+00-5.241033302E-16 1.013078510E-15 5.256212132E-16
1.059468810E-16
-6.862898108E-16 9.436895709E-16-1.136243877E-16 4.718447855E-16
6.145257914E-16
2 1 10
-5.230191280E-16 1.000000000E+00 4.145989108E-16-9.714451465E-17-
3.538903654E-16
-2.865359995E-16 9.978996796E-16 5.551115123E-16-9.532305500E-16-
1.526556659E-15
3 1 10
9.298117831E-16 4.198030812E-16 1.000000000E+00 7.331375090E-16
3.046777511E-16
1.229520839E-15-1.151856388E-15 7.259817747E-16-1.863093013E-15-
5.911070244E-16
4 1 10
5.232359684E-16 1.387778781E-17 7.334627697E-16 1.000000000E+00-
8.015506661E-16
5.400267026E-16-7.482079192E-16 1.373900993E-15-2.833562378E-16-
1.075528555E-16
5 1 10
1.059807624E-16-3.538835891E-16 3.047387375E-16-8.015100085E-16
1.000000000E+00
-6.278275968E-16 1.421070564E-15-2.245789275E-16-2.617128519E-16-
9.537997562E-16
6 1 10
-6.862627057E-16-2.865359995E-16 1.229553026E-15 5.400199263E-16-
6.278292908E-16

1.000000000E+00 5.329124728E-16 2.539387835E-16 6.123285879E-16
2.005342032E-16
7 1 10
1.054711873E-15 1.005489095E-15-1.096345237E-15-7.487500203E-16
1.421090893E-15
5.329056966E-16 1.000000000E+00-1.060950887E-15 5.551115123E-17-
5.210946692E-16
8 1 10
-1.118896642E-16 2.775557562E-16 7.251144130E-16 9.992007222E-16-
2.246399139E-16
2.539370895E-16-1.061160231E-15 1.000000000E+00 3.756760528E-16
4.163336342E-16
9 1 10
3.885780586E-16-9.549652735E-16-1.817990203E-15-2.837357085E-16-
2.617331807E-16
6.123184235E-16 2.220446049E-16 3.755947376E-16 1.000000000E+00
3.675043213E-16
10 1 10
6.132247488E-16-1.387778781E-15-5.932754288E-16 1.908195824E-16-
9.537048885E-16
2.005282740E-16-5.208778287E-16 3.330669074E-16 3.674896319E-16
1.000000000E+00
11 1 1
1.000000000E+00
Damping Reduced Matrix
10 10 6 1MYC 1P,5E16.9
1 1 10
5.000071763E-03 3.873466149E-11-1.577540911E-09-2.148505227E-12
2.120272274E-11
4.634663780E-12-5.998062267E-09 6.130234104E-11 8.114899100E-09
5.846266742E-11
2 1 10
3.822468555E-11 5.000072628E-03 1.108787270E-10 2.732089349E-09-
2.476957804E-11
-1.624223367E-12 6.456415505E-11 7.543952525E-09-2.001631344E-11
3.074546016E-09
3 1 10
1.055043695E-09-3.524203864E-11 5.000072655E-03-1.676906058E-11
1.731248434E-11
-1.053791003E-11 6.508603409E-09 2.472930399E-11 1.107571167E-09
8.114109434E-11
4 1 10
-1.797149974E-11 3.591259507E-09 4.340109256E-11 5.000072998E-03
2.847409067E-11

-2.749224305E-12-4.473315495E-11-1.885085110E-09-4.360177935E-11
3.343373995E-09
5 1 10
2.332813148E-11-2.848296745E-11 1.927747051E-11 3.324790549E-11
5.000239316E-03
1.505794511E-10-9.713366096E-12 2.464587190E-11 1.966202192E-12
1.697017432E-12
6 1 10
4.140914619E-12-1.555458381E-12-1.144567846E-11-2.670895966E-12
1.315946619E-10
4.999983799E-03 1.737415162E-11-7.106207060E-13 6.067877133E-12
9.644248614E-12
7 1 10
8.018616882E-10-3.045463881E-11 5.035296624E-09-2.661082465E-11-
1.130543228E-11
1.807118517E-11 4.183864443E+02-1.435369407E-11 5.675531156E-09
5.461750496E-11
8 1 10
1.487454604E-11-2.273736754E-11 2.135847055E-12 3.561943629E-09
2.331886767E-11
-8.297802549E-13-3.927720297E-12 4.183864443E+02-3.357245038E-11
2.650750730E-09
9 1 10
2.401748134E-09-3.695710404E-12-9.050182825E-10-3.402900184E-11
3.205380406E-12
6.109272810E-12 1.667672223E-09-2.457145598E-11 3.177337182E+03
1.489721690E-13
10 1 10
4.150813027E-11 6.508457773E-09 6.349054615E-11-3.972637330E-09
2.644315322E-12
9.723180594E-12 1.133670935E-11 2.425394996E-09-1.019986853E-12
3.177337182E+03
11 1 1
1.000000000E+00
Displacement Matrix
10 18 2 1DISPS 1P,5E16.9
1 1 18
-5.725273484E-03 4.897105021E+01 1.814914197E-01-5.725273440E-03-
1.338469173E+01
1.542014328E-03-5.725273441E-03-1.468376969E+01-2.206931641E-03-
5.725273475E-03
-7.833858958E+01-1.859052830E-01-5.725273484E-03 5.027012817E+01
1.852403657E-01
-5.725273475E-03-7.963766754E+01-1.896542290E-01
2 1 18

6.878894106E-03-7.837770591E-01 4.500789335E+01 6.878894923E-03-3.709646856E-01
-1.571242670E+01 6.878894923E-03-3.623644276E-01-1.697743337E+01 6.878894076E-03
5.904820352E-02-7.896276009E+01 6.878894106E-03-7.923773168E-01 4.627290002E+01
6.878894075E-03 6.764846157E-02-8.022776676E+01
3 1 18
-4.640478045E-03 6.242033030E+01 1.274265341E-01-4.640478083E-03 3.800752661E+01
-3.662169164E-01-4.640478083E-03 3.749892653E+01-3.765011549E-01-4.640478046E-03
1.257752277E+01-8.804288440E-01-4.640478045E-03 6.292893037E+01 1.377107726E-01
-4.640478046E-03 1.206892269E+01-8.907130826E-01
4 1 18
-8.151726126E-03-2.821312162E-01-6.534061104E+01-8.151726345E-03-2.185843793E-01
-3.710650867E+01-8.151726346E-03-2.172604869E-01-3.651829820E+01-8.151726104E-03
-1.523897576E-01-7.695985358E+00-8.151726125E-03-2.834551086E-01-6.592882151E+01
-8.151726104E-03-1.510658652E-01-7.107774892E+00
5 1 18
-4.027356970E+01-1.422761787E-02 2.087187310E-02-4.027356970E+01-2.492583555E-03
4.868075684E-03-4.027356970E+01-2.248104168E-03 4.534663849E-03-4.027356970E+01
9.731410162E-03-1.180254616E-02-4.027356970E+01-1.447209797E-02 2.120528590E-02
-4.027356970E+01 9.975889396E-03-1.213595906E-02
6 1 18
-2.330902251E-02-5.471316072E-03 1.204669488E-03-2.330902098E-02-5.440967243E-03
1.448676822E-03-2.330902098E-02-5.440334561E-03 1.453759798E-03-2.330902254E-02
-5.409353544E-03 1.702850700E-03-2.330902251E-02-5.471948148E-03 1.199585699E-03
-2.330902254E-02-5.408720726E-03 1.707934541E-03
7 1 18
-3.445047088E-10 7.679971460E+01-3.752014649E-01 3.381022614E-10-4.888758346E+01
2.388380352E-01 3.389452562E-10-4.895912846E+01 2.391875648E-01-3.788386178E-10

7.679971460E+01-3.752014648E-01-3.449784983E-10 8.054217579E+01-3.934850866E-01
-3.798123500E-10 8.054217579E+01-3.934850862E-01
8 1 18
6.421732885E-10-3.752014649E-01-7.679971460E+01-6.421338177E-10 2.388380351E-01
4.888758346E+01-6.420255012E-10 2.391875645E-01 4.895912846E+01 6.811001436E-10
-3.752014652E-01-7.679971460E+01 6.430028594E-10-3.934850867E-01-8.054217579E+01
6.827661449E-10-3.934850873E-01-8.054217579E+01
9 1 18
5.191526028E-11 7.420419088E+01-4.408696464E-01-5.411725662E-11-4.345534771E+00
2.581814252E-02-5.381548451E-11-5.283848536E-11 1.019021800E-11 5.063701659E-11
-7.420419088E+01 4.408696463E-01 5.197510951E-11 8.053071393E+01-4.784574422E-01
5.074529026E-11-8.053071393E+01 4.784574422E-01
10 1 18
4.527607466E-12 4.408696464E-01 7.420419089E+01-5.085716576E-12-2.581814255E-02
-4.345534771E+00-5.132649843E-12-3.080214588E-12-3.542962070E-11 5.501481321E-12
-4.408696464E-01-7.420419088E+01 4.531528795E-12 4.784574422E-01 8.053071393E+01
5.512596290E-12-4.784574422E-01-8.053071393E+01
11 1 1
1.000000000E+00
Eigenvalue Matrix
5 10 2 1LMAT 1P,5E16.9
1 1 10
-9.059906006E-06-8.359551430E-06-8.076429367E-06-7.424503565E-06 1.440569758E-05
2.641603351E-05 8.367628884E+04 8.367628884E+04 6.354664363E+05 6.354664363E+05
2 1 10
3.009967775E-03 2.891288887E-03 2.841905939E-03 2.724794224E-03 3.795483841E-03
5.139653053E-03 2.892685411E+02 2.892685411E+02 7.971614870E+02 7.971614870E+02
3 1 10
4.790512499E-04 4.601629183E-04 4.523033780E-04 4.336644697E-04 6.040700147E-04

```
 8.180011892E-04     4.603851819E+01     4.603851819E+01     1.268721911E+02
1.268721911E+02
    4    1   10
 1.000000000E+00     1.000000000E+00     1.000000000E+00     1.000000000E+00
1.000000000E+00
 1.000000000E+00     1.000000000E+00     1.000000000E+00     1.000000000E+00
1.000000000E+00
    5    1   10
-9.059906006E-06-8.359551430E-06-8.076429367E-06-7.424503565E-06
1.440569758E-05
 2.641603351E-05     8.367628884E+04     8.367628884E+04     6.354664363E+05
6.354664363E+05
    6    1    1
 1.000000000E+00
Force Matrix
    2   10    2    1PGTRA   1P,5E16.9
    1    1   10
 1.852403657E-01       4.627290002E+01       1.377107726E-01-6.592882151E+01
2.120528590E-02
 1.199585699E-03-3.934850866E-01-8.054217579E+01-4.784574422E-01
8.053071393E+01
    3    1    1
 1.000000000E+00
```

APPENDIX B

CONTINUOUS BEAM STATE SPACE FORMULATION

```
clear all;
close all;
clc;

% $$$$$$$$$$$$$$$$$$$$$$$$$$$$$$$$$$$$$$$$$$$$$$$$$$$$$$$$$$$$$$$$$$$$$$$$$$$$$$$$$$$$$$$$$$
%
%      Read matrices and compute Eigenvalue / Eigenvector              %
% $$$$$$$$$$$$$$$$$$$$$$$$$$$$$$$$$$$$$$$$$$$$$$$$$$$$$$$$$$$$$$$$$$$$$$$$$$$$$$$$$$$$$$$$$$
%



 [Kr,Mr] = read_out4('N:\vt\NVH\Abhishek\PhD\Model\run5_matlab\KMRed.txt');  %%
Read Reduced K & M

 [VV] = read_out4('N:\vt\NVH\Abhishek\PhD\Model\run5_matlab\eigval.txt');    %%
Read Eigenvalues
  V = diag(VV(:,1));


  num_modes_total = length(V);
  index_orig = 1:num_modes_total;
  omega2 = diag(V);

  freqvec = sqrt(omega2)/(2*pi); % Hz

 [fmod11] = read_out4('N:\vt\NVH\Abhishek\PhD\Model\run5_matlab\Force.txt');  %
[100 x 816][816 x 1]  = 100 x 1
                                          % Modal Force vector
  % As the amplitude is taken care of in the Freq2TimeLoadFix.m,
  % we need to eliminate the amplitude from the FORCE
  %

  fmod12 = ones(length(fmod11));
  fmod12 = [fmod12(:,1) fmod12(:,2)];
  fmod13 = zeros(length(fmod11));
  fmod13 = [fmod11(:,1) fmod13(:,2)];
 [Cmqchk] = read_out4('N:\vt\NVH\Abhishek\PhD\Model\run5_matlab\Disp.txt');   %
Read Displacement
```

```
% $$$$$$$$$$$$$$$$$$$$$$$$$$$$$$$$$$$$$$$$$$$$$$$$$$$$$$$$$$$$$$$$$$$$$$$$
%
%                State space for all modes                      %
% $$$$$$$$$$$$$$$$$$$$$$$$$$$$$$$$$$$$$$$$$$$$$$$$$$$$$$$$$$$$$$$$$$$$$$$$
%


% --------------------------- Principal coordinates -----------------

 SISO = 2;   % Load applied seperatly on 2 grids

% variable = zeros(length(Mr),1);
% tunableSS
% systune
 B11 = [ zeros(length(Mr),SISO) ; inv(Mr)*fmod11 ];  %
 len = length(B11);
 uni = [ones(len)];
uni2 = (uni(:,1));
%uni2 = [0 1;0 1;0 1;0 1;0 1;0 1;0 1;0 1;0 1;0 1;0 1;0 1;0 1;0 1;0 1;0 1;0 1;0 1;0 1];
 BB11 = B11 + uni2;
 [Dr] = read_out4('N:\vt\NVH\Abhishek\PhD\Model\run5_matlab\DampRed.txt');  %
Damping matrix based on rayleigh damp

 Z = 0.5 * inv(Mr) * Dr * inv(sqrt(V));      % Compute Z

 Cmv = zeros(size(Cmqchk));
 [rr,cc] = size(Cmqchk);


 C11 = [-Cmqchk*V   -Cmqchk*(2 * Z * sqrt(V))];
 [nOut,crp] = size(C11);


 D11 = Cmqchk*inv(Mr)*fmod11;
 len3 = length(D11);
 uni3 = [ones(len3)];
 uni4 = (uni3(:,1));
 %uni4 = 10000*[0 1;0 1;0 1;0 1;0 1;0 1;0 1;0 1;0 1;0 1;0 1;0 1;0 1;0 1;0 1;0 1;0 1];
 DD11 = D11 + uni4;

 AA11 = [ zeros(size(Mr))  eye(size(Mr)) ; -V -(2 * Z * sqrt(V)) ];
```

```
 mysystem3 =  ss(AA11,B11,C11,D11);   %% State Space System

 mysystem4 =  ss(AA11,BB11,C11,DD11);

tt = 0:0.0004:4;   %% Time of simulation



ff =[];
for p = 1:length(tt)
  qq = Freq2TimeLoadFix( tt(p) );    %% Load

  ff = [ff ; qq ];
end
UU = ff;

[Y, Tsim, X] = lsim(mysystem3,[UU'],tt');   %%   simulate  Linear model



 XX = csvread('N:\vt\NVH\Abhishek\PhD\Model\run5_matlab\export_results.csv');  % Time domain data from nastran from Org Model


 grids = find(XX(:,1)==4.000);
 xdat = XX(:,1);
 ydat = XX(:,2);

 ng = length(grids);
 if mod(ng,2) > 0
   ng = ng + 1;
 end
 if mod(ng,4) > 0
   mm = ng/3;
   nn = 3;
 else
   mm = ng/4;
   nn = 4;
 end

  resp = 3; % Z direction load

  for ii = 1 : length(grids)
  if ii == 1, mmm = 1;i=1;, else mmm = ii-1;i = grids(mmm)+ 1;,end
```

```
  xd = xdat(i:grids(ii));
  yd = ydat(i:grids(ii));

  ass = 3*ii - ( 3-resp );
  yres = Y(:, ass  );

  figure
  %subplot(mm,nn,ii);
  plot(xd, yd,'kx-','LineWidth',1,'MarkerIndices',1:50:length(yd)); hold on;
  %subplot(mm,nn,ii);
  plot(Tsim, yres,'ro','LineWidth',1,'MarkerIndices',1:100:length(Y)); hold on;

  xlabel('Time sec'); ylabel('Acc');

  legend('NAS','LSIM' ); ;
  end



%Define properties of unbalanced mass
m2 = 0.002;
e = 250;
 %Define properties of DC Motor
L = 0.5; %Henrys
R = 2; %Ohms
Kf = 0.2; %Nms
Kb = 0.1; %Back emf Constant
J = 0.02; %Kgm2/s2
Km = 0.1; %Torque Constant
```

APPENDIX C

TRUCK FRAME STATE SPACE FORMULATION

```
close all
clear all
clc
%  No Grids are SPC'd
%  Grids of interest are  10000340, 350, 10001423, 1433, 10267858, 10267946
%  Internal sequencing is 17, 18, 93, 97, 246420, 246438
%  Load applied on Grids 10257787, 788
%  Internal sequencing is 238530, 531
% $$$$$$$$$$$$$$$$$$$$$$$$$$$$$$$$$$$$$$$$$$$$$$$$$$$$$$$$$$$$$$$$$$$$$$$$
%
%      Read matrices and compute Eigenvalue / Eigenvector              %
% $$$$$$$$$$$$$$$$$$$$$$$$$$$$$$$$$$$$$$$$$$$$$$$$$$$$$$$$$$$$$$$$$$$$$$$$
%


[Kr,Mr] = read_out4('N:\vt\NVH\Abhishek\PhD\Model\AP\NasRun\KMRed.txt');  %%
Read Reduced K & M

 [VV] = read_out4('N:\vt\NVH\Abhishek\PhD\Model\AP\NasRun\eigval.txt');    %%
Read Eigenvalues
V = diag(VV(:,1));


num_modes_total = length(V);
index_orig = 1:num_modes_total;
omega2 = diag(V);

freqvec = sqrt(omega2)/(2*pi); % Hz

 [fmod11] = read_out4('N:\vt\NVH\Abhishek\PhD\Model\AP\NasRun\Force.txt');
% [100 x 816][816 x 1]  = 100 x 1
% Modal Force vector
% As the amplitude is taken care of in the Freq2TimeLoadFix.m,
% we need to eliminate the amplitude from the FORCE
%
```

```
[Cmqchk] = read_out4('N:\vt\NVH\Abhishek\PhD\Model\AP\NasRun\Disp.txt');   %
Read Displacement

% $$$$$$$$$$$$$$$$$$$$$$$$$$$$$$$$$$$$$$$$$$$$$$$$$$$$$$$$$$$$$$$$$$$$$$$$$$$
%
%                   State space for all modes                        %
% $$$$$$$$$$$$$$$$$$$$$$$$$$$$$$$$$$$$$$$$$$$$$$$$$$$$$$$$$$$$$$$$$$$$$$$$$$$
%


% ---------------------------- Principal coordinates ------------------
[Dr] = read_out4('N:\vt\NVH\Abhishek\PhD\Model\AP\NasRun\DampRed.txt');  %
Damping matrix based on rayleigh damp



%%% Individual Loads to be SIMULATED seperately
tt = 0:0.0004:4;   %% Time of simulation

%%>>>>>>>>>>>>>>>>>>>>>>>>>>>>>>>>>>>>>>>>>>
% for loads = 4:5
% UU = [];

SISO =1;
B11 = [ zeros(length(Mr),SISO) ; inv(Mr)*fmod11(:,14) ];  %
BB11 = [ zeros(length(Mr),SISO) ; inv(Mr)*fmod11(:,1) ];

Z = 0.5 * inv(Mr) * Dr * inv(sqrt(V));
% Compute Z

Cmv = zeros(size(Cmqchk));
[rr,cc] = size(Cmqchk);


C11 = [-Cmqchk*V   -Cmqchk*(2 * Z * sqrt(V))];
[nOut,crp] = size(C11);


D11 = Cmqchk*inv(Mr)*fmod11(:,14);
DD11 = Cmqchk*inv(Mr)*fmod11(:,1);

AA11 = [ zeros(size(Mr))  eye(size(Mr)) ; -V -(2 * Z * sqrt(V)) ];

mysystem3 =  ss(AA11,B11,C11,D11);   %% State Space System
mysystem4 =  ss(AA11,BB11,C11,DD11);
```

```
ff =[];
for p = 1:length(tt)
qq = Freq2TimeLoadFix( tt(p) );    %% Load

ff = [ff ; [qq  ]];  %
end
UU = ff;

[Y, Tsim, X] = lsim(mysystem3,  UU , tt');   %%   simulate  Linear model


mytxt =
strcat('/cae/vt/NVH/Abhishek/PhD/Model/AP/NasRun/Pg2_W',num2str(loads),'.csv');
XX = csvread(mytxt);  % Time domain data from nastran from Org Model

grids = find(XX(:,1)==4.000);
xdat = XX(:,1);
ydat = XX(:,2);
xd = XX(:,1);
resp = 3; % Z direction load
jj = 1;
for ii = 2 : size(XX,2)

xd = xdat(jj:grids(ii));
yd = ydat(jj:grids(ii));
yd = XX(:,ii);
ass = 3*(ii-1) - ( 3-resp );
yres = Y(:, ass  );

figure

plot(xd, yd,'kx-','LineWidth',1,'MarkerIndices',1:50:length(yd)); hold on;

plot(Tsim, yres,'ro','LineWidth',1,'MarkerIndices',1:100:length(Y)); hold on;

xlabel('Time sec'); ylabel('Acc');
thStr = strcat('NAS - ',num2str(loads));
legend(thStr,'LSIM' ); ;
jj = grids(ii) + 1;
end

end
m2 = 0.002;
e = 250;
```

```
%Define properties of DC Motor
L = 0.5; %Henrys
R = 2; %Ohms
Kf = 0.2; %Nms
Kb = 0.1; %Back emf Constant
J = 0.02; %Kgm2/s2
Km = 0.1; %Torque Constant
```